



The Hashemite Kingdom of Jordan Scientific Research Support Fund The Hashemite University

JJEES

Jordan Journal of Earth
and Environmental Sciences

Volume (9) Number (3)

Cover photo © Ahmad Masri, Lisan Marl Formation, Dead Sea, Jordan



JJEES is an International Peer-Reviewed Research Journal

ISSN 1995-6681

jjees.hu.edu.jo

December 2018

Jordan Journal of Earth and Environmental Sciences (JJEES)

JJEES is an International Peer-Reviewed Research Journal, Issued by Deanship of Scientific Research, The Hashemite University, in corporation with, the Jordanian Scientific Research Support Fund, the Ministry of Higher Education and Scientific Research.

EDITORIAL BOARD:

Editor –in-Chief:

- **Prof. Fayez Ahmad**
The Hashemite University, Jordan

Assistant Editor:

- **Prof. Nezar Hammouri**
The Hashemite University, Jordan

Editorial Board:

- **Prof. Najib Abou Karaki**
University of Jordan
- **Prof. Nizar Abu-Jaber**
German-Jordan University
- **Prof. Mohammad Atallah**
Yarmouk University
- **Prof. Anwar Jiries**
Mu'tah University
- **Prof. Atef Al-Kharabsheh**
Al Balqa Applied University
- **Prof. Khaled Al Tarawneh**
Al-Hussein Bin Talal University
- **Prof. Abdullah Al-Diabat**
Al al-Bayt University

THE INTERNATIONAL ADVISORY BOARD:

- **Prof. Sayed Abdul Rahman,**
Cairo University, Egypt
- **Prof. Abdullah Al-Amri,**
King Saud University, Saudi Arabia
- **Prof. Waleed Al-Zubair,**
Arabian Gulf University, Bahrain
- **Prof. Ute Austermann-Haun,**
Fachhochschule und Lipp, Germany
- **Prof. Ibrahim Banat,**
University of Ulster, UK
- **Prof. Matthias Barjenbruch,**
Technisch Universitat Berlin, Germany
- **Prof. Mohamed Boukhary,**
Ain Shams University, Egypt
- **Prof. Mohammad El-Sharkawy,**
Cairo University, Egypt
- **Prof. Venugopalan Ittekkot,**
Center for Tropical Marine Ecology, Bremen, Germany
- **Prof. Christopher Kendall,**
University of North Carolina, U.S.A.
- **Prof. Elias Salameh,**
University of Jordan, Jordan.
- **Prof. V. Subramanian,**
Jawaharlal Nehru University, India.
- **Prof. Omar Rimawy,**
University of Jordan, Jordan.
- **Prof. Hakam Mustafa,**
Yarmouk University, Jordan.
- **Dr. Michael Crosby,**
The National Science Board, National Science Foundation, Virginia, U.S.A.
- **Dr. Brian Turner,**
Durham University, U.K..
- **Dr. Friedhelm Krupp,**
Senckenberg Research Institute and Natural History Museum, Germany.
- **Dr. Richard Lim,**
University of Technology, Australia.

EDITORIAL BOARD SUPPORT TEAM:

- Language Editor
- **Dr. Halla Shureteh**
- Publishing Layout
- **Obada Al-Smadi**

SUBMISSION ADDRESS:

Manuscripts should be submitted electronically to the following e-mail:

jjees@hu.edu.jo

For more information and previous issues:

www.jjees.hu.edu.jo



Hashemite Kingdom of Jordan



Scientific Research Support Fund



Hashemite University

Jordan Journal of Earth and Environmental Sciences

JJEES

An International Peer-Reviewed Scientific Journal

Financed by the Scientific Research Support Fund

Volume 9 Number (3)

<http://jjees.hu.edu.jo/>

ISSN 1995-6681

المجلة الأردنية لعلوم الأرض والبيئة
Jordan Journal of Earth and Environmental
Sciences (JJEES)

<http://jjees.hu.edu.jo>

Hashemite University
Deanship of Scientific Research
TRANSFER OF COPYRIGHT AGREEMENT

Journal publishers and authors share a common interest in the protection of copyright: authors principally because they want their creative works to be protected from plagiarism and other unlawful uses, publishers because they need to protect their work and investment in the production, marketing and distribution of the published version of the article. In order to do so effectively, publishers request a formal written transfer of copyright from the author(s) for each article published. Publishers and authors are also concerned that the integrity of the official record of publication of an article (once refereed and published) be maintained, and in order to protect that reference value and validation process, we ask that authors recognize that distribution (including through the Internet/WWW or other on-line means) of the authoritative version of the article as published is best administered by the Publisher.

To avoid any delay in the publication of your article, please read the terms of this agreement, sign in the space provided and return the complete form to us at the address below as quickly as possible.

Article entitled:-----

Corresponding author: -----

To be published in the journal: Jordan Journal of Earth & Environmental Sciences (JJEES)

I hereby assign to the Hashemite University the copyright in the manuscript identified above and any supplemental tables, illustrations or other information submitted therewith (the "article") in all forms and media (whether now known or hereafter developed), throughout the world, in all languages, for the full term of copyright and all extensions and renewals thereof, effective when and if the article is accepted for publication. This transfer includes the right to adapt the presentation of the article for use in conjunction with computer systems and programs, including reproduction or publication in machine-readable form and incorporation in electronic retrieval systems.

Authors retain or are hereby granted (without the need to obtain further permission) rights to use the article for traditional scholarship communications, for teaching, and for distribution within their institution.

I am the sole author of the manuscript

I am signing on behalf of all co-authors of the manuscript

The article is a 'work made for hire' and I am signing as an authorized representative of the employing company/institution

Please mark one or more of the above boxes (as appropriate) and then sign and date the document in black ink.

Signed: _____ Name printed: _____

Title and Company (if employer representative) : _____

Date: _____

Data Protection: By submitting this form you are consenting that the personal information provided herein may be used by the Hashemite University and its affiliated institutions worldwide to contact you concerning the publishing of your article.

Please return the completed and signed original of this form by mail or fax, or a scanned copy of the signed original by e-mail, retaining a copy for your files, to:

Deanship of Scientific Research
The Hashemite University P.O. Box 150458, P.C.13115, Zarqa, Jordan
Tel.: 00962 53903333/ Ext. 4235
Fax: 00962 53826823
E-mail: jjees@hu.edu.jo

Subscription

Jordan Journal of Earth & Environmental Sciences (ISSN 1995-6681)
An International Peer- Reviewed Research Journal
Published by the Deanship of Scientific Research - The Hashemite University



Name:	الاسم:
Specialty:.....	التخصص:
Address:.....	العنوان:
P.O. Box:.....	صندوق البريد:
City & Postal Code:	المدينة: الرمز البريدي:
Country:.....	الدولة:
Phone:.....	رقم الهاتف:
Fax No:.....	رقم الفاكس:
E-mail:.....	البريد الإلكتروني:
Method of payment:	طريقة الدفع:
Amount Enclosed:.....	المبلغ المرفق:
Signature:.....	التوقيع:

Cheques should be paid to Deanship of Research - The Hashemite University

I would like to subscribe to the Journal:

For

- One year
 Two years
 Three years

One year Subscription Rates

	Inside Jordan	Outside Jordan
Individuals	10JD	70\$
Students	5JD	35\$
Institutions	20JD	90\$

Correspondence

Subscriptions and sales:

Professor Fayez Ahmad
Deanship of Scientific Research
The Hashemite University P.O. Box 150458, P.C.13115, Zarqa, Jordan
Tel.: 00962 53903333/ Ext. 4235
Fax: 00962 53826823
E-mail: jjees@hu.edu.jo

PAGES	PAPERS
134 - 138	The Effects of Biosolid Application on Water-Use Efficiency and the Growth Behavior of <i>Sesbania sesban</i> (L.) Merr in Arid Mediterranean Environments <i>Fakher J. Aukour, Nabeel Bani Hani, Salman D. Al-Kofahi and Shereen Abu Smeir</i>
139 - 145	The Detection of Toxic Boron in Groundwater and Sludge in Bethlehem Area <i>Reem Y. Zeitoun</i>
146 - 152	Microfacies analysis and Paleoenvironment Interpretation of Upper Oligocene Azkand Formation in Western Iraq <i>Mohammed F. Al-Ghreri, Amer S. Algibouri and Ali A. Abed</i>
153 - 166	Creating a Drinking Water Quality Index (WQI) Map Using the Geographic Information System (GIS) Technique for Karbala City, Iraq <i>Kamal B. Al-Paruany</i>
167 - 174	The Effectiveness of Continuous Contour Ridges and Intermittent Trenches Constructed Using the Vallerani in Water Harvesting in Arid Regions <i>Kefah I. Yousef, Ahmad M. Abu-Awwad and Michel Rahbeh</i>
175 - 184	Evaluation of the DSSAT Vertical Drainage Model for Vertisols <i>Fatima Ali Bani Khaled and Ayman A. Suleiman</i>
185 - 196	Characterization and Origin of Selected Basaltic Outcrops in Harrat Irbid (HI), Northern Jordan <i>Ali Al Smadi, Ahmad Al-Malabeh and Sana'a Odat</i>

The Effects of Biosolid Application on Water-Use Efficiency and the Growth Behavior of *Sesbania sesban* (L.) Merr in Arid Mediterranean Environments

Fakher J. Aukour*, Nabeel Bani Hani², Salman D. Al-Kofahi¹, and Shereen Abu Smeir¹

¹Department of Land Management and Environment, Faculty of Natural Resources and Environment, The Hashemite University, Jordan.

²Manager of Horticulture Directorate, Irrigation and Soil Researcher, National Center for Agriculture Research and Extension, Jordan.

Received 21 February, 2018; Accepted 6 August, 2018

Abstract

Improving water-use efficiency (WUE) of cultivated crops serves as a key solution for maintaining high crop production levels under limited water resources. The main objective of this study is to investigate the potential use of municipal biosolids as soil amendments for the improvement of the production and WUE of *Sesbania sesban* (L.) Merr. Different levels of fermented dewatered biosolid were applied and mixed with the soil surface at the rates of 0.0 (control), 2.0, 4.0, 6.0, 8.0, and 10.0 ton/ha. Experimental treatments were arranged in a randomized complete block design with three replicates. The biological yield and water-use efficiency were significantly affected by biosolid applications. The highest increase in the biological yield (49.83 ton/ha) and water-use efficiency at the biological yield harvest stage (5.46) were obtained at the highest rate of biosolid application (10 ton/ha). Lower levels of biosolid applications (2, 4ton/ha) did not affect the biological yield. Moreover, grain yield, water-use efficiency at grain yield stage, Harvest Index, and average stem diameter were not significantly affected by biosolid applications. The biological yield and water-use efficiency showed a high increase (29 %) in their outputs compared to the control treatment.

© 2018 Jordan Journal of Earth and Environmental Sciences. All rights reserved

Keywords: Sesbania species, sewage sludge, grain and biological yield, forages, Mediterranean basin.

1. Introduction

The estimated agriculture production in 2050 must increase by 60 % globally to satisfy the food needs of the growing populations, particularly (up to 100 %) in developing countries (UN, 2015). The increasing demand for water in agriculture has increased the pressure on fresh water resources (Molden et al., 2010). The potential livestock production possibly will be negatively affected because of the continuous need for water for agricultural crops. Several researches were done in this regard to investigate the potential improvement in water-use efficiency aiming to increase the agricultural production at low water contents, especially for fodder production (Mendoza-Grimón, et al., 2015).

Water-Use Efficiency (WUE) is defined as the ratio of total biomass produced to the water supply used, and is considered an efficient tool in detecting the conservative plant properties. WUE is a measure of specific crop capacity to convert absorbed water into plant biomass, including other plant metabolic activities (Molden and Oweis, 2007), and therefore, it is considered a key factor in securing environmental sustainability of food production in dry areas. The improvement in plant biomass and crop yield is possible by increasing the percentage of WUE by plants, while maintaining the production levels at economically feasible levels (Aggarwal, 2000; Wang et al., 2011).

Municipal wastewater treatment plants transform sewage

biosolids into a uniform waste type referred to as biosolids. The biosolids, which are treated and managed appropriately complying with the national and international standards, can be used to support plant nutrition (Albaladejo et al., 2008). Biosolids are rich in several macronutrients such as N, P, K, Ca, Mg, S and micronutrients, such as Cu, Zn, Fe, Mn, B and Mo (Usman et al., 2012). For this study, biosolids were brought from the Municipal Water Treatment Plant (MWTP) of Ramtha in Northern Jordan. They were dewatered using an Infrared radiation (IRD) process, where moisture is removed, and pathogens in sewage sludge were destroyed, to confirm their compliance with the standards and regulations, set by the Jordanian national authorities to regulate the environmental and health issues (JOB, 2006).

The moisture content was measured and found to be (<10 %), with non-traceable pathogens. After grinding, the biosolids were distributed manually over the plots, based on the treatment specified for each plot. The biosolids were mixed and incorporated into the soil, using a rotovator to a depth of 20 cm, and then covered with black plastic mulch before sowing *Sesbania* seeds. The area of each plot was 6 m² (2×3 m).

(L.) Merr is a fast growing shrub belonging to the Fabaceae family. It is a short-lived tree with a high foliage percentage, and is characterized by its deep-root system with a single or multiple stems reaching a height of 6 m (Hang

* Corresponding author. e-mail: fakagr67@gmail.com

et al., 2011; Mani et al., 2011) and a diameter of 20 cm. It is a nitrogen-fixing species with a high nitrogen content (Dinendra and Azad-ud-doula, 2001; Gupta et al., 2011; Pandhare et al., 2011) that could be used as an effective source of protein to support the low-protein roughages for livestock feeds (Patra et al., 2006). The rapid *Sesbania* growth and its high nutritive value, make it a very promising nutritive source of cut-and-carry forages (Gupta et al., 2011; Manaye et al., 2009; Naik et al., 2011; Pandhare et al., 2011; Sabra et al., 2010).

S. sesban can be grown in a variety of soil characteristics and can tolerate salinity especially at a maturity stage. The production of *S. sesban* under low soil-moisture content possibly can be improved using soils with a high-nutrient content, such as those treated with fermented biosolids. The efficiency of such protocols can be assessed using biological and grain yields and harvest indices (Bolinder et al., 2007; Bondeau et al., 2007). These indices are considered ideal measurement to estimate the effect of certain treatments used to improve the crop progression rate and production, and to show variability in the harvested components of interest to compare the effects of different treatment application rates. Several plant parameters were used to evaluate the effect of biosolid application on *Sesbania* growth and the potential benefits that might be attained.

The objective of this research is to assess the effect of applying different levels of municipal biosolids on the biological yield and the WUE of the forage crop *S. sesban* at the stages of grain yield, and to measure other parameters of plant growth such as the harvest index (HI), and the average stem diameter (ASD).

2. Materials And Methods

The current study was executed at Deir-Alla agriculture station in Jordan Valley-the Northern Ghorat 32°11'36.3"N 35°37'16.7"E. Deir-Alla is considered a subtropical steppe of a low-latitude and a semi-arid hot climate. The annual average temperature is 23.6 °C with an average annual precipitation of 280 mm. According to the National Soil Map Project (NSM and LUP, 1993), the soil is fine and loamy.

The experiment was set up based on randomized complete block design (RCBD) with three replicates and six treatment levels. The biosolids were applied at different levels: 0, 2, 4, 6, 8, 10 ton/ha. This study did not cover the biosolid chemical or nutrient analysis, since several other studies have already reported the beneficial use of biosolid application on plant production due to the appropriate content of plant-required nutrients. Such studies reported that the digested and dewatered biosolids contain 3-6 % N, 1-4 % P, 0.2-1 % K and 50-60 % organic matter.

Sesbania seeds were planted for two seasons on the 5th of June, 2014 and 2015 and were harvested after ninety-nine days on the 14th of September, 2014 and 2015. The planting spaces were 40 cm within lines and 60 cm between lines. Seedlings were irrigated using an inline drip irrigation system with emitters (4 L/h), with a spacing of 0.4 m and 0.6 m between laterals. The amount of irrigation water was based on the potential evapotranspiration that was calculated based on Penman-Monteith equation, and crop coefficient was obtained from FAO 56 hand book. The meteorological

data were obtained from the meteorological climatic station in Deir-Alla. Supplemental irrigation was added after the rainfall to reach the crop evapotranspiration point based on 100 % ET. The total accumulated amounts of added water during the growing seasons were 613 and 650 mm for 2014 and 2015, respectively.

Water-Use Efficiency (ton/m³) was measured by dividing the biological or grain yield (ton/ha) over the total amount of water added (m³). The rate of dry matter increase was the best measure to evaluate plant performance and its success in any environment (Vasudevan et al., 2005). BY, GY, HI, and the average stem diameter (ASD) were measured in both growing seasons. For BY, leaves from the selected plants were taken and oven-dried at 68 °C for twenty-four hours for dry weight estimation. The total biomass or biological yield was calculated by adding the woody biomass weight and the dry leafy biomass weight. The GY was estimated by the recurrent harvest of random plants in different rows, while HI was used to quantify the yield of *Sesbania* species versus the total amount of biomass that has been produced. HI was measured using grain yield in weight base (ton/ha) of the harvested product divided by the total mass of the aboveground plant as a percentage. The stem diameters (SD) were measured as an average value of the stem diameters taken at the knee height (DKH) above the average ground level at 50 cm height, outside bark and at the breast height (DBH).

The data for the two years were merged and averaged (data were normally distributed) because the analysis output showed similar results between years. The collected data were analyzed using Statistical Analysis Software (SAS Institute, 2011). Treatments were considered statistically significant, when the model statement showed α value (< 0.05). LSD (Least Significance Difference) was used to separate means whenever the significant variability was detected.

3. Results and Discussion

The statistical analysis shows that there were significant differences in BY (Table 1), and WUE at the biological yield stage (WUE_{BY}), as represented in table 2, with the different biosolid application rates. The same was seen in WUE at the grain yield stage (WUE_{GY}, Table 2). There was an increase by about 39 % in BY (Tables 1 and 2), as well as WUE_{BY} (Tables 2). The analysis of variance shows no significant effects at different biosolid application rates on GY.

Table 1. *Sesbania* BY and GY significance distribution using different rates of biosolid.

Treatment	Mean for Biol.	Std Err Mean	Mean for Grain.	Std Err Mean
T1-0	38.42c	1.12	2.69c	0.85
T1-10	49.83a	1.22	3.9a	0.44
T1-2	39.06c	0.64	2.76c	0.52
T1-4	39.16c	0.97	2.83bc	0.49
T1-6	42.98bc	0.51	3.15b	0.55
T1-8	43.73b	1.01	3.73a	0.20

Values in a column followed by the same letter are not significantly different according to the Newman-keuls test at $p < 0.05$.

Table 2. Sesbania WUE Biol. and WUE grain signficancy

Treatment	Mean for WUE boil	Std Err Mean	Mean WUE grain.	Std Err Mean
T1-0	4.21c	0.12	0.29c	0.09
T1-10	5.46a	0.13	0.43a	0.05
T1-2	4.28c	0.07	0.30c	0.06
T1-4	4.29c	0.11	0.31c	0.05
T1-6	4.71b	0.06	0.35b	0.06
T1-8	4.7b	0.11	0.41a	0.02

Values in a column followed by the same letter are not significantly different according to the Newman-keuls test at $p < 0.05$.

The applied biosolids underwent what is called Vector attraction reduction (EPA, 2000), which is referred to as the processing of biosolids to make them less attractive to vectors or organisms, such as rodents and insects (EPA, 2002), which, at the end, reduced the potential for transmitting diseases. Microbial analysis indicated the absence of harmful pathogens, and the biosolids were found to be safe.

The results obtained underwent statistical analysis for signficancy of the data obtained, and were represented in tables and figures, as well as linear regression analysis. None documented analysis of Pearson correlations indicates that there was a high correlation between the biosolid application rate and BY (0.872), whereas BY increased as the biosolid rate increased. This was approved when measuring the R- square, in which less than 76.1 % of variability in the biosolid application rate can be accounted for the quantity of the biosolid applied. Also, the adjusted R- square (0.75) of variability and the difference between the R- square and the adjusted R- square becomes smaller as the sample size becomes larger, since the standard deviation was positive.

A biosolid application rate of (10 ton/ha) showed the highest biological yield value (Table 1). The biological yield tended to increase with the increase of the biosolid application rates, which was represented also in mean plots diagram. The line of fit in the fitting curve histogram (Figure 1) was suspended away from the horizontal by the points through confidence curve. This figure shows that the biological yield is statistically significant. Grain yield exhibits the same trend (Figure 2), in which it was statistically significant, while the intercept value (Figure 3) shows how much the grain yield can increase with the increase of the biosolid rate; it goes down as the biosolid application rate gets down.

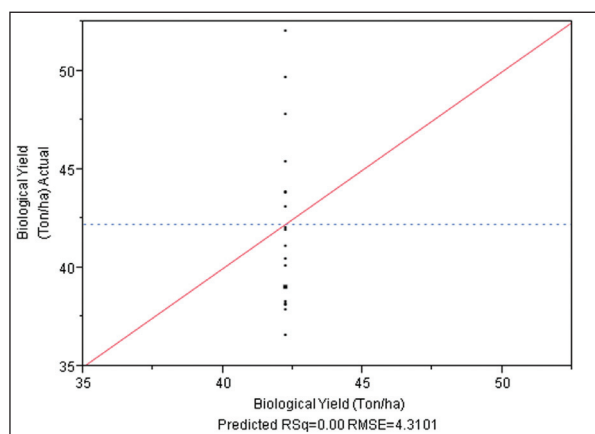


Figure 1. Actual predicted plot of the whole model response of biological yield (ton/ha) in Sesbania

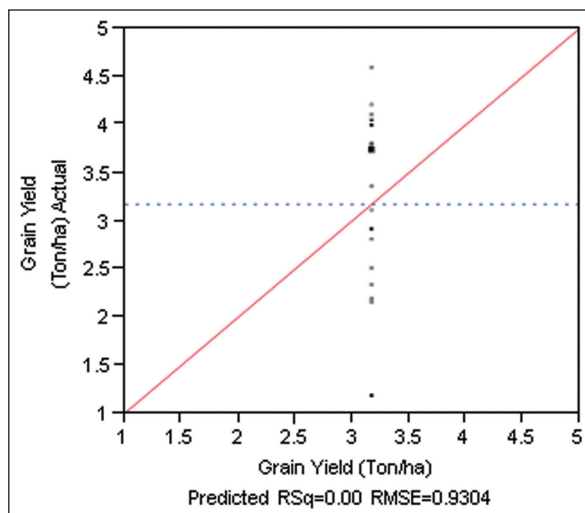


Figure 2. Actual predicted plot of the whole model response of Grain yield (ton/ha) in Sesbania

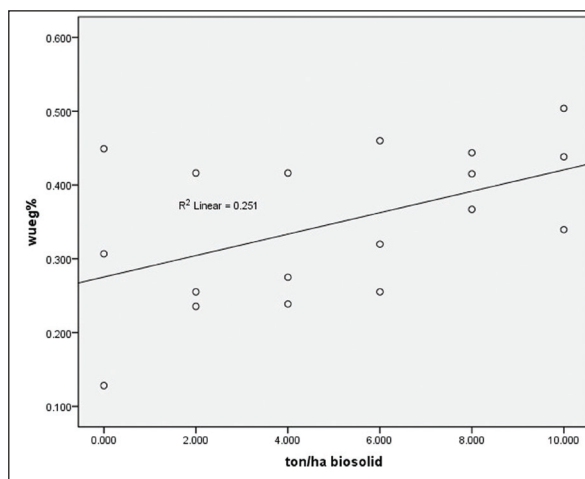


Figure 3. Scattered plot distribution of WUE at grain yield in Sesbania

The improvements obtained with the increase of biosolid application rate was consistent with the results of Garcia et al. (2000), where they reported an increase in the biomass production of some herbaceous plants in response to biosolid application. This is probably because the biosolid application improved plant growth rates and conditions, as a positive effect (Fernández-Luqueño et al., 2010; McLaughlin et al., 2007).

The responses of Sesbania to the addition of biosolids were also noticed through its effects on the WUE (Table 2). There were significant differences of the WUE for the biological yield of Sesbania under the different levels of biosolid applications (Table 2).

The same trend of improvement was obtained in the WUE for the biological yield level by the same amount of increment (23 %), at the rate of 10.0 ton/ha of biosolids when compared to the control treatment rate. Results obtained shows that there was a relationship between the amount of the biological yield obtained, and the improvement in WUE, in which a significance difference occurs clearly at 10.0 ton/ha of the biosolid application rate in comparison to the lower biosolid application rates (8.0 ton/ha). These results show an increase in both parameters of about 12 %, while measuring the change in these parameters when compared to the differences between the lower biosolid application

rates, at 8.0 ton/ha and 6.0 ton/ha, or much lower rates, the results show an increase in just about 2 % of them. These results support the findings of other researchers (Rostagno, 1998; Moffet, 1997; Harris-Pierce et al., 1995; Aguilar et al., 1994), who stated that using biosolids can increase soil water availability. At the same time, it can be said that the biosolid application rate may act as any other organic form of fertilizer, in which the N conversion to plant state—available inorganic forms increase, especially in the case of legumes, and to a certain limit much higher than non nodulated crops were steady – being not reached yet.

Although the statistical analysis shows no significant differences among the grain yield, and WUE at the grain stage (Table 2) with respect to the different biosolid application rates, the amount of increment produced in grain yield was (33 %) at 10.0 ton/ha, when compared to the control treatment rate. The responses of the harvest index and average stem diameter parameters to different biosolid application rates were not significant, and show the same trend, but in a lower percentage, in which the increase in their values was up to (10 %), when compared to the control.

Davis et al. (2014) reported similar results, where they noticed that the vegetative growth of Irish potato due to the inorganic fertilizers addition was higher than that for the tuber formation. The results of this research emphasize the current obtained results which show that the outcome of using biosolids to improve the biological yield and the water-use efficiency of *Sesbania* plant was achieved.

The (*S. Sesbania*) crop is expected to serve as a source for animal feeds especially in arid regions where water is in a very limited supply. It might be necessary, later on, to run further studies to study the presence of biosolid residues in the soil after harvesting crops at higher levels of application rates (>10 ton/ha). Although Garrido et al. (2005) did not find a significant increase in organic matter and the total nitrogen in the soil, which is possibly due to the use of low biosolid rate (4.5 ton/ ha), as well as the short-term nature of biosolids application, and the relatively low concentrations of trace elements in the biosolids.

It can be concluded that the effect of biosolid application on the plant biological yield and WUE is detectable with a possible minimal effect on the grain yield and grain related indices. This conclusion encourages farmers to look after such crops for the sake of their herds, and their production sustainability, especially under arid and semi-arid conditions.

4. Acknowledgment

This work has been funded by the National Center for Agricultural Research and Extension in Jordan.

References

Aggarwal, P.K. (2000). Application of system simulation for understanding and increasing yield potential of wheat and rice. Published Ph.D. Thesis, Wageningen, The Netherlands. <http://edepot.wur.nl/197264>.

Aguilar, R., Loftin, S.R., Ward, T.J., Stevens, K.A., and Gosz, J.R. (1994). Sewage sludge application in semiarid grasslands: Effects on vegetation and water quality. Technical completion report 285. New Mexico Water Resources Research Institute-USDA Forest Service-Univ. of New Mexico-New Mexico State Univ. Las Cruces, N.M 75 pp.

Albaladejo, J., Lobez, J., Boix-Fayos, C., Barbera, G.G., and Martinez-Mena, M. (2008). Long-term effect of a single application of organic refuse on carbon sequestration and soil physical properties. *J. Environ. Qual.*, 37: 2093-2099.

Bolinder, M.A., Janzen, H.H., Gregorich, E.G., Angers, D.A., and Vanden Bygaart, A.J. (2007). An approach for estimating net primary productivity and annual carbon inputs to soil for common agricultural crops in Canada. *Agric. Ecosyst. Environ.* 118: 29–42.

Bondeau, A., Smith, P.C., Zaehle, S., Schaphoff, S., Lucht, W., Cramer, W., Gerten, D., Lotze-Campen, H., Muller, C., Reichstein, M., and Smith, B. (2007). Modelling the role of agriculture for the 20th century global terrestrial carbon balance. *Glob. Change Biol.* 13: 679–706.

Davis, JD; Davidson, RD; Essah, SYC (2014). Fertilizing Potatoes. Colorado State University Extension. Fort Collins, Co80523; (970) 491-2061. USA.

Dinendra, N.S, Azad-ud-doula Prodhan, A.K.M. (2001). Anatomy of *Sesbaniasesban*. *Bangladesh Agri. Uni. Mymensingh, Bangladesh* 35(4): 211-218.

EPA, (2000). United States Environmental Protection Agency. Biosolids Technology Fact Sheet Land Application of Biosolids. EPA 832-F-00-064.

EPA, (2002). US Environmental Protection Agency. Pathogen and Vector Attraction Reduction Requirements. EPA Guide to the Part 503 Rule.

Fernández-Luqueño, F., Reyes-Varela, V., Martínez-Suárez, C., Salomón-Hernández, G., Yáñez-Meneses, J., Ceballos-Ramírez, J.M., and Dendooven, L. (2010). Effect of different nitrogen sources on plant characteristics and yield of common bean (*Phaseolus vulgaris* L). *Bioresource Technology* 101: 396–403.

Garcia, S., Cuevas, G., Martinez, F., and Walter, I. (2000). Effect on vegetation cover of the application of organic urban waste residues on a degraded soil near Madrid. *Ecol. Madrid* 14: 79-87.

Garrido, S., Del Campo, G.M., Esteller, M.V., Vaca, R., and Lugo, J. (2005). Heavy metals in soil treated with sewage sludge composting, their effect on yield and uptake of broad bean seeds (*Vicia faba* L.). *Water, Air, and Soil Pollution*, 166: 303–319.

Gupta, A.M., Su, S.W., and Chen, Z.S. (2011). Heavy-metal bioavailability and chelate mobilization efficiency in an assisted phytoextraction process by *Sesbaniasesban* (L.) Merr., *Common. Soil Sci. Plant Anal.* 42(2): 231-245.

Harris-Pierce, R.L., Redente, E.F., and Barbarick, K.A. (1995). Sewage-sludge application effects on runoff water quality in a semiarid rangeland. *J. Environ. Qual.* 24: 112–115.

JOB. Jordanian Official Bulletin. Jordanian Regulations for Biosolids Reuse and Disposal. (2006). No. (1145/2006).

Manaye, T., Tolera, A., and Zewdu, T. (2009). Feed intake, digestibility and body weight gain of sheep fed Napier grass mixed with different levels of *Sesbaniasesban*. *Livestock Sci.* 122: 24-29.

Mani, R.P., Pandey, A., Goswami, S., Tripathi, P., Kumudhavalli, V., and Singh, A.P. (2011). Phytochemical screening and in-vitro evaluation of antioxidant activity and antimicrobial activity of the leaves of *Sesbaniasesban* (L) Merr. *Free Radic. Antioxidants*, 3(1): 66-69.

McLaughlin, M.J., Warne, M.St.J., Whatmuff, M.S., Heemsbergen, D., Broos, K., Barry, G., Bell, M.J., Nash, D., Pritchard, D., and Penney, N. (2007). Australia's National Biosolid Research Program -how it came about, and what has it discovered? *Water Pract. Technol.* 2(4): 1–9.

Mendoza-Grimón, V., Hernández-Moreno, J.M, and Palacios-Díaz, M.P. (2015). Improving water use in fodder production. *Water* 2015, 7(6), 2612-2621; doi: 10.3390/w7062612.

Moffet, C.A. (1997). Quantity and quality of runoff from two biosolids-amended Chihuahuan Desert grassland soils. M.S. Thesis, Texas Tech Univ., Lubbock, Tex.

Molden, D., Oweis, T., Steduto, P., Bidraban, P., Hanjra, M.A., and Kijne, J. (2010). Improving agricultural water productivity: Between optimism and caution. *Agricultural Water Management* 97: 528-535.

- Molden, D.J., and Oweis, T. (2007). Pathways for increasing agricultural water productivity. In: Molden, D. (ed.). *Water for food, water for life. Comprehensive assessment of water management in agriculture*. Earthscan, London and International Water Management Institute, Colombo.
- Naik, N.N., Tare, H.L., Sherikar, A.K., Deore, S.R., and Dama, G.Y. (2011). Central nervous system stimulant effect of extracts obtained from the barks of *Sesbania sesban*. *Int. J. Inst. Pharm. Life Sci.* 1(1): 77-92.
- NSM and LUP (1993). Hashemite Kingdom of Jordan, ministry of agriculture, hunting technical services ltd., soil survey and land research centre. *National Soil Map and Land Use Project. The soils of Jordan. Level 1, Reconnaissance Soil Survey, Volume 2, Main Report*. Amman.
- Pandhare, R.B., Sangameswaran, B., Mohite, P.B., and Khanage, S.G. (2011). Antidiabetic activity of aqueous leaves extract of *Sesbania sesban* (L.) Merr. in streptozotocin induced diabetic rats. *Avicenna J. Med. Biotech.* 3(1): 37-43.
- Patra, A.K., Chhonkar, P.K., and Khan, M.A. (2006). Effect of green manure *Sesbania sesban* and nitrification inhibitor encapsulated calcium carbide (ECC) on soil mineral-N, enzyme activity and nitrifying organisms in a rice-wheat cropping system. *Eur. J. Soil Biol.* 42: 173- 180.
- Rostagno, C.M. (1998). Biosolids application on southwest Texas rangelands: its influence on the soil and sediment properties and on runoff water quality. Ph. D. Diss., Texas Tech Univ., Lubbock, Tex.
- S.A.S. Institute. 2011. SAS for Windows. Version: 9.3. SAS Institute, Cary, NC.
- Sabra, H.A., Hassan, S.G., and Mohamed, M.I. (2010). Effect of *Sesbania sesban* (*Sesbaniaegyptiaca*) supplementation on the reproductive performances of baladi sheep as compared to berseem (Egyptian clover). *J. Reprod. Infertil.* 1(3): 66-70.
- Thu Hang BP, Lam V, Bich Phuong TT, Preston TR (2011). Water hyacinth (*Eichhornia crassipes*): an invasive weed or a potential feed for goats? *Livestock Res. Rural Dev.* 23 (7), Article #152.
- United Nations. (2015). Sustainable Development Goals. <http://www.un.org/sustainabledevelopment/hunger/> accessed 13/09/17.
- Unkovich, M., Baldock, J., and Forbes, M. (2010). Chapter book. Variability in harvest index of grain crops and potential significance for carbon accounting: Examples from Australian Agriculture. *Advances in Agronomy*, Volume 105. ISSN 0065-2113.
- Usman, K., Khan, S., Ghulam, S., Khan, M.U., Khan, N., Khan, M.A., and Khalil, S.K. (2012). Sewage sludge: An important biological resource for sustainable agriculture and its environmental implications. *American Journal of Plant Sciences*, 3: 1708-1721.
- Vasudevan, P., Sharma, S., and Kumar, A. (2005). Liquid fuel from biomass: an overview. *Journal of Scientific and Industrial Research*, 64: 822–31.
- Wang, B., Liu, W., and Dang, T. (2011). Effect of phosphorus on crop water and nitrogen use efficiency under different precipitation year in dryland. *Proceedings of International Symposium on Water Resources and Environmental Protection, ISWREP-2011, Xi'an, China.*

The Detection of Toxic Boron in Groundwater and Sludge in Bethlehem Area

Reem Y. Zeitoun¹

¹Chemistry Department, Faculty of Science, Bethlehem University, Bethlehem, Palestine.

Received 23 March, 2018; Accepted 4 November, 2018

Abstract

Bethlehem is located in the Eastern Basin of the Mountain Aquifer. This part of the Aquifer is hydrologically important as one of the main sources of water supply in the southern part of the West Bank. This analytical study is carried out to determine the permissible amounts of boron in water samples from the Bethlehem area during the wet and dry seasons of 2014-2015. Boron (B) is a dark brown/black element which occurs naturally in fresh and saline waters. It can also result from pollution occurring from sewage or industrial discharges. The excessive use of boron in the industrial production of detergents and glass products increase boron concentration in wastewater. Boron is an essential nutrient for plants at low concentrations, but it is toxic to plants above 0.5 – 2.0mg/L. The Curcumin method is used for the detection of boron in drinking water by spectrophotometer at wavelength of 540 nm. The results show that the average concentration of boron in wells was the same (0.00333 mg/L) during the summer and winter seasons. The average concentration of boron in springs during the winter season was 0.00422 mg/L and it was 0.00556 mg/L during the dry season. The detection of boron in the sludge samples of Wadi Nar was conducted by the spectrophotometric method of Azomethine – H at a wavelength for 420 nm. The average concentration of boron in the sludge samples during the dry season was 1.523 mg/L and 1.135 mg/L for the wet season. Finally, the results of the analysis of the samples taken from wells and springs show that boron concentration was within the acceptable limits according to WHO standards of 2011.

© 2018 Jordan Journal of Earth and Environmental Sciences. All rights reserved

Keywords: Bethlehem, boron, springs, wells, wastewater, sludge.

1. Introduction

Boron (B) is a natural dark brown/black element; it is widely found in sedimentary rocks and sediments especially in clay marine sediments. (Khayat et al., 2006). A high boron concentration of 4.5 mg B/L in seawater ensures that marine clays or sediments are rich in boron rather than other elements. Boron, as a natural element, is slowly released into the environment by natural weathering processes. Boron's mobility depends on soil acidity and rainfall because of its affinity to leach. (Keren and Mezuman, 1981). As a result, boron toxicity is more problematic in arid climates rather than temperate climates. Boron is widely used in detergent manufacturing as a major component because it is an excellent bleaching and cheap agent. As a result, it increases boron contents in sewage. However, wastewater with high boron concentration is not easily removed during standard sewage treatment processes. (Moss and Nagpal, 2003).

Boron is used in the industry as boric acid and sodium salts of boron primarily borax, or disodium tetraboratedecahydrate in a variety of products. It is widely used in the manufacture of glass and housing materials such as fiber-glass insulation and porcelain varnish, ceramic glazes and metal alloys. It is a major ingredient in many cleaning products, and is typically used in cleansers, cosmetics, detergents and laundry additives. It is also used in the manufacture of agrochemicals, insecticides and fertilizers in which boron is an essential element for plant growth. Boron compounds are also used as fertilizers and pesticides especially in areas with low

boron constituents and high precipitation; boron fertilizers are added to increase the B content of soil fluids. Boric acid, borates, and perborates have been used in mild antiseptics and in the pharmaceutical industry. The U.S. Environmental Protection Agency (EPA) also identifies boron neutron capture therapy in cancer treatment (EPA, 2008).

The EPA classifies boron as a Group D element, meaning that there is inadequate or no evidence that boron is carcinogenic for humans or animals. Boric acid or sodium tetraborate in the diet causes growth retardation in mammals but low dietary levels protect against fluorosis and bone demineralization and may indirectly influence calcium, phosphorus, magnesium and cholecalciferol (Vitamin D3) metabolism. Long-term exposure may produce negative reproductive impacts on human health (WHO, 1998). The EPA limitations showed variation in the permissible concentration among adults and infants.

The EPA does not regulate boron in water, but it does monitor it in foods, and the Occupational Safety and Health Administration (OSHA) sets standards for workplace exposure especially in the industrial branch. The WHO (1998) suggests that the concentrations of boron for human consumption should not exceed 0.3 mg/l. as a guideline value.

The Bethlehem area has an arid to semi-arid climate with an increasing aridity towards the eastern slopes of the Jerusalem desert. The eastern basin of the Mountain Aquifer, in which the Bethlehem area is located, is the

* Corresponding author. e-mail: rzeitoun@bethlehem.edu

principal source of water in the southern part of the West Bank. The mismanagement of wastewater, especially over the highly permeable areas of limestone overlying the West Bank aquifer, endangers the quality of the groundwater. The hydrology of Bethlehem area is affected by the presence of fissures, fractures, joints and karstification in addition to the rock porosity and permeability. (Rofe and Raffety, 1963).

The sewage network serves 40.4 % of the total population in the Bethlehem Governorate which had 210484 inhabitants in 2014 while cesspits and open channels serve wastewater collection for the remainder. (PCBS, 2009a; PCBS, 2017; PWA, 2009). Direct disposal of wastewater into the environment can pollute the soil, surface water and groundwater. Increased modernization and the use of chemicals add more dangerous materials to the wastewater and increase the potential for environmental damage. As the population increases, the wastewater will also increase with more hazardous materials harming the environment (PCBS, 2009b). The lack of a sewage treatment plant in the Bethlehem area will increase the negative influence and create real problems for public health. Groundwater will be polluted as a result of seepage. Although wastewater in Bethlehem is collected through the municipality sewage networks, it is discharged as raw sewage into the Wadi Nar where it flows unprotected through the neighboring agricultural lands. In addition to this improper disposal of wastewater, there are also solid waste products such as glass, electrical conductors, and other commercial products which are rich in boron. The frequent disposal of sewage water from the Israeli settlements into Palestinian areas has a serious impact on human health by polluting the environment especially groundwater. A checkup survey is conducted to determine whether the concentrations of boron in waste water and in the local aquifer are within the permissible WHO guidelines.

2. Study Area

The study area is the Bethlehem governorate which lies in the Eastern Basin of the Mountain Aquifer. Bethlehem governorate is between 158 and 198 East and between 98 and 128 North on the Palestinian Grid. According to (ARIJ, 2010b) the governorate has a total area of approximately 659.1 km². Conferring to Palestinian Meteorological Department, the average annual rainfall for the Bethlehem governorate is 518.4 mm/yr. The average annual rainfall for Bethlehem during 1900 to 2006 from Cremisan Monastery of coordinates 166.4 East to 126 North and at an elevation of 820 m is 574.7 mm/yr. More than 80 % of the rainfall is received during the winter season that is from December to May (Zeitoun, 2011). Bethlehem contributes to the arid and semi-arid climate with an increase in aridity towards the Eastern Slopes in the Jerusalem desert (Rofe and Raffety, 1963).

2.1. Soil Type

In the Bethlehem area Cenomanian, Turonian and Senonian stages of the Upper Cretaceous Period are represented by limestones, dolomites, marls and, at the top of the sequence, chalk with chert layers and bands of nodular chert.

Bare rocks cover some of the area and the soil types include Lithosols, Brown Lithosols and Loessial Arid Brown

soils, Brown Rendzinas and Pale Rendzinas, Terra Rossas, Brown Rendzinas and Pale Rendzinas and Brown Lithosols and Loessial Serozems. The major soil types in the study area are Brown Lithosols and Loessial Arid Brown soils and Brown Rendzinas and Pale Rendzinas (Rofe and Raffety, 1963). The major soil types are shown in Figure (1).

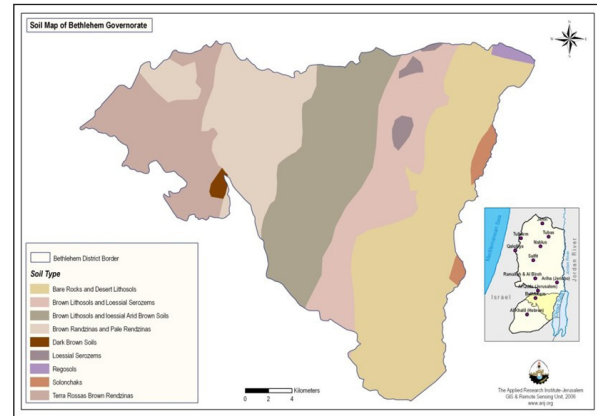


Figure 1. Soil map of Bethlehem governorate. (ARIJ, 1997)

2.2. Land-use

The total area of the Bethlehem Governorate is 659.1 km². The land-use map shows that most of the agricultural areas, forests, permanent crops, seasonal crops and plastic houses are located to the west of the Bethlehem region. Agricultural irrigation is provided by local village springs.

Agricultural land makes up 621.748 km², which is 94.3 % of the 659.1 km² of the Bethlehem Governorate. The Palestinian built-up areas cover 9.715 km² with a percent of 1.47 % of the total area of the Bethlehem Governorate (ARIJ, 2010b). The main activities are shown in the land-use map of Figure (2).

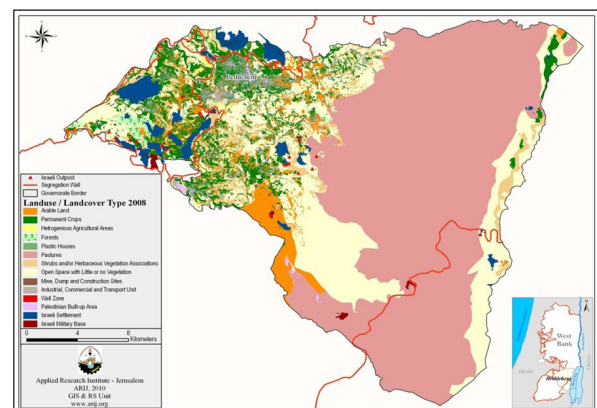


Figure 2. Land-use map of Bethlehem Governorate. (ARIJ, 2010b)

2.3. Water Resources

Discharge from springs and bore-hole well extraction from the eastern basin of the Mountain Aquifer provide the water supply for the Bethlehem Governorate. Of the three wells in this study Beit Fajjar is owned by the Water Supply and Sewerage Authority (WSSA), while "PWA 3" and "PWA 11" are owned by the Palestinian Water Authority (PWA) (PWA, 2015). Other wells in the area are owned by the occupational controller Mekorot.

The majority of the springs are located in the western part of Bethlehem region as shown in Figure (3).

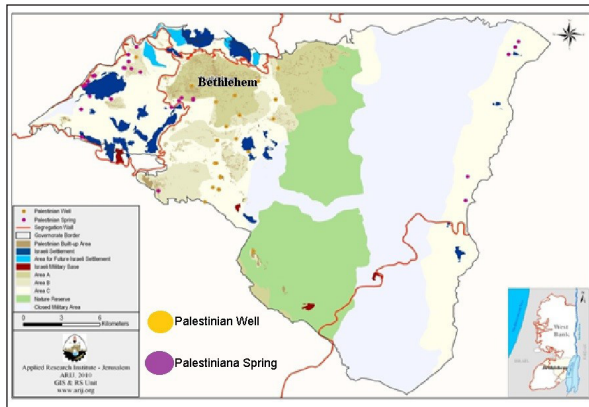


Figure 3. Water Resources map of Bethlehem Governorate modified after (ARIJ, 2010a).

Most of the villagers depend on local springs for irrigating their crops. As the network does not provide a regular supply, householders also have to make use of spring water for domestic requirements.

Although the main cities and refugee camps are connected to the sewage networks, there is no sewage treatment plant in the Bethlehem Governorate at all. Final discharge goes, without any primitive treatment, into open areas, agricultural land and into wadis such as the Wadi Nar. The sewage network serves about 40.4 % of the population the Bethlehem Governorate, while the remainder makes use of cesspits and open channels for wastewater collection (PWA, 2015).

3. Methodology

Implementation of the analysis for B concentration was completed for the wet and dry seasons of 2014-2015. The samples were collected at the end of May 2014 for the dry season and in January 2015 for the wet season. The survey was done for the available local wells and springs along the Bethlehem area as well as waste water and sludge from Wadi Nar in the wet and the dry seasons. Some more duplicate samples are also tested for the analysis and showed similar results.

In addition samples of waste water and sludge were collected from the Wadi Nar for both wet and dry seasons. The total number of samples for both seasons was about thirty samples for the study. In some cases, duplicate samples

were collected for analysis and showed similar results.

3.1 Sludge Samples

The sludge samples were taken for a depth of 30cm from three different locations along 100 meter apart from the Wadi Nar stream. The standard chemical analysis for water was followed. Boron in soil is found in the crystalline structures of soil minerals. The detection of boron in soil is by the spectrophotometric method by Azomethine – H as a complex agent with the boric acid H_3BO_3 in aqueous media at a wavelength for 420 nm. Over a concentration range of 0.5 to 10 mg of B, Azomethine –H with H_3BO_3 forms a stable complex (APHA et al., 2005). A calibration curve is prepared with a linearity of 98.6 % for standards of boron in ppm as: 0.0ppm, 0.25ppm, 0.5ppm, 1.0ppm, 2.0ppm, 4.0ppm. The absorbance was: 0.00, 0.026, 0.67, 0.145, 0.298 and 0.648, respectively.

3.2 Water Samples

The concentration of boron in drinking water is no more than 1mg B/L and generally contains less than 0.1 mg B/L, and in seawater it is approximately 5mg/L. The standard chemical analysis for water was implemented. The Curcumin method is used for the detection of B in drinking water. The sample is acidified and evaporated in the presence of curcumin which is red in color, and rosocyanine is formed. The rosocyanine is compared with a standard curve by the spectrophotometric method at a wavelength of 540 nm (APHA et al., 2005). A calibration curve is prepared with a linearity of 99.6 % for standards of Boron in ppm as: 0.0ppm, 0.01ppm, 0.02ppm, 0.03ppm, 0.04ppm and absorbance was : 0.00, 0.046, 0.171, 0.237 and 0.330, respectively.

4. Results and Discussion

The experimental check on boron in the wet and dry seasons of the period 2014-2015 is successfully accomplished. The results show that almost all the samples are within the permissible limits although with a variety in concentration among soil and sewage samples. The results show that the average concentration of boron in wells for both the summer and winter seasons is the same at 0.00333 mg/L. The maximum concentration in both seasons was the same at 0.005 mg/L as shown in Table (1) and Figure (4).

Table 1. Boron concentration for well samples in the wet and dry season in 2014-2015. The wells coordinates are according to (Scarpa, 2006).

Boron in Wells – Bethlehem					
Name	Location	Coordinates	Date	B mg/L	WHO 2011
PWA 11	Teqou	169.30/116.35	22/1/2015	0.003	1.5 mg/L
PWA 3	Teqou	171.25/120.25	22/1/2015	0.005	
Beit Fajjar	Teqou	169.60/115.10	22/1/2015	0.002	
Average: 0.003333 mg/L					
Minimum: 0.002 mg/L					
Maximum: 0.005 mg/L					
PWA 11	Teqou	169.30/116.35	20/5/2014	0.003	
PWA 3	Teqou	171.25/120.25	20/5/2014	0.005	
Beit Fajjar	Teqou	169.60/115.10	20/5/2014	0.002	
Average: 0.003333 mg/L					
Minimum: 0.002 mg/L					
Maximum: 0.005 mg/L					

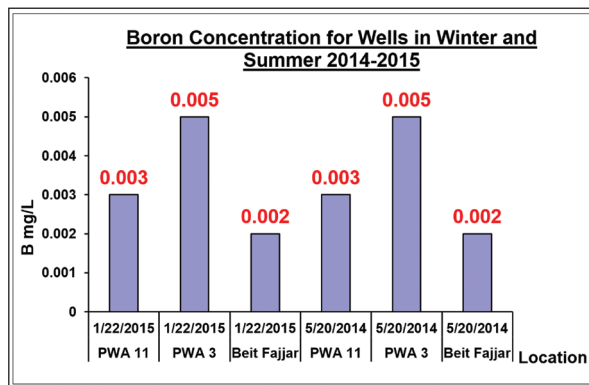


Figure 4. Boron concentration for well samples in the wet and dry season of 2014-2015.

The production wells are in the Herodian – Beit Fajjar field. The yield of the tested wells are within 230 – 250 m³/hr and the pumpage rate is 1.72 – 1.8 MCM. Based on the World Health Organization recommendations, each person should receive a minimum quantity of 100 liters of fresh water per day. However, Bethlehem receives an average supply of no more than 58 liters per capita per day (PWA, 2015), whereas the daily distribution per capita from consumed water for

domestic purposes is 79.1 liters/capita/day (l/c/d) in the West Bank in 2014. As an alternative, the villagers depend on the local springs for their daily domestic use in case of shortage of municipal water supply (Scarpa, 2004).

The average concentration of Boron in springs for the winter season is 0.00422 mg/L with a maximum of 0.01 mg/L and a minimum of 0.002 mg/L. The maximum concentration of 0.01 mg/L is for the sample from Wadi Nar, which is a surface running sewage stream. This is due to high boron contents in detergents, soaps and laundry additives. Sodium perborate (NaBO₃·H₂O) is widely used as a bleaching agent in domestic and industrial cleaning products. Boron, like other inorganic ions, is not removed during waste water treatment. It accumulates in domestic water and consequently in natural aquatic systems (Frenkel et al., 2010). The data shows that boron concentration is still within the acceptable limits which are below 1.5 mg/L according to (WHO, 1998; WHO, 2004; WHO, 2011). The average boron concentration in springs for the dry season is 0.00556 mg/L with a maximum of 0.01 mg/L and a minimum of 0.001 mg/L. The results of the analysis of the spring samples are illustrated in Table (2) and in Figure (5).

Table 2. Boron concentration for spring samples in the wet and dry seasons of 2014-2015. Springs Coordinates are from (Abed Rabbo et al., 1999).

Boron in Springs – Bethlehem					
Name	Location	Date	B mg/L	Code	Coordinates
Beir Ona	Beit Jala	22/01/2015	0.002		167.5/125.7
EinBalad	Ertas	22/01/2015	0.002	CB30	167.5/121.8
Wadi Nar	Wadi Nar	22/01/2015	0.01		
EinJame'-Battir	Battir	22/01/2015	0.004	BB21	162.8/125.6
EinBalad-Battir	Battir	22/01/2015	0.003	BB20	163.3/126.3
EinBalad-Nahalin	Nahalin	22/01/2015	0.005	BB28	161.1/121.6
EinBalad-WadiFukin	WadiFukin	22/01/2015	0.006	BB30	159.3/124.6
Namous-Hussan	Hussan	22/01/2015	0.002	BB27	161.2/123.1
EinBalad-Hussan	Hussan	22/01/2015	0.004		161.9/123.9
Average: 0.00422 mg/L					
Minimum: 0.002 mg/L					
Maximum: 0.01 mg/L					
Beir Ona	Beit Jala	20/05/2014	0.001		167.5/125.7
EinBalad	Ertas	20/05/2014	0.005	CB30	167.5/121.8
Wadi Nar	Wadi Nar	20/05/2014	0.01		
EinJame'-Battir	Battir	20/05/2014	0.003	BB21	162.8/125.6
EinBalad-Battir	Battir	20/05/2014	0.006	BB20	163.3/126.3
EinBalad-Nahalin	Nahalin	20/05/2014	0.006	BB28	161.1/121.6
EinBalad-WadiFukin	WadiFukin	20/05/2014	0.005	BB30	159.3/124.6
Namous-Hussan	Hussan	20/05/2014	0.008	BB27	161.2/123.1
EinBalad-Hussan	Hussan	20/05/2014	0.006		161.9/123.9
Average: 0.00556 mg/L					
Minimum: 0.001 mg/L					
Maximum: 0.01 mg/L					

Almost all the samples taken from the springs and wells showed similarity in concentrations which were below the acceptable limit of 1.5 ppm recommended by WHO in 2011

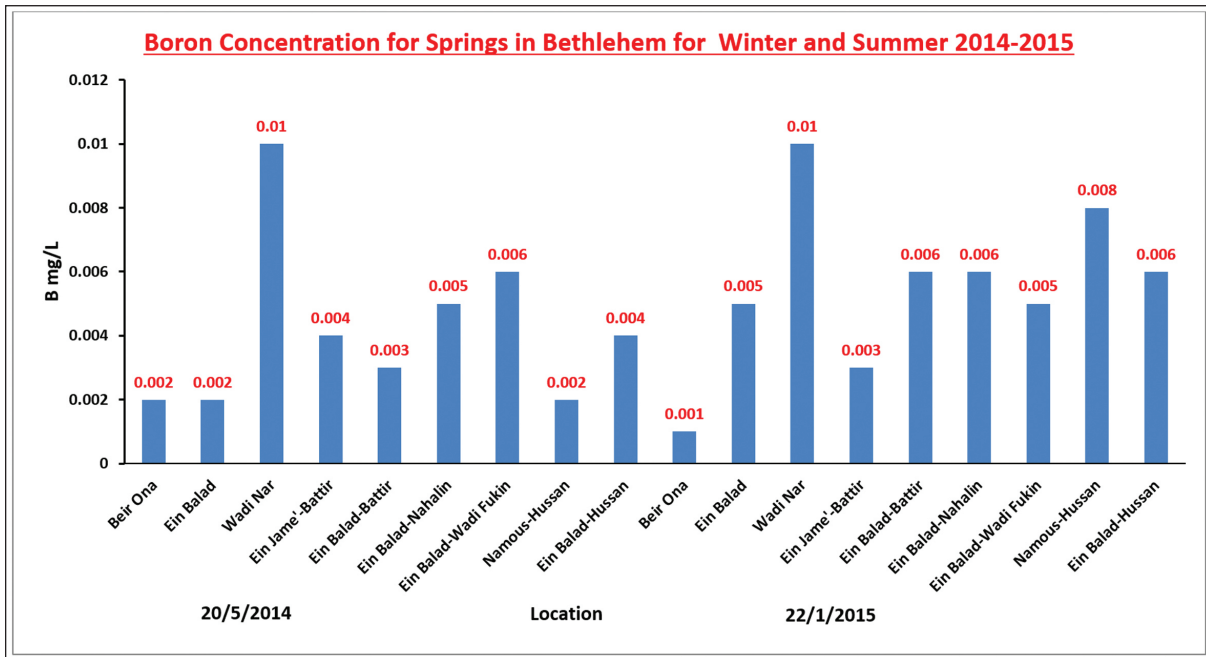


Figure 5. Boron concentration for spring samples in the wet and dry seasons of 2014-2015

The sludge samples taken from Wadi Nar showed acceptable values. The sludge samples were taken per season from three different locations for a depth of 30 cm with 100 m apart. The standard chemical analysis for water was followed. The results of the analysis of the sludge samples are illustrated in Table (3) and in Figure (6).

Table 3. Boron concentration for sludge samples in the wet and dry seasons of 2014-2015.

Boron in Sludge- Bethlehem				
Name	Location	Soil	Date	B mg/L
sludge 1	Wadi Nar	Soil	22/1/2015	1.145
sludge 2	Wadi Nar	Soil	22/1/2015	1.11
sludge 3	Wadi Nar	Soil	22/1/2015	1.15
Average: 1.135 mg/L				
Minimum: 1.11 mg/L				
Maximum: 1.15 mg/L				
sludge 1	Wadi Nar	Soil	20/5/2014	1.537
sludge 2	Wadi Nar	Soil	20/5/2014	1.51
sludge 3	Wadi Nar	Soil	20/5/2014	1.522
Average: 1.523 mg/L				
Minimum: 1.51 mg/L				
Maximum: 1.537 mg/L				

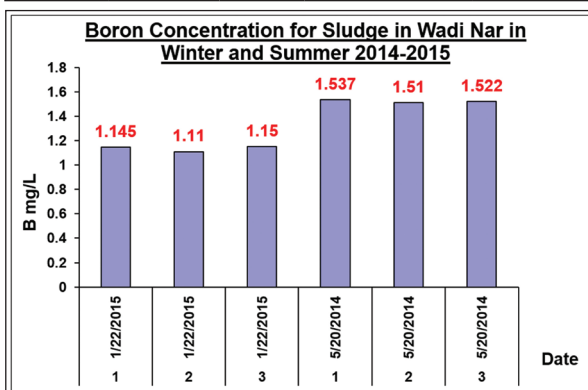


Figure 6. Boron concentration for sludge samples in the wet and dry seasons in 2014-2015.

Although a survey over one year provides interesting data, further study over two or three successive years would provide more precise indicators.

The average concentration of boron in the sludge samples for the dry season was 1.523 mg/L, whereas for the wet season the average was 1.135mg/L. These concentrations are high when compared with concentrations in fresh water. The high level of boron in Wadi Nar in the dry season is higher than that in the wet season due to direct evaporation. The high level of boron in the Wadi Nar is due to the excessive presence of detergents and cleaning products rich in boron contents such as borax. Moreover, many sewage tanks discharge sewage directly into the stream and some sewage tanks are filled with calcium sludge from neighboring stone cutting plants which may have boron traces (WSI, 2005). However, the increased concentration of boron in the sludge samples can be attributed to the accumulative sedimentation of boron over time. Although it shows higher concentrations than in the samples from wells and spring, it is still within the permissible limits for surface running water. However, the concentration of boron in sludge samples may increase over time due to the excessive use of borax in detergents and bleaching. Boron concentration may also rise over time in wells and springs due to the locations of springs near intensive neighborhood activities which depend mostly on cesspits for their sewage water. The common use of cesspits in some neighborhoods may be the cause for the higher concentrations of boron in local spring discharge.

Bethlehem has six major soil types which are mainly rich in calcium, sodium, potassium, clay, marl, limestone, chalk and conglomerates. These soil types enhance the presence of boron as a natural constituent particularly in clay-rich marine sediments (Vengosh et al., 2005). According to laboratory analysis conducted by the Water and Soil Environmental Research Unit (WSERU) at Bethlehem University for the period 2013-2014, the average concentration of calcium as Ca mg/L in the Bethlehem wells is 72.6 mg/L and 77.4 mg/L

in the Bethlehem springs (WSERU, 2014).

Finally, the results of Boron concentration in wells and springs in Bethlehem Governorate show that boron concentrations are below 1.5 mg/L and are within the acceptable limits of the WHO guidelines of 2011. The sludge samples also indicate acceptable concentrations in comparison to the quality of the sewage samples.

5. Conclusions

Boron is a naturally occurring element that is found mainly in sedimentary rocks rich in clay marine sediments. Some industrial commercial products release boron into the environment. This includes the use of borate compounds such as borax, boric acid, and other refined products in the manufacture of glass, fiberglass, washing products, alloys and metals, fertilizers, wood treatments and insecticides. Boron is an essential micronutrient for plant growth at low levels depending on the plant species.

The survey examined samples from available wells and springs in the Bethlehem area and from waste water and sludge from the Wadi Nar in the wet and dry seasons of 2014-2015.

The total number of samples for both seasons was around thirty samples for the study. The sludge samples were taken from a depth of 30cm. The chemical analysis was performed by the standard method of water analysis. The Curcumin method was used for the detection of boron in drinking water. The samples were acidified and evaporated in the presence of red curcumin forming rosocyanine. The rosocyanine is compared with the standard curve by the spectrophotometric method at a wavelength of 540 nm. Boron in soil is found in the crystalline structures of soil minerals. The detection of boron in soil is by the spectrophotometric method of Azomethine – H as a complex agent with the boric acid H_3BO_3 in aqueous media at a wavelength for 420 nm. Finally, the results of the analysis show that the concentration of boron in the water and sludge samples are within the permissible limits of WHO guidelines.

Recommendations

Implementing the survey of boron presence in other parts of the West Bank is highly recommended in order to have additional scientific information on the presence of boron in the West Bank for future generations. Further studies on other parameters such as nitrates, phosphates, salinity and with major cations and anions in water resources will be very useful to check for its correlations with the presence of boron. In addition, an elaborate study on the presence of boron in agricultural field crops irrigated or sprayed with water or fertilizers that might be rich in boron is also highly recommended.

Acknowledgement

The researcher would like to extend sincere thanks to Bethlehem University for providing financial support for this Internal Research Grant. The researcher is also grateful to Dr. Alfred Abed Rabbo, the director of the Water and Soil Environmental Research Unit (WSERU) at Bethlehem University, for his support and the provision of laboratory facilities. Special thanks are extended to Mr. Joseph Danho and Mr. Mohamad Harbouk from WSERU for their help in the field sampling and their support during this study.

Special thanks also go to the Water Supply and Sewerage Authority (WSSA), for their help in collecting water samples from the wells.

References

- Abed Rabbo, A., Scarpa, D.J., Qannam, Z., Abdul Jaber, Q., and Younger, P. (1999). Springs in the West Bank - Water Quality and Chemistry, Bethlehem University, Palestinian Hydrology Group and Newcastle University.
- APHA, AWWA, WEF, (2005). Standard Methods for the Examination of Water and Wastewater, 21st ED, Washington, DC, USA, 2005. (Greenberg, A., Clesceri, L., Eaton, A).
- ARIJ - Applied Research Institute-Jerusalem, (1997). The status of the Environment in the West Bank, Jerusalem.
- ARIJ - Applied Research Institute-Jerusalem, (2007). Soil map in Bethlehem governorate.
- ARIJ - Applied Research Institute-Jerusalem, (2010a). Wells and Springs location map in Bethlehem governorate.
- ARIJ - Applied Research Institute-Jerusalem, (2010b). Bethlehem City Profile, Jerusalem.
- EPA, U.S. Environmental Protection Agency, (2008). Health Effects Support Document for Boron, Washington, DC 20460 [Online] http://www.epa.gov/safewater/ccl/pdfs/reg_determine2/healtheffects_ccl2-reg2_boron.pdf [Accessed: 12/1/2014]
- Frenkel, O., Yermiyahu, U., Forbes, G., Fry, W. and Shtienberg, D. (2010). Restriction of potato and tomato late blight development by sub-phytotoxic concentrations of boron. [Online] Plant Pathology 59: 626–633. <http://www.onlinelibrary.wiley.com/doi/10.1111/j.1365-059.2010.02301.x/pdf> [Accessed: 13/2/2014]
- Keren, R., and Mezuman, U. (1981). Boron Adsorption By Clay Minerals Using A Phenomenological Equation I, [Online] Clays and Clay Mineral, 29(3): 198-204, <http://www.clays.org/journal/archive/volume%2029/29-3-198.pdf> [Accessed: 13/2/2014]
- Khayat, S., Hotzl, H., Geyer, S., and Ali, W. (2006). Hydrochemical investigation of water from the Pleistocene wells and springs, Jericho area, Palestine, [Online] Hydrogeology Journal 14: 192-202. <http://www.environmental-expert.com/Files/6063/articles/8787/1.pdf> [Accessed: 12/1/2014]
- Moss, S., and Nagpal, N. (2003). Ambient water quality guidelines for boron. Water Protection Section, Ministry of Water, Land and Air Protection, <https://www2.gov.bc.ca/assets/gov/environment/air.../boron/boron-tech-appnx.pdf>
- Palestinian Meteorological Department - Ministry of Transport. Rainy Season. <http://www.pmd.ps/viewSeasonRainEng.do>
- PCBS - Palestinian Central Bureau of Statistics, Population, (2009a). Housing and Establishment Census 2007, Final Results - Housing Report – Bethlehem Governorate, Palestinian Central Bureau of Statistics, Ramallah, Palestine.
- PCBS - The Palestinian Central Bureau of Statistics, (2009b). A press release on World Environment Day. The Palestinian environment to where?. http://www.pcbs.gov.ps/Portals/_pcbs/PressRelease/Envirm-DayE.pdf
- PCBS - The Palestinian Central Bureau of Statistics, (2017). Estimated Population in the Palestinian Territory Mid-Year by Governorate, 1997-2016. http://www.pcbs.gov.ps/Portals/_Rainbow/Documents/bethlm.htm
- PWA - Palestinian Water Authority, (2009). Water Supply in the West Bank. Ramallah, Palestine.
- PWA -Palestinian Water Authority, (2015). Personal communication with Palestinian Water Authority -Water sector office.
- Rofee and Raffety, (1963). Jerusalem District water supply, Geological and Hydrological Report. Hashemite Kingdom of Jordan, Central Water Authority. (Unpublished).
- Scarpa, D. (2004). Hydropolitics in recent Israeli – Palestinian relations, Hydrology: Science and Practices for the 21st Century, 2, British Hydrological Society, 147-152.

- Scarpa, D. (2006). The Southern West Bank Aquifer: Exploitation and Sustainability. Edited by Hambright, K. D., Rageb, F. J., and Ginat, J. Water in the Middle East: Cooperation and Technological Solutions in the Jordan Valley, International and Security Affairs series; Vol.3, University of Oklahoma Press, pp:90. <https://books.google.ps/books?isbn=0806137584>
- Vengosh, A., Kloppmann, W., Marei, A., Livshitz, Y., Gutierrez, A., Banna, M., Guerrot, C., Pankratov, I., and Raanan, H. (2005). Sources of salinity and boron in the Gaza strip: Natural contaminant flow in the southern Mediterranean coastal aquifer. Water Resources Research, Vol.41, W01013, doi:10.1029/2004WR003344 .
- WHO - World Health Organization, (1998). Guidelines for Drinking-water Quality, 2nd Ed. Vol. 2. Geneva, 1998. http://www.who.int/water_sanitation_health/dwq/gdwq2v1/en/
- WHO - World Health Organization, (2004). Guidelines for Drinking-water Quality, 3rd Ed., Vol. 1, Recommendations, WHO, Geneva, Switzerland, 2004.
- WHO - World Health Organization, (2011). Guidelines for Drinking-water Quality: Potable water – standards, Water – standards, Water quality - standards, 4thEd., 2011. www.zaragoza.es/contenidos/medioambiente/onu/624-eng-ed4.pdf
- WSERU – Water and Soil Environmental Research Unit, (2014). Personal communications with Water and Soil Environmental Research Unit.
- WSI –Water Studies Institute, (2005). Prospects of Efficient Wastewater Management and Water Reuse in Palestine, Water Studies Institute – Birzeit University, Palestine.
- Zeitoun, R., (2011). Runoff Estimation by the Curve Number for Wadi Ta'amira in Bethlehem – Palestine. Tempus, Birzeit University.

Microfacies analysis and Paleoenvironment Interpretation of Upper Oligocene Azkand Formation in Western Iraq

Mohammed F. Al-Ghreri¹, Amer S. Algibouri^{1*}, and Ali A. Abed²

¹Department of Applied geology, Faculty of Science, The University of Anbar, Anbar, Iraq.

²Department of geology, Faculty of Science, Salahaldeen University, Erbil, Iraq.

Received 28 April, 2018; Accepted 11 November, 2018

Abstract

This paper deals with the microfacies and paleoenvironment interpretation of the Azkand Formation at the high Euphrates river cliffs in north-western Iraq. In this study, the main components are dominated by the coexistence of large benthic hyaline perforated walls (Nummulitidae, Lepidocyclinidae, Amphisteginidae, Miogypsinidae, and Rotaliidae) and porcelaneous imperforate walls (Miliolidae, Peneroplidae, and Alveolinidae) with minor components of small benthic foraminifera. Other fossils are dominated by coralline algae, corals, bryozoans, mollusks, and shell fragments. These microbiota are considered beneficial in the biofacies analysis and recognition of paleoecology. On the basis of large benthic foraminiferal assemblages and microfacies features, eleven microfacies types have been recognized and interrelated. They indicate two depositional environments interpreted as shallow inner- to middle- ramp environments. The shallowest part in the studied section occurs in the photic zone which is characterized by the association of miliolids, peneroplids, and alveolinids. The middle ramp is classified into two shallow middle ramps characterized by dominant miogypsinis amphisteginids, and rotaliids, while the deeper middle-ramp setting is dominated by coralline algae along with nummulitids and lepidocyclinids.

© 2018 Jordan Journal of Earth and Environmental Sciences. All rights reserved

Keywords: Azkand Formation, benthic foraminifera, paleoenvironment, ramp.

1. Introduction

The Azkand Formation represents the upper division of Kirkuk Group of the Iraqi Oligocene outcrop to north Iraq. Bellen, 1956 (in Bellen et al 1959) described the type section of Azkand Formation from the outcrops of Azkand cirque, three miles N-65°-E of the village of Azkand on the southern dome of the Qarah Chauq Dagh structure. The thickness of the formation is variable from one area to another. At the type area, it consists of 104m (Buday, 1980). Lithologically, it consists mainly of massive, dolomitic, and recrystallized limestone. The abundance of *Heterostegina cf. assilinoides* indicates a Late Oligocene age. The study area represents a fore slope facies of a marine platform (fore-reef) facies (Bellen et al., 1959). The outcrops are limited to Anah anticline, Muger Al-Dheeb vicinity and Wadi Houran (Sissakian, and Mohammed, 2007). In all other areas, they are exposed as small patches only in deep cut valleys, particularly speaking in wadi Khazgah Al-Sharje northwest of Anah town in western Iraq (Al-Twaijri, 2000).

The objective of this research is to interpret the depositional environments of the Azkand Formation in western Iraq, based upon the microfacies and faunal contents.

2. Geological Setting

The study area is located within the western desert of the upper Oligocene carbonate platform that developed along the southern Hadetha vicinity. Tectonically, it is represented as part of the stable shelf of the Arabian platform, which is characterized by the presence of block tectonics and the

absence of tectonic folds (Buday and Jassim, 1987). The rocks of Oligocene in the Iraqi western desert have very limited extensions in the stable shelf either as outcrops or subsurface, located mainly within the Mesopotamian and low folded zones of the unstable shelf (Jassim and Karim, 1984). No Oligocene rocks are exposed in the southern desert due to the uplifting of the Salman zone and the Euphrates and Zubair subzones of the Mesopotamian zone in the Oligocene time (Jassim and Goff, 2006).

3. Study Area and Methods

This study is based on one outcrop section measured and sampled in the area located ten kilometers to the south of Hadetha Town, at the right bank of the Euphrates river (Figure 1). A total of seventeen samples were collected and studied, more than thirty-five thin-sections were prepared and examined in the laboratory. In addition, two samples were taken directly above the boundary from the basal conglomerates for comparison, and the outcrops were sampled at one- meter intervals (Figure 2).



Figure 1. Location map of the study area.

* Corresponding author. e-mail: aalgibouri@yahoo.com

The lower contact of the Azkand Formation is unexposed, but covered by fluvial recent deposits, while the upper contact is always unconformable and is marked by a significant Saviian break on the Oligocene/Miocene boundary, which is marked by basal conglomerates of the lower unit of the Euphrates Formation (Al-Ghreri et al., 2013).

Time unit	Rock unit	Sample no.	Thickness (m)	Lithology	Lithological description
Upper Oligocene	Azkand Formation	17	3	[Lithology symbol]	Massive limestone white in colour
		16			
		15			
		14	1	[Lithology symbol]	Caralline limestone with fragments of molluscan
		13			
		12	4	[Lithology symbol]	Limestone with molluscan, white to gray in colour
		11			
		10			
		9	1	[Lithology symbol]	Coralline limestone, showing algal facies
		8			
		7	3.5	[Lithology symbol]	Massive lomestone white to gray in colour
		6			
		5			
		4	1.5	[Lithology symbol]	Coralline limestone, showing algal facies
		3			
		2			
		1	3	[Lithology symbol]	Massive limestone with fragments of coralline algae, a shoal nummulitic facies, white to gray in colour

Figure 2. Lithological section of Azkand Formation in the study area.

4. Microfacies Analysis and Depositional Environments

Eleven different microfacies types could be distinguished in the Oligocene Azkand Formation by thin-section studies of the composition and structure which are described and illustrated here together with their environmental interpretation (Figures 3 and 4).

4.1 Microfacies 1: *Lepidocyclus nummulitidae* wacke/Packstone (MF1)(Figure 3-A)

Description: The major components of this microfacies are the small and ovate tests of the large benthic foraminifera, namely (*Lepidocyclus* spp., *Rotaliaviennoti* and *Amphistegina* sp.) with textures ranging from wackestone to packstone. Other biocontents include fragments of coralline red algae, bryozoans, and echinoids plate. They are one-meter thick and dominate the lower part of the studied section.

Interpretation: The presence of large benthic foraminifera (*Lepidocyclus* spp. and *Rotalia* sp.) indicates full marine environments within the euphotic zone, because symbiotic-bearing foraminifera are restricted to the euphotic zone, below the wave base (Corda and Brandano, 2003; Bassi et al., 2007; Hottinger, 1997; Romero et al., 2002).

The occurrence of the perforated foraminifera such as *Lepidocyclinidae* and *Nummulitidae* reflects deposition in the lower part of photic zone at the distal middle ramp (Hottinger, 1983).

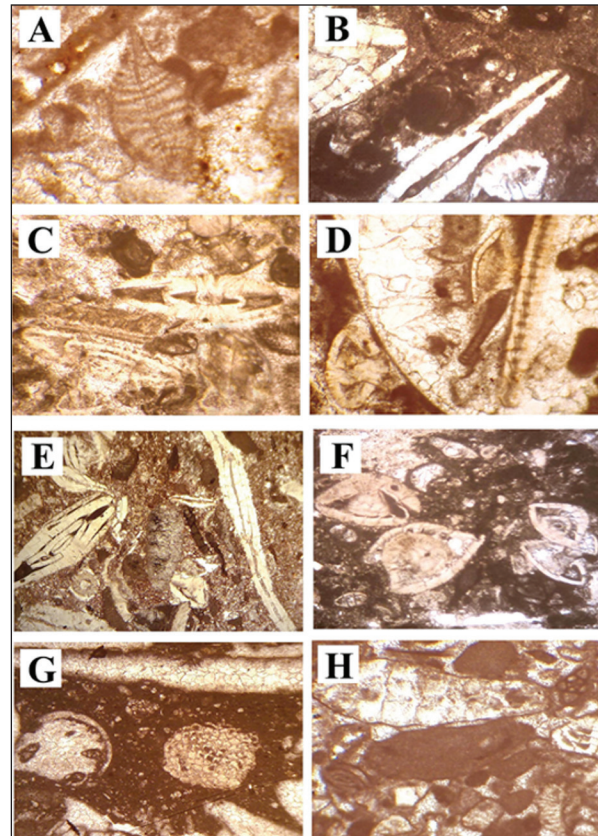


Figure 3. Microfacies types (MF) which recognized in the Azkand Formation:

- A-MF1: *Lepidocyclus nummulitidae* wacke/packstone X25.
- B, C-MF2: *Nummulitidae* wackestone to packstone. X25.
- D, E-MF3: *Heterostegina* packstone, X30.
- F-MF4: *Amphistegina* grainstone, X50.
- G, H-MF5: *Miogypsina* corallinean wackestone to packstone, X50.

4.2 Microfacies 2: *Nummulitidae* Wacke/Packstone (MF2) (Figures 3 B-C)

Description: This microfacies consists of large and flat perforate foraminifera represented by the individuals of nummulitids such as (*Nummulites* sp., *Operculina complanata* and *Heterostegina assilinoidea*) among the most common genera representing more than 60 %; they include *Rotalia* sp., *miliolids* sp., bryozoans, and fragments of red algae were presents. They dominate the lower part of the Azkand Formation.

Interpretation: The presence of large flat perforated tests (*Nummulites* sp., *Operculina* sp. and *Heterostegina* sp.) with coralline algae indicates deposition near a fair-water wave base on a proximal middle shelf (Corda and Brandano, 2003; Cosovic et al., 2004). Members of the genus *Operculina* only live in the warm waters of normal marine salinity, and show relatively high ecological tolerances compared to other biota (Langer and Hottinger, 2000). *Operculina* spp. are dominant foraminifera on deep reef fronts and inter-reef channels in Indonesia (Remena, 2006). They were also common in main reef, back-reef, patch reef, intra-reef, and deeper off-reef facies similar to those of the modern Indo-Pacific (Bosellini, 2006).

According to Hallock and Glenn (1986), the porcelaneous tests (mainly *Heterostegina* sp. and *Amphistegina* sp.) live in

a tropical-subtropical environment over a wide bathymetric range, but are particularly frequent between depths of 40 and 70 m. Furthermore, they are most abundant in the mesophotic and oligophotic zones of subtropical seas, but thrive in tropical environments (Hottinger, 1983, 1997; Reiss and Hottinger, 1984). Such assemblage indicates that these deposits were formed in the distal part of the middle ramp well below the fair-weather wave base since there are no signs of wave hydraulic turbulence in these microfacies (Moghaddam et al., 2011).

4.3 Microfacies 3: *Heterostegina* Packstone (MF3) (Figures 3 D-E)

Description: This facies is composed of bioclasts of perforated foraminifera characterized by relatively diverse assemblage of Nummulitids such as (*Heterostegina* assilinoidea, *Heterostegina involuta*, *operculina* sp., and *Nummulites* sp.), with fragments of small foraminifera which are distributed irregularly among the large foraminifera. Coralline algae are also present. This microfacies is most prominent in the lower parts of the Azkand Formation, attaining a thickness of 1 m.

Interpretation: The presence of high diverse large perforated foraminifera nummulitids such as *Heterostegina* spp. and *operculina* sp., indicates deposition in the distal part of the middle ramp well below the fair-weather wave base (Beavinton and Racey, 2004). Nummulitidae protect themselves from ultraviolet light by producing very thick lamellated test walls or by occurring in relatively deeper waters. (Rasser et al., 2005).

The Oligocene nummulitid facies consists of *Heterostegina*, *Operculina*, *Nummulites*, and *Spiroclypeus* occurring in the middle-ramp deposits of the circum-Alpine area, northern Slovenia, and Malta (Nebelsick et al., 2005). Larger benthic foraminifera (*Heterostegina*, *Amphistegina*, *Asterigerina*) and calcareous red algae are the main components in the deeper ramp facies (Brandano et al., 2009). In general, *Operculina*, inhabit shallow-water soft substrates under the influence of a mixed siliciclastic carbonate environment (Reiss and Hottinger, 1984); whereas, *Heterostegina* occurs abundantly in calm-water environments being protected at shallow depths or in deeper parts of the sea down to 85 m (Geel, 2000). In the Oligo-Miocene, *Heterostegina* inhabited high energy foreereef environments (BouDagher-Fadel and Wilson, 2000), of 20–30 m depth (Banner and Hodgkinson, 1991).

4.4 Microfacies 4: *Amphistegina* Grainstone (MF4) (Figure 3-F)

Description: The main components of this facies are *Amphistegina* sp., *Rotalia* sp. and *Heterostegina* sp. with some minor components which include fragments of mollusca, echinoids plate and coralline algae fragments. This microfacies is dominant in the upper part of the Azkand Formation of (1) meter thick.

Interpretation: The interpretation of this microfacies is based on the abundance of large benthic perforated wall such as *Amphistegina* sp., *Operculina* sp. *Rotalia* sp. and *Miogyopsina* sp. The association indicates shallow water environments photic zone of high-energy condition. The

occurrence of *Amphistegina* sp. and *Heterostegina* sp. Indicate warm marine water with low to medium energy in photic zone and in the long range of depths between 40 and 70 m (Hallock and Gleen, 1986). Hallock et al. (1986) found in the study of the influence of environments on the test shape of *Amphistegina* sp. that the test shape varies with depth; they are robust and spherical in shallow environments, and thinner and flatter as depth increases. Finally, the dominant benthic foraminiferal genus is *Amphistegina*, which is considered a shallow water genus (McDougall et al., 1999).

4.5 Microfacies 5: *Miogyopsina* coralline wacke/packstone (MF5) (Figures 3 G-H)

Description: *Miogyopsinidae*, coralline and *Rotalids* fragments are the dominant bioclasts with minor skeletal grains of echinoids plates and of mollusk red algae fragments. The depositional textures reflect poorly sorted wackestone; some other grains have been partially micritized. This microfacies dominates the upper part of the Azkand Formation with a thickness of 1 m.

Interpretation: This facies is dominated by a high diversity of benthic foraminifera mainly *Miogyopsinidae* which are dominant in the lagoon and shallow subtidal depositional environments of the upper Oligocene-lower Miocene limestones (Flügel, 2004). This biota can contribute to coral-reef frameworks by successfully competing with coralline algae for space on hard substrates (Barattolo et al., 2007). Moreover, the abundance of *Miogyopsina* spp. in rhodoliths decreases substantially with the increase of depth from 20 to 70 m (Minnery, 1990).

The occurrence of perforated-walled foraminifera such as *Miogyopsinidae* with coralline red algae fragments, indicates deposition in the moderate to high-energy environment of an upper part of a carbonate shelf slope, at less than 50m of depth and in waters of normal salinity (Geel, 2000).

4.6 Microfacies 6: Coral Boundstone (MF6) (Figures 4 A-B)

Description: Coral has a wide distribution in the Azkand Formation, represented by two beds, at the middle and upper parts, usually capping most of the top section, with each bed ranging in thickness between 1 m and 1.5 m. It was formed by the growth of coral networks. The framework of this microfacies comprises in situ and unbroken coral. This is the most abundant type in the studied section, representing more than 50 %, and is composed mainly of corals. The associated fauna includes large benthic foraminifera such as miliolids and various types of calcareous coralline algae such as (*Lithophyllum* sp. and *Lithothamnium* sp.) echinoderms debris; *rotaliida* can rarely be seen.

Interpretation: Miliolids are common components in this facies indicating shallow-water, and low-energy environments in many modern and ancient examples of carbonate platforms (Reiss and Hottinger, 1984). Also, this facies is formed in patch reefs and represents the mid-ramp environment (Buxton and Bedley, 1989). According to Wilson (1975), and expanded by Flügel (2004), the allochems of this facies must have been derived from the reef.

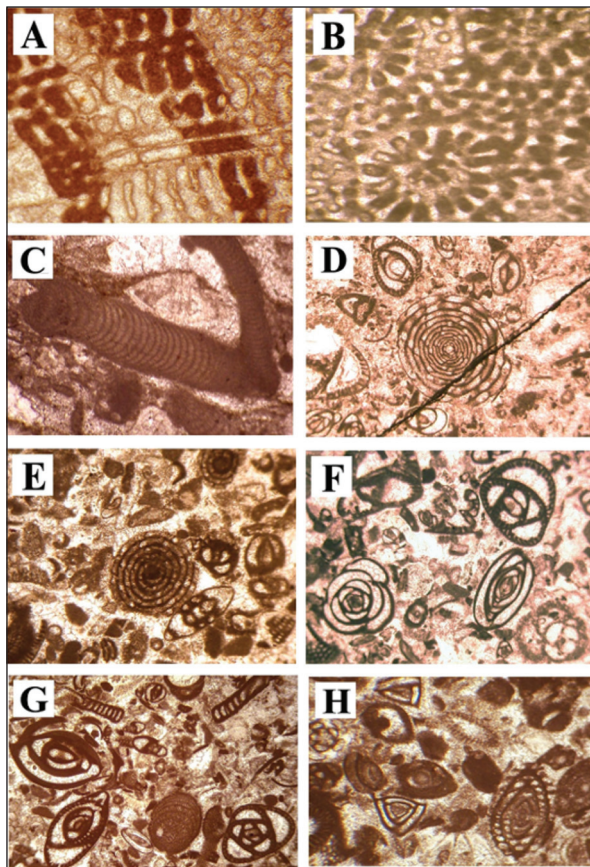


Figure 4. Microfacies types (MF) which recognized in the Azkand Formation:

- A, B-MF6: Coral (boundstone) X25.
 C-MF7: Articulated Coralline algae grainstone X 25.
 D, E-MF8: Alveolinids miliolids packstone- grainstone X60.
 F-MF9: Miliolids packstone – grainstone X 60.
 G-MF10: Miliolids peneroplids grainstone X 60.
 H-MF11: imperforate foraminifera packstone-grainstone X40.

4.7 Microfacies 7: Coralline algae grainstone (MF7) (Figure 4 C)

Description: in the Coralline Algae Grainstone, the articulated coralline algae are the most abundant constituents. *Lithothamnion* sp. and *Mesophyllum* sp. are the most conspicuous algae and *Jania* is rare. Large and small benthic foraminifera *Amphistegina* sp., *Heterostegina* sp., and bryozoans, echinoid and molluscan fragments are present. Small rhodoliths (*Sporolithon* sp., and *Lithophyllum* sp.) are locally common; they rarely include encrusting foraminifera such as *Miogypsina*. Sparry calcite is common.

Interpretation: Firstly, coralline red algae are used as a potential tool for paleoecology, paleoenvironment and paleobathymetry, builder of porous and permeable carbonate reservoir rocks for hydrocarbon and reefs rich in hydrocarbon (Kundal, 2011). Geographical ranges are controlled by water temperature, depth ranges, and light intensity (Johansen, 1981).

As for the abovementioned factors, this facies is widely distributed in tropical to polar normal marine waters, from intertidal depths to the base of the photic zone (Wray, 1977), at the depths of 20-80 m, but could be also present at the depths of 80-160 m depth (Flügel, 2004).

Articulated branching coralline algae are characterized by the dominance of crustose coralline thalli composed

primarily of melobesoids (*Lithothamnion* sp. and *Mesophyllum* sp.), both genera grow most profusely in well-illuminated waters usually attached to hard substrates in low-energy conditions at depths of more than 50 m (Kishore et al., 2006). They are restricted to environments that are deeper inner- to mid-ramp ranging from 40 to 80 m depths at the upper photic zone (Misra et al., 2006). Similar associations have been recorded by Pomar et al. (2004) in the slope and outer ramp. In addition, to the *Lithothamnion*-dominated association typical for shallow warm-temperates to tropical environments, there is an association dominated by *Mesophyllum* characteristic of the lower photic zone in warm-temperate to tropical environments (Kroeger et al., 2006). Moreover, the occurrence of coralline algae with perforated walls such as (*Amphistegina*, *Heterostegina*) indicates that this facies was formed in the photic zone (Brandano et al., 2008).

4.8 Microfacies 8: Alveolinids miliolids packstone grainstone (MF8) (Figures 4 D-E)

Description: The main components of this microfacies are imperforate benthic foraminifera, namely alveolinids and miliolids, with less abundant of peneroplids. All other components are subordinate and are distributed irregularly among the facies. Some fragmentation of coralline algae, bivalves, and gastropods are present. This microfacies is observed in the lower part of the Azkand Formation with a thickness of 1.5 m.

Interpretation: This facies is characterized by abundant imperforate benthic foraminifera mainly Alveolinidae (*Borelismelo* spp.), miliolids such as (*Austrotrillina* howchin, *Quinqueloculina* sp.), and peneroplids (*Peneroplis evolutus*). Alveolinids are important faunal contributors to open-water sediments of the inner platform in shallow water or possibly hypersaline (Hottinger, 1997). According to (Murray, 1973) alveolinids, peneroplids, and miliolids are common in lagoons, shallow-water, and other quiet environments and are generally miliolids capable of tolerating higher salinities than other biota. However, all of this biota are very common in reef to backreef environments at normal marine salinities (Brasier, 1975; Hallock, 1984a; Reiss and Hottinger, 1984).

The occurrence of a large number of porcelaneous foraminifera suggests that the deposition took place in a shelf-lagoon setting, with very limited circulation and relatively hypersaline environments (Romero et al., 2002). A similar microfacies was reported from the shelf-lagoon environment of Asmari Formation, Iran (Brandano et al. 2008; Sadeghi et al. 2009; Vaziri-Moghaddam et al., 2006).

4.9 Microfacies 9: Miliolids packstone – grainstone (MF9) (Figure 4 F)

Description: This microfacies consists of predominant imperforate-walled foraminifera that include miliolids (*Austrotrillina* howchini, *Austrotrillina* sp., *Spiroloculina* sp., *Quinqueloculina* sp., and *Triloculina* sp.), with small miliolids, fragments of coralline red algae. Echinoid are present with debris of mollusks. The miliolids particles are heavily micritized, especially on their outer borders, and the spaces between grains are filled with sprite or micrite.

Interpretation: Porcelaneous foraminifera are regarded as the major components of this microfacies reported from

open and restricted platform conditions (Hallock and Glenn, 1986). Miliolids are commonly present in back-reef-lagoon environments and the sheltered areas on the reef banks (Ghosh, 2002). The occurrence of porcelaneous such as miliolids (*Austrotrillina* spp.) preferentially live in waters of low turbulence, where abundant fine sediments occur and are characteristic of restricted lagoonal and/or relatively nutrient-rich back reef environments. (Brandano et al., 2008) and (Allahkarampour Dill et al., 2010) believed that the prevalence of porcelaneous foraminifera strongly suggests deposition in a protected inner-shelf lagoon- environment.

In general, the occurrence of imperforate foraminifera mainly *Quinqueloculina* sp. and *Triloculina* sp. indicates that deposition took place in a restricted shelf lagoon environment. Furthermore, whole porcelaneous foraminifera often dominate near-shore environments in water depths of less than 50 m, and can live in environments with extreme temperatures and salinity (Murray, 1973; Flügel, 2004).

4.10 Microfacies 10: Miliolidspeneroplids grainstone (MF10) (Figure 4-G)

Description: The main components of this microfacies are large benthic imperforate foraminifera, characterized by a relatively diverse assemblage of imperforate walls; examples include (*Austrotrillina howchini*, *Austrotrillina*, *asmariensis*, *Peneroplis evolutus*, *Quinqueloculina*, *Dendritina*, and *Spirolina*, in addition to coralline algae (*Lithophyllum* sp.), echinoderm plates and bryozoan fragments. This microfacies dominates the lower-middle parts of the Azkand Formation attaining a thickness of 2 m.

Interpretation: Generally, porcelaneous foraminifera are abundant where CaCO₃ availability is high and the water is warm and hypersaline (Ghosh, 2002). In this facies, the coexistence of foraminifera with porcelaneous walls such as (miliolids and peneroplids), indicates environments with very limited circulation and relatively hypersaline conditions (Amirshahkarami et al, 2007; Hallock and Glenn, 1986). Moreover, the larger porcelaneous foraminifera (such as *Peneroplis* and *Archaias*), hosting dinoflagellate, rhodophycean and chlorophycean endosymbionts dominate the upper photic zone (Romero et al., 2002).

The association of the large number of porcelaneous imperforate foraminiferal tests such as *Austrotrillina*, *Peneroplis*, *Dendritina*, and other miliolids, indicates that this assemblage is described in association with the inner-ramp environment (Brandano et al., 2008; Flügel, 1982, 2004; Vaziri-Moghaddam et al., 2006; Wilson, 1975).

4.11 Microfacies 11: Imperforate foraminifera packstone-grainstone (MF11) (Fig.4-H)

Description: The main components of this microfacies are larger benthic foraminifera with imperforate walls, such as *Triloculina tricarinata*, *Triloculina trigonula*, *Archaias hensoni*, *Dendritina rangi*, *Austrotrillina howchini*, *Quinqueloculina* sp., *Peneroplis* and miliolids. Coralline algae, corals, bryozoans; molluscan shells' fragments are also present. The minor components are small benthic foraminifera. This microfacies dominates the lower-middle parts of the Azkand Formation with a thickness of 2 m.

Interpretation: Large foraminifers with imperforate walls dominate the near-shore environments at water depths

between 0 and 50m, and can live in environments with extreme temperatures and salinity (Murray, 1991; Flügel, 2004). Miliolids often dominate the modern reefs in normal oceanic salinities in addition to metahaline environments such as Shark Bay, Western Australia (Hallock and Glenn, 1985; James et al., 1999).

Porcelaneous foraminifera such as miliolids (*Triloculina* spp. and *Quinqueloculina* spp.) are common throughout the Azkand Formation. *Triloculina* spp. are often found in association with *Quinqueloculina* spp. in the Mediterranean Sea, the Caribbean Sea, and Western Australia (Murray, 1991). Benthic foraminifera such as *Quinqueloculina* spp. generally live on protected sedimentary subenvironments, and are commonly associated with sea grass beds and sandy and muddy substrates in waters at depths of less than 12 m (Murray, 1973, 1991; Betzler et al., 1997). They also live on reefal sediments and are among the most abundant foraminifera on the modern Great Barrier Reef, Australia (Uthicke et al., 2010). Furthermore, porcelaneous foraminifera mainly (*Peneroplis* and *Archaias*) live in recent tropical and subtropical shallow-water environments, hosting dinoflagellate, rhodophycean and chlorophycean endosymbionts (Lee, 1990). Due to the presence of epiphytic foraminifera, this microfacies could have originated in sea-grass-dominated environments (Brandano et al., 2008).

5. Microfacies Association and Depositional Model

The distribution of larger benthic foraminiferal assemblages are excellent indicators used as valuable tools to reconstruct palaeoenvironmental models in warm, shallow marine environments, especially in monotonous carbonate platform successions (Geel, 2000). In this study, two main environmental gradients can be identified in the Azkand formation. These include inner-ramp and middle-ramp environments. A general depositional scheme is provided in (Figure 5).

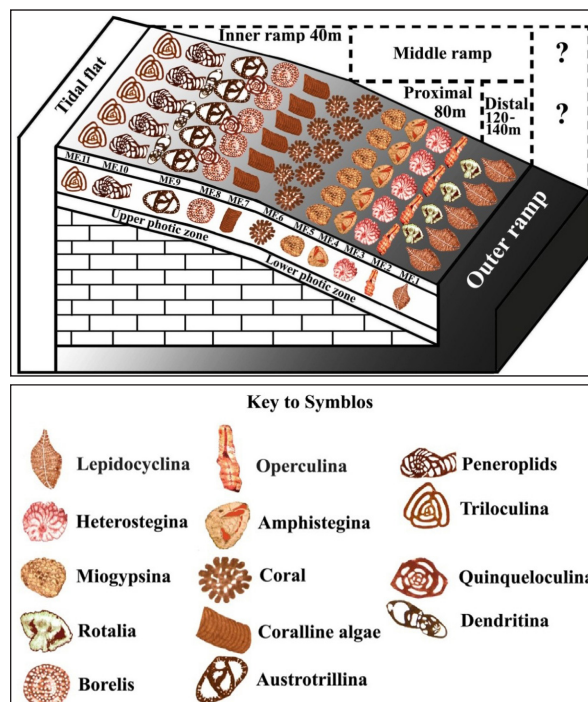


Figure 5. Depositional model for the carbonate platform of the Azkand Formation.

5.1 Inner- Ramp Environments

The most common microfacies of the inner ramp environment is the imperforate foraminifera types such as *Peneroplis* sp., *Austrorillina* sp., *Dendritina* sp., *Archaias* sp., *Borelis* sp., *Meandropsina* sp., and miliolids. Other components include coralline algae and coral fragments dominating the restricted shallow sub-tidal environments or restricted lagoon environments (Hallock and Glenn, 1986; Geel 2000; Romero, 2006).

The occurrence of the large porcellaneous foraminifera type such as *Archaias* sp., *Peneroplis* sp., *Borelis* sp., *Meandropsina* sp., *Dendritina* sp. and miliolids indicates tropical and subtropical shallow-water environments (Lee, 1990), in the upper part of the upper photic zone (Brandano et al., 2008). The common association of coralline algae and coral fragments with miliolids and *Austrorillina* sp. indicates the very shallow water at upper part of the upper photic zone in the inner-ramp environment.

5.2 Middle- Ramp Environment

This setting is represented by an assemblage of larger perforate foraminifera such as nummulitids (*Operculina complanata*, *Heterostegina assilinoidea* and *Heterostegina* sp.), *Lepidocyclinids* (*Nephrolepidina* sp. and *Eulepidina* sp.), *Asterigenids* (*Amphistegina* sp.) and *Miogypsinoid* (*Miogypsinoides complanata* and *Miogypsina* sp.). Furthermore, the most common smaller foraminiferal fauna are *Rotalia*, coralline red algae, and scattered coral fragments.

The abundant occurrence of perforate foraminifera (such as *Operculina* sp. and *Lepidocyclina* sp.) and *Rotalia* sp. along with red algae places the oligophotic zone in the middle- ramp setting (Bassi et al., 2007; Brandano et al., 2008). Generally, the upper part of the lower photic zone is dominated by perforate hyaline foraminifera such as (*Operculina* sp., *Heterostegina* sp., *Amphistegina* sp. and *Miogypsina* sp.) with red algae association places the middle ramp in an oligophotic zone (Brandano et al. 2008; Corda and Brandano, 2003) to mesophotic zone (Hottinger, 1997).

Furthermore, *Operculina complanata* was found in the lower parts of the photic zone and in quiet settings away from the effect of waves (Beavington-Penney and Racey, 2004; Hohenegger et al., 2000). This species seems to tolerate a high amount of terrigenous sediments that reduce the light intensity (Bassi et al., 2007).

In this study, the middle-ramp setting can be divided into two parts, namely the proximal middle-ramp facies dominated by coralline algae with (*Operculina* sp., *Heterostegina* sp., *Amphistegina* sp., *Miogypsina* sp. and *Rotalia* sp.) and the distal middle- ramp facies which is characterized by dominant coralline algae with *Nummulites* sp. and *Lepidocyclina* sp.

6. Conclusions

The paleoenvironmental recognition of the Azkand Formation in Western Iraq based on the biofacies analysis suggests two major depositional settings. These depositional environments are the inner- and the middle-ramp environments. In the inner-ramp setting, the most abundant microfacies are wackestone-packstone with an imperforate wall. Examples include *Peneroplis* sp., *Austrorillina* sp.,

Dendritina sp., *Archaias* sp., *Borelis* sp., *Meandropsina* sp., and miliolids which indicate the low-energy upper photic zone, and the shallow shelf lagoon depositional environment.

The middle-ramp setting is generally dominated by bioclast packstone-grainstone with perforate walls, and can be divided into (A) shallow part of the middle-ramp environment (proximal middle-ramp) characterized by the occurrence of large foraminifera with perforate walls such as *Operculina* sp., *Heterostegina* sp., *Amphistegina* sp., *Rotalia* sp., and *Miogypsina* sp., and (B) a deeper middle-ramp setting (distal middle-ramp), dominated by large perforated foraminifera such as, *Nummulites* sp. and *Lepidocyclina* sp. along with fragments of corallina.

References

- Al-Ghreeri, M.F., Al-gibouri, A.S., and Al-Ahmed, A.A. (2014). Facies architecture and sequence development of the Euphrates formation in western Iraq. *Arabian Journal of Geosciences*. 7: 2679-2687.
- Allahkarampour, D., Seyrafian, A., and Vaziri-Moghaddam, H (2010). The Asmari Formation, north of the Gachsaran (Dill anticline, southwest Iran): facies analysis, depositional environments and sequence stratigraphy. *Carbonates and Evaporites*. 25(2): 145-160.
- Al-Twajjri, F.S.S. (2000). Sequence Stratigraphic Analysis of the Oligocene Succession in Western Iraq. M. Sc. Thesis, Baghdad University, 166p.
- Amirshahkarami, M., Vaziri-Moghaddam, H., and Taheri, A. (2007). Sedimentary facies and sequence stratigraphy of the Asmari Formation at Chaman_Bolbol (Zagros Basin Iran). *J. Asian Earth Sci.*, 29: 947-959.
- Banner, F.T., and Hodgkinson, R.L. (1991). A revision of the foraminiferal subfamily Heterostegininae. *Revista Espanola de Micropaleontologia* 23: 101-140.
- Barattolo, F., Bassi, D., and Romero, R. (2007). Upper Eocene larger foraminiferal-coralline algal facies from the Klokova Mountain (south continental Greece) *Facies* 53: 361-375.
- Bassi, D., Hottinger, L., and Nebelsick, H. (2007). Larger Foraminifera from the Upper Oligocene of the Venetian area, northeast Italy: *Paleontology* 5(4): 845-868.
- Beavington – Penney, S.J., and Racey, A. (2004). Ecology of extant nummulitids and other larger benthic foraminifera. Applications in Paleoenvironmental analysis: *Earth Science Review* 67(3-4): 219-265.
- Bosellini, F.R. (2006). Biotic changes and their control on Oligo-Miocene reefs: a case study from the Apulia Platform margin (southern Italy): *Palaeogeography, Palaeoclimatology, Palaeoecology*, 241: 393-409.
- BouDagher-Fadel, M.K., and Wilson M.E. (2000). A revision of some large foraminifera from the miocene of East Kalimantan. *Micropaleontology*, 46: 153-165.
- Brandano, M., Frezza, V., Tomassetti, L. and Cuffaro M. (2008). Heterozoan carbonates in oligotrophic tropical waters: The attard member of the Lower coralline limestone Formation (Upper Oligocene, Malta). *Palaeogeography, Palaeoclimatology, Palaeoecology*, 272: 1-10.
- Brasier, D. (1975). Ecology of Recent sediment-dwelling and phyla foraminifera from lagoons of Barbuda, West Indies: *Journal of Foraminiferal Research*, 5: 42-62.
- Buday, T. (1980). The Regional Geology of Iraq. *Stratigraphy and Paleogeography*, edit. by Kassab, I. and Jassim, S.Z., GEOSURV, Baghdad, 1: 445.
- Buday, T., and Jassim, S.Z. (1987). The Regional Geology of Iraq. *Tectonism, Magmatism and Metamorphism*, GEOSURV, Baghdad, Iraq, 2: 352.
- Buxton, M.W.N., and Pedley, H.M. (1989). Short Paper: A standardized model for Tethyan Tertiary carbonate ramps: *Journal Geological Society*, London 146: 746-748.

- Corda, L., and Brandano, M. (2003). A photic zone carbonate production on a Miocene ramp Central Apennines, Italy. *Sedimentary Geology*, 61: 55–70.
- Cosovic, V., Drobne, K., and Moro, A. (2004). Paleoenvironmental model for Eocene foraminiferal limestones of the Adriatic carbonate platform (Istrian Peninsula). *Facies*, 50: 61-75
- Flügel, E. (1982). *Microfacies analysis of limestones*. Translated by K. Christenson. Springer, Berlin 633 p.
- Flügel, E. (2004). *Microfacies of carbonate rocks. Analysis interpretation and application*. Springer, Berlin, 976 p.
- Ghosh, A.K. (2002). Cenozoic coralline algal assemblage from southwestern Kutch and its importance in palaeoenvironments and palaeobathymetry. *Current Science* 83 (2): 153-158.
- Hallock, P., and Glenn, E.C. (1985). Numerical analysis of foraminiferal assemblages: a tool for recognizing depositional facies in Lower Miocene reef complexes: *Journal of Paleontology*, 59: 1382-1394.
- Hallock, P., and Glenn, E. C. (1986). Larger foraminifera: A tool for Paleoenvironmental analysis of Cenozoic carbonate depositional facies: *Palaios*, 1: 55–64.
- Hallock, P., Forward, L.B., Hansen, H.J. (1986). Environmental influence of test shape in Amphistegina. *Journal of Foraminiferal Research*, 16: 224–231.
- Hottinger, L. (1983). Processes determining the distribution of larger foraminifera in space and time: *Utrecht Micropaleontology* 30: 239–253.
- Hottinger, L. (1997). Shallow benthic foraminiferal assemblages as signals for depth of their deposition and their limitations. *Bulletin Society Geology France*, 168(4): 491–505.
- James, N.P., Collins, L.B., Bone, Y., and Hallock, P. (1999). Subtropical carbonates in a temperate realm: modern sediments on the southwest Australian shelf. *Journal of Sedimentary Research*, 69: 1297-1321.
- Jassim, S.Z., and Goff, J. (2006). *Geology of Iraq*. Dolin and Moravian Museum, Prague. 341p.
- Johansen H.W. 1981. *Coralline Algae, a First Synthesis*: Boca Raton, CRC Press 239 p.
- Kishore, S., Misra, P.K., Jauhri, A.K., and Singh, S.K. (2006). Paleocene coralline algae from the Cauvery Basin South India. *Journal of Geological Society. India*, 68 (11): 789-796.
- Kroeger, K. F., Reuter, M., and Brachert, T.C. (2006). Palaeoenvironmental reconstruction based on non-geniculate coralline red algal assemblages in Miocene limestone of central Crete. *Facies*, 52: 381–409.
- Kundal, P. (2011). Generic Distinguishing Characteristics and Stratigraphic Ranges of Fossil Corallines: *Journal geological society, India*, 78: 571-586.
- Lee, J.J. (1990). Fine structure of rodophycean prophyridium purpureum insitu in Peneroplis pertusus and P. asicularis. *Journal of Foraminiferal Research*. 20:162-169.
- McDougall, K.A., Poore, R.Z. and Matti, J.C. (1999). Age and paleoenvironment of the Mediterranean. *Sedimentology*, 51: 627-651.
- Minnery, G.A. (1990). Crustose coralline algae from the Flower Garden banks, northwestern Gulf of Mexico: controls on distribution and growth morphology: *Journal of Sedimentary Petrology*. 60: 992-1007.
- Misra, P.K., Jauhri, A.K., Singh, S.K., and Kishore, S. (2006). Coralline algae from the Fulra Limestone (Middle Eocene) of Kachchh, Gujarat, W. India. *Journal. Geological. Society*, 67(4): 495-502.
- Murray, J.W. (1973). Distribution and Ecology of Living Benthic Foraminiferids: *Palaeogeography, Palaeoclimatology, Palaeoecology* 179: 43-56.
- Murray, J.W. (1991). *Ecology and Palaeoecology of Benthic Foraminifera*: Essex, Longman Scientific and Technical 397p.
- Nebelsick, J.H., Rasswer, M., and Bassi, D. (2005). Facies dynamic in Eocene to Oligocene Circumalpine carbonates. *Facies*, 51: 197–216.
- Pomar, L., Brandano, M., and Westphal, H. (2004). Environmental factors influencing skeletal grain sediment associations: a critical review of Miocene examples from the western Mediterranean: *Sedimentology*, 51: 627-651.
- Rasser, M.W., Scheibner, C., and Mutti, M. (2005). A paleoenvironmental standard section for Lower Eocene tropical carbonate factories (Pyrenees, Spain; Corbieres, France). *Facies*, 51: 217–232.
- Reiss, Z., and Hottinger, L. (1984). *The Gulf of Aqaba: Ecological Micropaleontology*: Berlin, Springer - Verlag, 354 p.
- Remero, W. (2006). Habitat variables determining the occurrence of large benthic foraminifera in the Berau area (East Kalimantan, Indonesia): *Coral Reefs*, 25: 351-359.
- Romero, J., Caus, E., and Rossel, J. (2002). A model for the palaeoenvironmental distribution of larger foraminifera based on late Eocene deposits on the margin of the Pyrenean Basin (SE Spain): *Palaeogeography, Palaeo climatology, Palaeoecology*, 197:3-56.
- Sadeghi, R., Vaziri-Moghaddam, H., and Taheri, A. (2009). Biostratigraphy and paleoecology of the Oligo-Miocene succession in Fars and Khuzestan areas (Zagros Basin, SW Iran). *Hist Biol.* [http:// www.informaworld.com/smpp/title *content=t713717695](http://www.informaworld.com/smpp/title*content=t713717695).
- Sissakian, V.K., and Mohammed, B.S. (2007). *Geology of Iraqi Western Desert*. *Iraqi Bulletin of Geology and Mining. Special Issue*, 51–124.
- Uthicke, S., Thompson, A., and Schaffelke, B. (2010). Effectiveness of benthic foraminiferal and coral assemblages as water quality indicators on inshore reefs of the Great Barrier Reef: *Coral Reefs*, 29: 209-225.
- Van-Bellen, R.C., Dunnington, H.V., Wetzel, R., and Morton, D.M. (1959). *Lexique Stratigraphique International. Asie, Fascicule 10 a*, Iraq, Centre National De La Recherche Scientifique, Paris, 333 p.
- Vaziri-Moghaddam, H., Kimiagari, M., and Taheri, A. (2006). Depositional environment and sequence stratigraphy of the Oligo–Miocene Asmari Formation in SW Iran. *Facies*, 52:41–51.
- Wilson, J.L. (1975). *Carbonate facies in geologic history*: Berlin, Heidelberg, New York, Springer 471 p.

Creating a Drinking Water Quality Index (WQI) Map Using the Geographic Information System (GIS) Technique for Karbala City, Iraq

Kamal B. Al-Paruany

Ministry of Science and Technology, Iraq,

Received 6 May, 2018; Accepted 11 November, 2018

Abstract

The geographic information system (GIS) technique is applied in the present study to produce a drinking water quality index map for the Karbala city in Iraq. Ninety-two samples of groundwater were collected from different sites in the study area and analyzed in terms of different chemical parameters affecting the quality of drinking water. The piper diagram is used to estimate the chemical type of groundwater in the study area. $\text{Na}^+\text{-SO}_4^{-2}$ and $\text{Na}^+\text{-Cl}$ facies were found to be the dominant major groundwater types. At few locations, the groundwater chemistry belongs to mixed $\text{Mg}^{2+}\text{-Ca}^{2+}\text{-SO}_4^{-2}$ and mixed $\text{Mg}^{2+}\text{-Ca}^{2+}\text{-Cl}$ facies. Cations and anions were used to create a water quality database in the study area using (GIS) for the purpose of producing a spatial distribution map for each parameter using the Reverse Interpolation Technique (IDW). The results of these determinants were also used to calculate the values of the water quality index and the production of the index map of the quality of drinking water. The analysis of the WQI map results shows that only 1 % of the water samples fall within class II which represents good water quality and 57 % of the available well samples fall under class III which indicates poor water quality, 21% of the water samples fall in class IV which indicates a very poor water quality, and 20 % of the samples indicate unsuitable water. Wilcox and United State Salinity Laboratory (USSL) diagrams are also applied in the current study to evaluate the available water wells in the area, and to determine its suitability for irrigation purposes. To achieve this goal the Electrical Conductivity (EC) has been measured and the sodium percentage (Na %) and sodium Adsorption Ratio (SAR) have been calculated based on the chemical analysis of Ca_2^{2+} , Mg^{2+} , Na^+ , K^+ . The results show that only 4 % of the water samples fall under the good to permissible category, and are suitable for irrigation

© 2018 Jordan Journal of Earth and Environmental Sciences. All rights reserved

Keywords: "GIS, Water Quality Index, Karbala, Iraq"

1. Introduction

River water constitutes the main source for drinking water, irrigation and other purposes in Iraq. However, river water has been exposed to many problems in recent years, the most important of which include the scarcity of rainfall, the construction of dams on the Tigris and Euphrates rivers by the neighboring countries, in addition to the fact that rivers have become a dumping ground for industrial waste (Alhadithi, 2016). Therefore, there is an urgent need to find other sources of water to meet people's water needs. Groundwater is one of the most reliable sources of water, which is almost believed to be clean and uncontaminated water (Alhadithi, 2004; Israil, et al., 2006). Hence, there is a general tendency in Iraq to drill more wells to meet the growing water needs for potable water, and water for agricultural purposes and all daily uses.

The current research is conducted to look for other sources of water and to study their suitability for drinking purposes using GIS and the water quality index technique in the Karbala province. These techniques have been used successfully in recent years to assess groundwater quality as they provide an overview of the water quality by incorporating composite data and giving a result that describes the condition of the groundwater. Several researchers around the world

have applied the WQI model to evaluate the quality of drinking water. Horton (1965) has been the first to use the WQI concept successfully, which was then developed and improved by Brown et al., (1970). The improvement of WQI for groundwater is described in a number of studies (Backman et al., 1998; Ramakrishnalal et al., 2009; Soltan, 1999; Saeedi et al., 2009; Stigter et al., 2006a; Stigter et al., 2006b). In Iraq, this method has also been used in many studies and for multiple areas (Alhadithi, 2014, 2016; Al-Saadi, 2013; Amal et al., 2013; Khalid, 2011; Rizwan and Gurdeep, 2010). In the current study, the GIS technique has been used to create a water quality database and generate a WQI map to evaluate the groundwater in the Karbala province.

1.1 Study Area

The study area is located in the center of Iraq about 100 km south of Baghdad. It is bounded by latitudes $32^\circ 8' 00''$ to $32^\circ 51' 00''$ North and longitude $34^\circ 10' 00''$ to $44^\circ 17' 00''$ East (Figure 1). The study area is about 5,043 km² and has a population of about 1.067 million according to the census of 2011 (Al-Jiburi, 2002). The climate there is characterized by a cold weather in winter with low precipitation and hot dry summers (Al-Jiburi, 2002). The mean annual values of

precipitation, temperature and evaporation are 9.9 mm, 23.07 C° and 266.81 mm respectively while the relative humidity has a negative trend compared to the temperature and evaporation (Al-Jiburi, 2002).

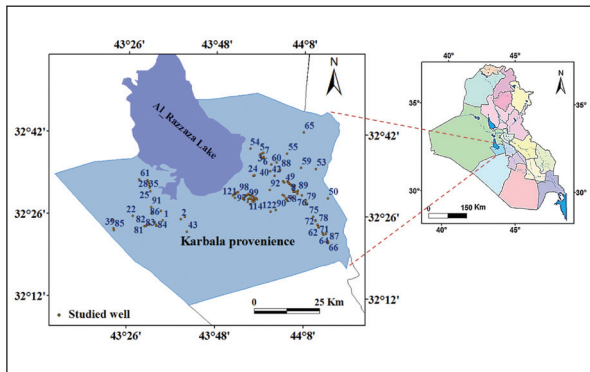


Figure 1. Location map of the study area

1.2 Geology and Hydrology of the Study Area

The geological outcrops in the studied area represent the Dammam, Euphrates, Nfayl, Fatha, Injana, Zahar and Dibdiba Formation as well as the Quaternary deposits which cover 80 % of the studied area. All the geological formations of the study area are described in Table 1. These formations represent part of two structural areas: Salman Zone which belongs to the stable shelf, and the Mesopotamia zone which belongs to the unstable shelf (Al-Jawad et al., 2002).

The study area can be divided into three regions from a topographic point of view, namely, the Mesopotamian plain, the Desert plain, Bahr Al-Najaf, and the Raazaza depression. The main groundwater aquifers in the west of the studied area are Dammam and Umm ErRathuma Formation while the main aquifer within the terregenous deposits of the desert plain is the Injana Formation. Dammam and umm ErRdhuma Formations represent the first and second aquifers within the carbonate rocks respectively.

Table 1. Geological Formations in the studied area

Era	Period	Age	Formation	Description
Cenozoic	Quaternary	Pliocene – Pleistocene	Dibdiba	Sandstone, which is generally white, pink and light grey, well-sorted, fine-coarse grained small pebbles are often reported. Sandstones contain mud balls, occasionally cross bedded. Other rock types are silty clay stone-clayey siltstone.
		Late Miocene	Injana (upper fares)	Generally, the formation consists of red, partly greenish silty, sandy calcareous claystone and lentils of grey, brownish, greenish and yellowish sandstone. Thin beds (0.30 m.) of marly and chalky limestone are occasionally present in the sequence
	Neogene	MiddleMiocene	Fatha (Lower Fars)	Generally consist of green, partly reddish in places sandy, dolomitic and gypseous marl with interbedded calcareous, partly sandy claystone and fossiliferous limestone
		Middle. Miocene	Nfayil	Lenticular sequence of reddish sandy calcareous claystone and brownish coarse grained sandstone, with limestone intercalations (0.2-2.0 m.)
		Early. Miocene	Euphrates	Basal breccia, limestone and marl. sub rounded, re-crystallized and dolomitized a nummulitic limestone, fragments ranging in size from 1 cm. - 20 cm. cemented by limy material
	Paleogene	Eocene	Dammam	Recrystallized anummulitic limestone, grey, creamy, yellowish and white in color, cavernous and Karstified
		Upper Paleocene	Umm Er Radhuma	Phosphates Limestone/ Dolostone, Dolomite
Mesozoic	Cretaceous	Cretaceous	Tayarat	Dolomitic limestone, silty clay sandstone

The main aquifer in the eastern part of studied area is the Quaternary deposits of the Mesopotamian plain. Figure (2) illustrates the extensions of the Formation of Dammam and its stratigraphical position with other formations along the studied area. The depth of the groundwater varies from one location to another (ranging between 12 and 270), and generally deepens towards the central part of the studied area as shown in Figure (3).

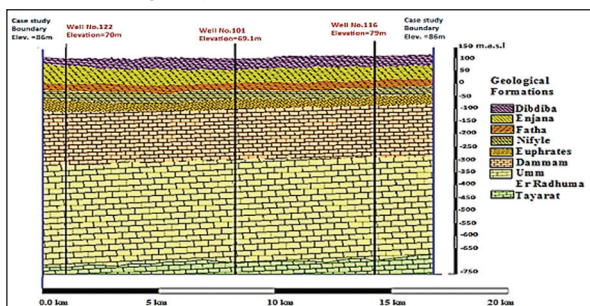


Figure 2. Stratigraphic correlation between the wells in the study area developed from Sissakian (1995) and Consortium-Yugoslavia (1977).

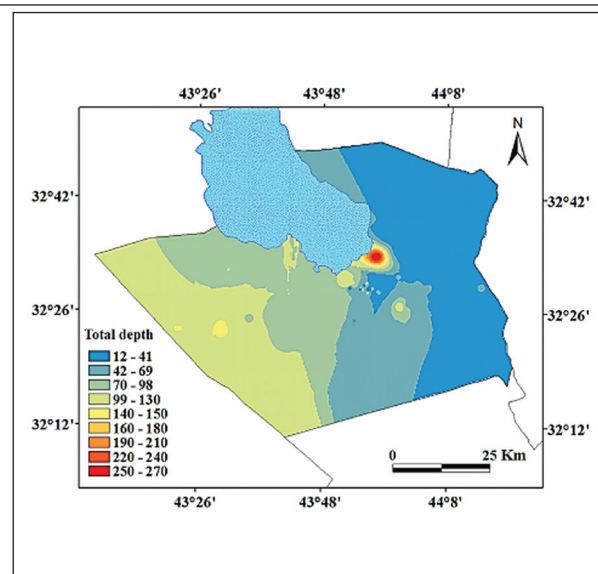


Figure 3. Total depth of groundwater map of the study area

The general direction of the groundwater flow is from west to east and from southwest tonortheast at the western parts of the area,while the groundwater flow is from northwest toward southeast at the Mesopotamian plain with local diversions (Rasul and Waqed, 2015). The most hydrogeological feature in the studied area is the lake of Al-Razzaza.

2. Martial and Methods

Ninety-two samples were collected from ninety-two water wells distributed along the study area; analysis is based on standard roads approved. The locations of these sites are shown in Figure 1. The parameters such as pH, TDS and EC were measured in the field after collecting the samples, while anions and cations were measured in all the groundwater samples in the laboratory. Cations (Ca²⁺, Na⁺, and K⁺) have been analyzed by flame photometer, and Ca²⁺+Mg²⁺ by the EDTA titration method. Bicarbonate has been analyzed by the H₂SO₄ titration method and chloride has been analyzed by the AgNO₃ titration method (Jackso, 1976).

All the measured values were transferred to GIS environment to create a spatial distribution map for each parameter using the Reverse Interpolation Technique (IDW). The results of these determinants were also used to calculate the values of water quality index, sodium percentage (Na %), and the sodium adsorption ratio (SAR).

2.1 Calculating Water Quality Index (WQI)

The groundwater chemical analyses have been used to calculate the water quality index values. The Iraqi drinking water standards for 1992 were taken into consideration also when calculating WQI as shown in Table 2. The weight (*wi*) for each chemical parameter has been assigned in the first step depending on its relative importance in the quality of water used for drinking purposes as presented in Table 4. Five is the maximum weight assigned for specific chemical parameters which are believed to be of great importance in the evaluation of water quality and a minimum weight of (2) is given for the chemical parameter that is believed to be not detrimental to the overall quality of water (Table 3).

Table 2. Drinking Water Quality Iraqi Standards (Khalid, 2011)

Parameters	Unit	Iraqi standards for drinking water
TDS	mg/L	500
pH		8.5
Ca ²⁺	mg/L	50
Mg ²⁺	mg/L	125
Na ⁺	mg/L	200
K ⁺	mg/L	12
Cl ⁻	mg/L	200
HCO ₃ ⁻	mg/L	200
SO ₄ ²⁻	mg/L	500
NO ₃ ⁻	mg/L	50

According to Ramakrishnalal et al. (1999) a higher weightage is given to nitrite (NO₃⁻) parameter than to the others because it plays an important role in the quality of drinking water, while a lesser weight was assigned to other parameters such as magnesium Mg²⁺, calcium Ca²⁺ and sodium Na⁺ because they are not harmful to the quality of groundwater for drinking purposes. In the second step and in order to assign the relative individual weight of each parameter, standardization was achieved using equation No.1 that is called the relative weight.

Table 3. Relative weight (Wi) values of each groundwater parameter.

Chemical parameters	Unit	Weight (wi)	Relative weight (Wi)
TDS	mg/L	4	0.13
pH		4	0.13
Ca ²⁺	mg/L	2	0.06
Mg ²⁺	mg/L	2	0.06
⁺ Na	mg/L	2	0.06
⁺ K	mg/L	2	0.06
⁻ Cl	mg/L	3	0.10
HCO ₃ ⁻	mg/L	3	0.10
SO ₄ ²⁻	mg/L	4	0.13
NO ₃ ⁻	mg/L	5	0.16
		31	1.000

$$Wi = wi / \sum_{i=1}^n wi \dots\dots\dots 1$$

Where *Wi* is relative weight, *wi* is the weight of each parameter, and *n* is the number of parameters. In the third step the quality rating scale (*qi*) is calculated according to equation number 2 by dividing each chemical parameter concentration (Ci) in each water sample by its respective Iraqi standards for drinking (Si) as shown in Table 5 and the result is multiplied by 100.

$$qi = (Ci / Si) * 100 \dots\dots\dots 2$$

In the fourth step, the sub index of the parameter (*SLi*) is calculated for each chemical parameter using the following relationship

$$SLi = Wi . qi \dots\dots\dots 3$$

Finally, WQI has been computed using the following relationship:

$$WQI = \sum SLi \dots\dots\dots 4$$

The method of calculating the water quality index was explained in detail as an example of well number one in Table 4.

Table 4. Calculating of the water quality index (WQI) of well No. 1

Chemical parameters	Sl	Weight (wi)	Relative weight (Wi)	Ci	qi	SLi	WQI
TDS	500	4	0.13	1945	389.0	50.19	114.7
pH	8.5	4	0.13	7.14	84.0	10.84	
Ca ²⁺	50	2	0.06	130	260.0	16.77	
Mg ²⁺	125	2	0.06	89	71.2	4.59	
Na ⁺	200	2	0.06	140	70.0	4.52	
K ⁺	12	2	0.06	10	83.3	5.38	
Cl ⁻	600	3	0.10	250	41.7	4.03	
HCO ₃ ⁻	200	3	0.10	63	31.5	3.05	
SO ₄ ²⁻	500	4	0.13	576	115.2	14.86	
NO ₃ ⁻	50	5	0.16	1.3	2.6	0.42	
		31	1.00				

2.2 Statistical Analysis

Statistical analysis of chemical parameters of water has been reported from the different divisions of India and other parts of the world (Dewangan et al., 2010; Dhirendra et al., 2009; Navneet and Sinha, 2010; Suhaimi- Othaman et al., 2007 and Antonopoulou et al., 2001). A statistical analysis of the chemical parameters of water was carried out using the statistical package for social sciences SPSS, 2009 version 18 to identify the physiochemical parameters that deviate from the Iraqi standards for the quality of drinking water.

The basic statistical test mean, standard deviation and

spearman's correlation matrix (assuming $p < 0.01$) are applied as shown in Tables 5 and 6. It can be noted that the mean for all the parameters are more than the limits of Iraqi standards except for the pH values, which fall within the limits. The standard deviation for TDS, Ca²⁺, Na⁺, K⁺, HCO₃⁻ and SO₄²⁻ is more than the limits, while the remaining parameters are within the limits of Iraqi standards for the quality of drinking water. The degree of a linear association between any two of the water quality parameters measured by the simple correlation coefficient (r) presented in Table 6.

Table 5. Descriptive statistics for all the studied wells

	TDS	pH	Ca ⁺²	Mg ⁺²	Na ⁺	K ⁺	Cl ⁻	HCO ₃ ⁻	SO ₄ ⁻²	NO ₃
Minimum	1100	7.1	70.0	32.0	81.0	2.0	149.0	63.0	293.0	0.1
Maximum	15200	7.9	1102.0	540.0	2331.0	273.0	3799.0	2013.0	3269.0	9.0
Mean	3342	7.3	262.3	130.5	451.4	41.6	621.5	373.0	999.7	3.0
Std. Deviation	2231	0.2	163.8	79.4	307.9	53.2	489.2	277.1	568.9	2.1
Iraqi St.	500	8.5	50	125	200	12	600	200	500	50

Table 6. Correlation coefficient for a studied well water sample and WQI

	TDS	pH	Ca ⁺²	Mg ⁺²	Na ⁺	K ⁺	Cl ⁻	HCO ₃ ⁻	SO ₄ ⁻²	NO ₃ ⁻³	WQI
TDS	1										
pH	-.084	1									
Ca ⁺²	.950	-.067	1								
Mg ⁺²	.841	-.070	.891	1							
Na ⁺	.946	-.058	.924	.767	1						
K ⁺	.639	-.020	.680	.655	.667	1					
Cl ⁻	.942	-.074	.950	.802	.963	.626	1				
HCO ₃ ⁻	.910	-.068	.897	.707	.936	.625	.916	1			
SO ₄ ⁻²	.886	-.062	.919	.926	.870	.772	.836	.766	1		
NO ₃ ⁻³	-.087	.240	-.106	-.133	-.112	-.266	-.118	-.034	-.182	1	
WQI	.972	-.068	.970	.874	.956	.781	.946	.917	.938	-.136	1

The correlation of the analysis measures the convergence in the relationship between the selected chemical variables. If the correlation coefficient is closer to +1 or -1, it represents the optimal linear relationship between the two chemical variables. The analysis of this method attempts to prepare the nature of the relationship among the drinking water chemical parameters determinants.

In the current study, only NO₃⁻ shows a poor negative correlation with all the ions and a poor positive correlation with pH. PH also indicates a poor negative correlation with all

the parameters. All other negative and positive correlations of the pairs are observed as moderate to good correlations. Good correlation indicates chemical weathering and leaching of secondary salts contribution followed by multiple source inputs such as the industrial and agricultural effluents, which exhibit a poor correlation in the groundwater (Udayalaxmi et al., 2010). In addition, good correlation reveals that most of the ions are related in different physiochemical reactions such as the ion exchange in the groundwater pattern.

2.3 Hydrochemical Classification

Hydrochemical facies or hydrochemical zonation for the present investigation has been carried out by plotting the percentage of the reacting values of major ions in Pipers (1944) trilinear diagrams (Figure 4). It has been observed that 80 % of the water samples fall in the zone of no dominant cation type, and 12 % of the water samples fall in the zone of sodium-potassium type, and that 8 % of the water samples fall in the zone of the calcium type. The alkalis type of water ($\text{Na}^+ + \text{K}^+$) exceeds the alkaline earth type of water ($\text{Ca}^{2+} + \text{Mg}^{2+}$) whereas strong acid anions ($\text{Cl}^- + \text{SO}_4^{2-}$) exceed the weak acids (HCO_3^-) which indicate non-carbonate hardness in all the samples. $\text{Na}^+ - \text{SO}_4^{2-}$ and $\text{Na}^+ - \text{Cl}$ facies, are of a bulk groundwater type in the study area representing 51 % and 31 % from the total water samples respectively.

The dominance of the $\text{Na}^+ - \text{SO}_4^{2-}$ facies reflects the presence of the evaporate minerals, which are the main source of these ions and it is evidence of recharge areas. The $\text{Na}^+ - \text{Cl}$ water type reflects the effect of geological formations on the quality of the studied groundwater which comprises halite. At few locations, the groundwater belongs to mixed $\text{Mg}^{2+} - \text{Ca}^{2+} - \text{SO}_4^{2-}$ and mixed $\text{Mg}^{2+} - \text{Ca}^{2+} - \text{Cl}$. Mixed water types ($\text{Ca}^{2+} \text{Mg}^{2+} \text{Cl}$) suggest the dissolution of rock forming minerals such as halite's and carbonate-bearing minerals and an ion exchange process.

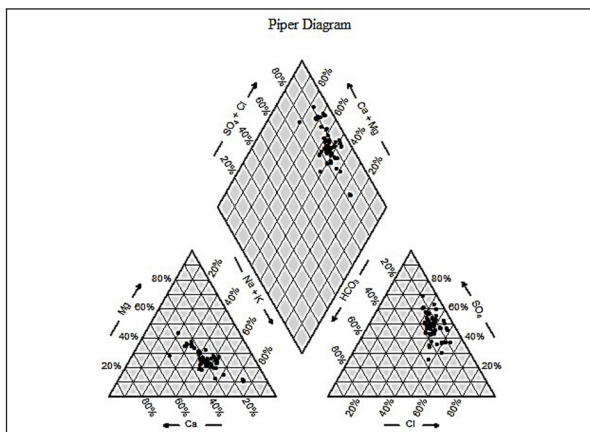


Figure 4. Piper diagram showing the chemical composition of groundwater in the study area

3. Results and Discussion

3.1 Total Dissolved Solid (TDS) and pH

The total dissolved solid (TDS) values for the studied wells ranged from 1200 to more than 14000 (mg/L). A spatial distribution map for TDS using the Reverse Interpolation Technique (IDW) has been prepared as shown in Figure 5a. It can be seen that the water samples show high values of TDS in all the studied wells, being much higher than the Iraqi standards for the quality of drinking water. According to Rao (1986), the high values of TDS may be attributed to the reduction of the osmotic activity of the plants, which interferes with the absorption of water and nutrients from the soil.

The pH values in the studied groundwater ranged from 7.1 to 7.9 as shown in Figure 5b. The pH values of water control the nature and environment of solubility of chemical constituents in the water. The decreasing in the value of pH in the water affects the balance of carbonates and bicarbonate. This results in the release of carbon dioxide and leads to an increase in the water's ability to dissolve increasing the concentration of dissolved salts (Abawi et al., 1990).

3.2 Cations and Anions

In the studied wells, calcium (Ca^{+2}) concentrations ranged from 71 to 1190 mg/L (Figure 5c). All the water samples exceeded the permissible limits of the Iraqi drinking water standards. The increased calcium concentration in the water samples of the studied wells can be ascribed to the geological nature of the area as well as the frequent use of the water wells. Magnesium (Mg^{+2}) values in the studied samples ranged from 32 mg/L to 540 mg/L as shown in Figure 5d.

In general, the source of magnesium in groundwater is the minerals containing magnesium; it is washed from rocks and subsequently ends up in water. Magnesium is used for many different purposes and consequently may end up in water through different ways (Deshpande and Aher, 2012). Chemical industries add magnesium to plastics and other materials as a fire protection measure or as filler. It also ends up in the environment from fertilizers' application and from cattle feed. The rock type in the study area is indurate to compacted clastic sediments hence the source of magnesium in the groundwater is clay.

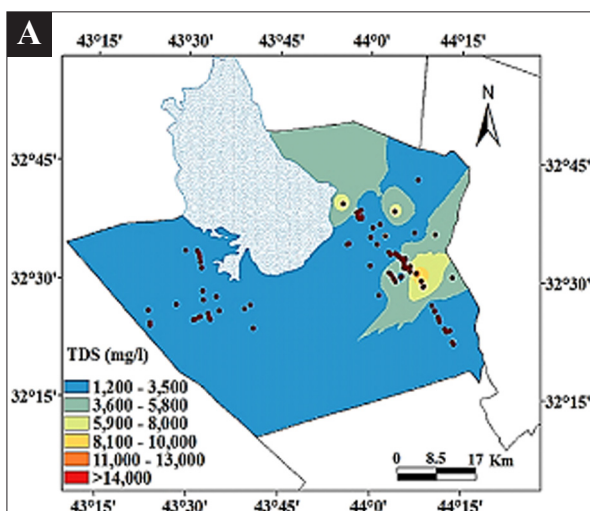


Figure 5.a: Spatial distribution map of TDS

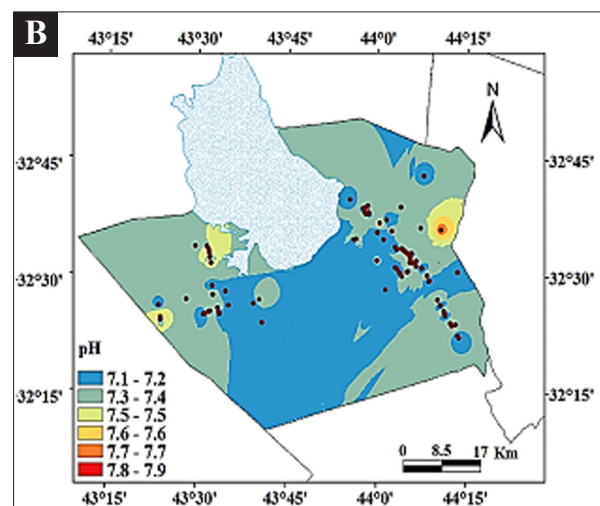


Figure 5.b: Spatial distribution map of pH

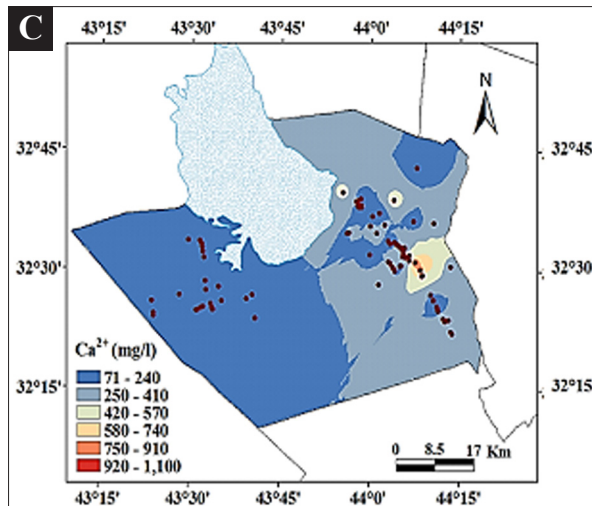


Figure 5.c: Spatial distribution map of Ca^{2+}

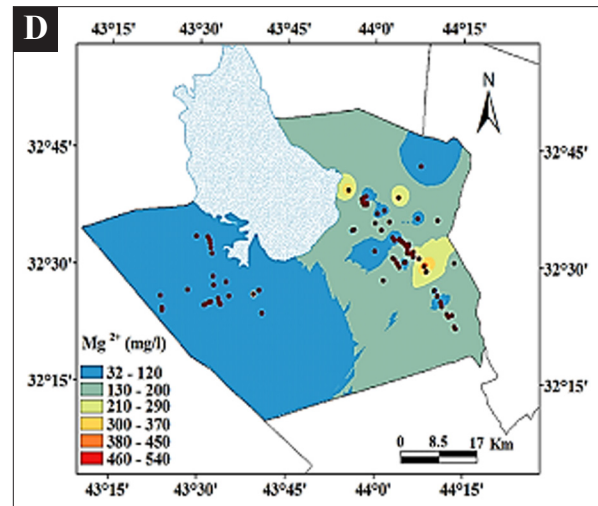


Figure 5.d: Spatial distribution map of Mg^{2+}

Potassium ion (K^+) is found in all the studied wells in higher concentrations than the allowable rates as is evident in Figure 5e. Sodium ion (Na^+) is usually present in groundwater and in high quantities. The upper limit of sodium allowed in drinking water exceeds 200 mg/L according to the Iraqi drinking water quality standards. In

general, each groundwater contains some sodium because most of the rocks and soils contain sodium ions, which dissolve easily (Alhadithi, 2014). Accordingly, 80 % of the water samples contain an acceptable sodium content in the south-eastern part of the study area which rises towards the north-eastern part as shown in Figure 5f.

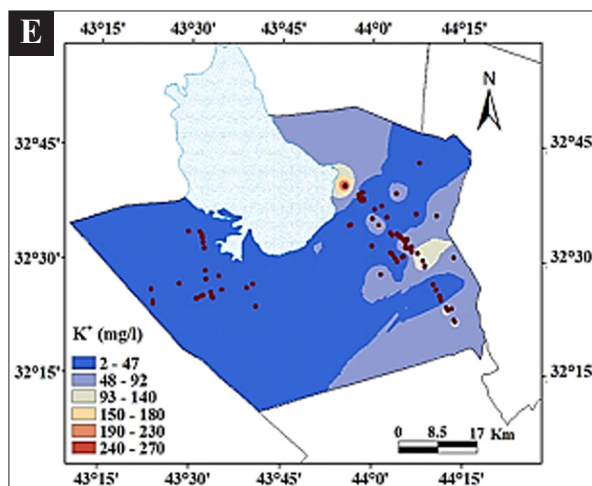


Figure 5.e: Spatial distribution map of K^+

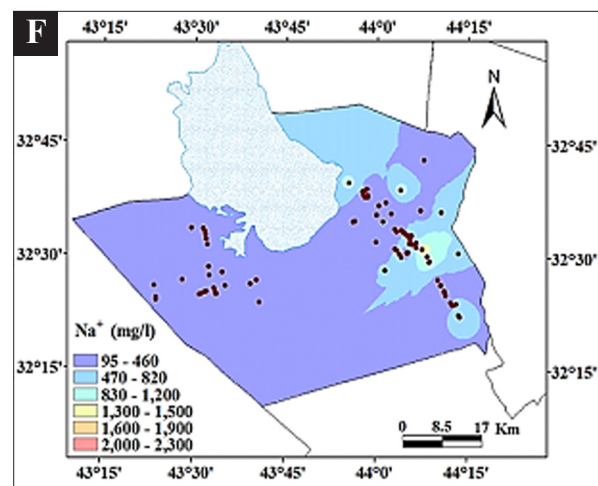


Figure 5.f: Spatial distribution map of Na^+

Bicarbonate (HCO_3^-) contents in the studied wells vary between 65 and 200 mg/L as shown in Figure 5g. Accordingly, 15 % of the studied water samples are within the limits of the Iraqi standards for drinking water quality, whereas the remaining wells have bicarbonate (HCO_3^-) rates higher than

the permissible limits. The chloride values were within the limits of Iraqi standards for drinking water quality in 2 % of studied water samples, but the remaining samples showed higher rates than the permissible limits as shown in Figure 5h.

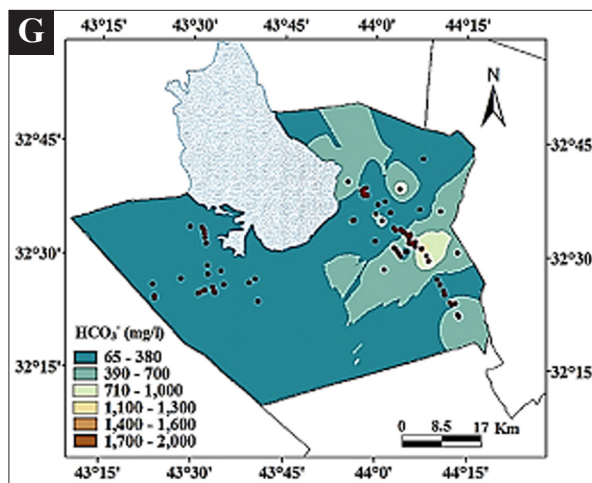


Figure 5.g: Spatial distribution map of HCO_3^-

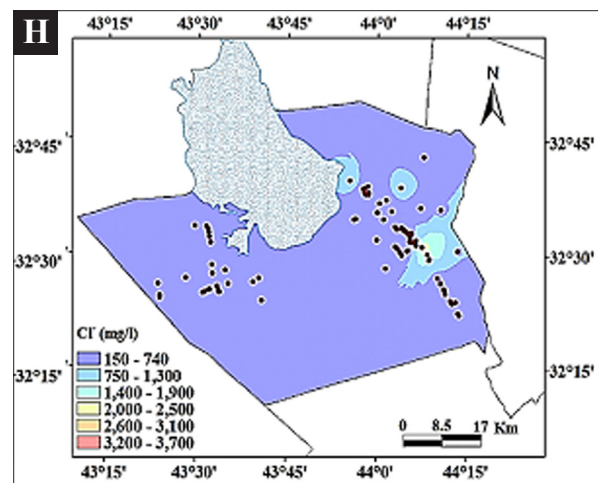


Figure 5.h: Spatial distribution map of Cl^-

Chloride (Cl⁻) is a broadly distributed element in all kinds of rocks in different forms. Therefore, it is mostly high in groundwater, where the rainfall is less and the temperature is high (Ramakrishnalal et al., 2009). Some soil characteristics such as porosity and permeability play a key role in building up the chlorides concentration (Chanda, 1999).

The concentration of Nitrate (NO₃⁻³) ranges between 0.024 and 8.8 mg/L in the studied wells (Figure 5i). The main

source of nitrate in the groundwater is either sewage and waste decomposition of organic substances or the excessive use of fertilizers (Karanth, 1987). The values of Sulphate (SO₄⁻²) vary from 300 to 3300 mg/L in the studied wells as shown in Figure 5j. Accordingly, water samples collected from only 2 % of studied wells have concentration higher than the permissible limits.

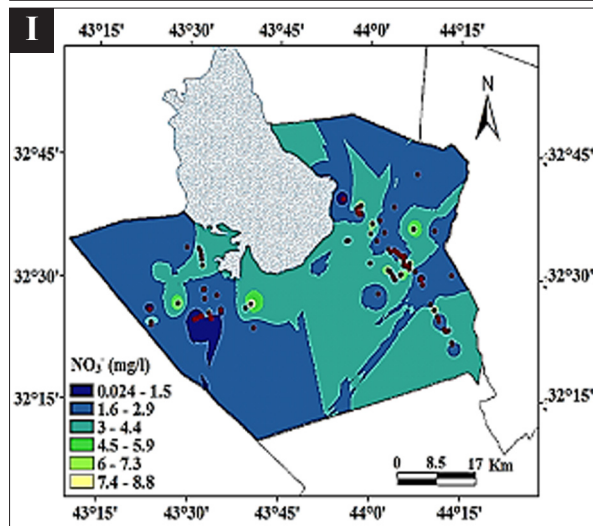


Figure 5.i: Spatial distribution map of NO₃⁻

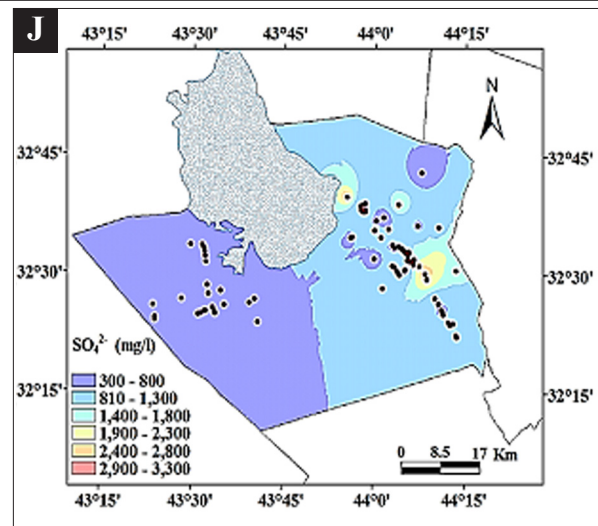


Figure 5.j: Spatial distribution map of SO₄⁻²

The spatial distribution maps of the constituents with the chemical analysis discussed above were made to evaluate the quality of Karbala groundwater for drinking uses depending on the data of ninety-two wells representing Karbala region. It is found that the tendency of the Karbala groundwater flow is in the north and northeast direction. The spatial distribution maps of the concentrations of the contaminants in Karbala groundwater give acceptable presentation of groundwater quality distribution due to the good correlation between the observed and estimated values of these concentrations. Therefore, these maps can be approximately used to estimate the suitable locations of new wells containing minimum harmful contaminants.

The analyses reveal that the major cation Na⁺ in the Karbala groundwater generally has dominant representation at an average of 59 % of all the cations. The major anions SO₄⁻² and Cl⁻ are also dominant at the average of 44 % and 43%, respectively of all the anions. Na₂SO₄ and NaCl components are mainly found in Karbala groundwater, therefore, it tends to have permanent hardness. The average concentration of all major ions in the Karbala groundwater is found in the order SO₄⁻²>Cl⁻>Na⁺>HCO₃⁻>Ca⁺²>Mg⁺²>K⁺>NO₃⁻. According to the average TDS value of 3342 mg/l, the Karbala groundwater is too unsuitable for drinking uses.

3.3 Generation of Water Quality Index (WQI) Map

According to Ramakrishnalal et al. (2009), the computed WQI values have been classified into five types, namely excellent water to unsuitable for drinking as indicated in Table 7. Based on the classification, only 1% of water samples fall within class II which represents a good water quality, and 57 % of the available water wells fall under class III which

indicates a poor water quality, 21% of the water samples fall in class IV which indicates a very poor water quality and 20 % of the samples are unsuitable water.

Table 7. Percentages of studied water well samples based on WQI values

WQI value	Class	Water quality	Percentage of studied water sample
<50	I	Excellent	Nil
50-100	II	good water	1%
100-200	III	poor water	57%
200-300	IV	very poor water	21%
>300	V	Unsuitable water	20%

All calculated WQI values have been transferred to GIS environment to create a spatial distribution map of WQI. It has been produced using then reverse interpolation technique (IDW) which can be considered as a general suited map for providing information and observation data visually about drinking water in the study area represented by the spatial distribution of the index of the quality of water used for drinking. This map enabled decision-makers to evaluate water for drinking purposes easily and for large areas because it shows the spatial distribution of groundwater quality as an index value. Figure (6) shows the spatial distribution map of WQI which has shown that the water in the study area is unstable for drinking purposes.

The reasons behind this could be the excessive depletion of groundwater and the cultivation of crops which consume a lot of water such as grass, in addition to not using modern irrigation methods. Another reason could be the mixing of Al-Razaza Lake waters with the groundwater.

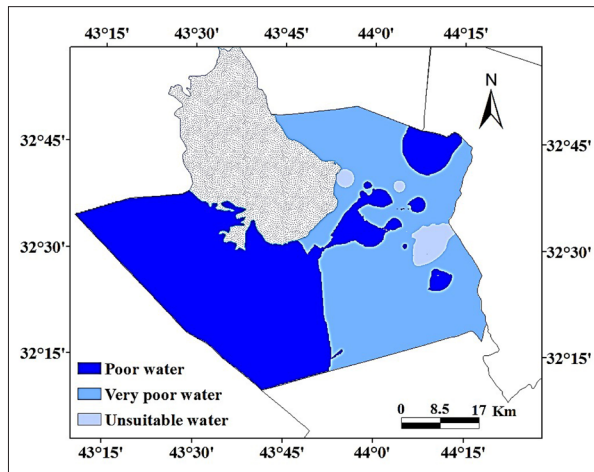


Figure 6. Spatial distribution map of WQI

3.4 Water Quality for Irrigation Purposes

Since most groundwater in the studied wells is not suitable as drinking water the outcome of the current study can be discussed further in attempting to provide water for purposes, other than the drinking purposes, such as irrigation in the city of Karbala. A standard diagram (Wilcox, 1955 and USSL, 1954) has been used to assess the suitability of water for irrigation purposes in the study area. Accordingly, the Electrical Conductivity (EC) has been measured in the field and the sodium percentage (Na %) and Sodium Adsorption Ratio (SAR) have been calculated based on the chemical analysis of Ca^{2+} , Mg^{2+} , Na^+ , K^+ using the following equations:

$$Na\% = (Na^+ + K^+) * 100 / Ca^{2+} + Mg^{2+} + Na^+ + K^+ \dots 5$$

$$SAR = Na^+ / \sqrt{(Ca^{2+} + Mg^{2+})/2} \dots\dots\dots 6$$

The percentages of sodium (Na %) ranging between 20 % and 76 % were plotted against specific conductance in the Wilcox diagram as shown in Figure 7. It shows that the groundwater of the study area is in bad condition. It is unsuitable in 34 % of the water samples, and is of a doubtful to unsuitable quality in 28 % of the samples. Only 2% of the

samples are of a good to permissible quality (Table 8). It is noted that 36 % of the water samples are out of the limits of the diagram because of the high value of the EC which can be considered or added to the proportion of unsuitable water quality.

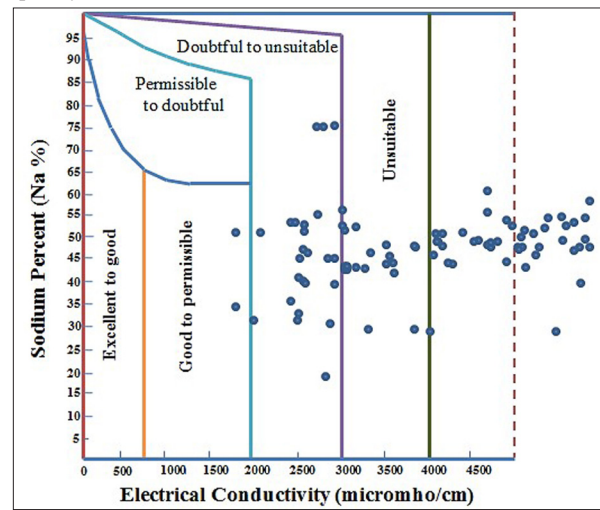


Figure 7. Diagram of the quality of irrigation water classification (Wilcox, 1955)

The calculated values of SAR in the study area varied from 4 to 16 meq which have been plotted on the US salinity. It is taken as an alkalinity hazard and the electrical conductivity (EC) is taken as a salinity hazard which is summarized in Table (8) and is shown in Figure (8). As is clear, only 4 % of samples fall in the C3-S1 fields, indicating a medium to high salinity and low alkalinity water; this means that this water can be used for irrigation, where a moderate amount of leaching and a moderate permeability with the leaching soil occur. Furthermore 96 % of the water samples fall in C4-S1, C4-S2, C4-S3 and C4-S4 field, is indicating a very high salinity and a low to medium sodium hazard. This water is not suitable for irrigation under normal conditions and further action of salinity control is required in the remediation of such problem.

Table 8. Classification of groundwater for irrigation in the study area

Wilcox, 1948	Well No	% of sample	USLL 1954	Well No	% of sample
Excellent	Nil	0	C3-S1	86,84,71,69	4
Good to permissible	71,84	2			
Doubtful to unsuitable	1,2,6,18,20,25,28,33,35,36,42,43,59,61,65,68,69,70,73,80,81,83,85,86,91,92	28	C4-S1	1,2,3,18, 42,59,70, 88	9
Permissible to Doubtful	Nil	0	C4-S2	4,6,7,8,9,10,11,12,13,19,22,24,26,28,30,31,33,35,36,37,38,39,40,41,44,45,46,47,48,49,50,52,53,57,60,61,62,63,65,66,67,68,72,73,74,75,77,78,81,82,83,85,87,90,91,92.	62
Unsuitable	3,4,5,9,10,11,12,13,14,19,22,24,26,30,38,39,40,52,60,62,66,67,72,74,75,77,78,82,87,88,7,8,15,16,17,21,23,27,29,31,32,34,37,41,45,46,47,48,49,50,51,53,54,55,56,57,58,63,64,76,79,89,90.	70	C4-S3	5,14,15,16,17,20,21,23,25,32,34,43,51,56,58,64,89	18
			C4-S4	27,29,54,55,76,79	7

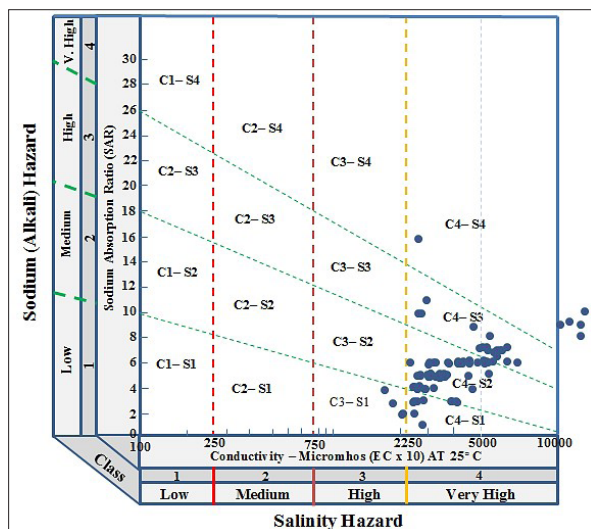


Figure 8. Diagram for irrigation water quality classification (USSL, 1954)

4. Conclusions

The GIS technique has been applied in the present study to create a water quality index map to evaluate the quality of groundwater in the Karbala province used for drinking purposes in a precise manner. Chemical parameters of the water samples including cations and anions have been considered to calculate WQI. It has been observed that the water samples fall in the poor water to unsuitable water categories. More detailed analyses have been conducted by plotting analytical data on USSL and Wilcox diagrams to assess the suitability of well water for irrigation purposes.

The results show that only 1 % of the studied groundwater samples can be used for drinking purposes, and 4 % can be used for irrigation purposes. Also, the current study has clearly shown that the techniques of GIS and water quality index are efficient, economic, fast, and easy means to evaluate the quality of groundwater for drinking purpose.

Recommendation

Conducting hydrogeological studies and detailed examinations of the water-bearing formations, including the exposed ones along with studies and interpretations of the subsurface geology from the lithology data along with selected subsurface geological sections.

The use of modern irrigation methods instead of the traditional ones.

The construction of dams which recharge the aquifer to prevent the circulation of the Al-Razzaza Lake waters with groundwater.

Preventing the cultivation of crops which consume large quantities of water.

Monitoring the amounts of water pumped out of wells.

References

Abawi, Suad, A. R and Hassan Salman, M. (1999). Scientific Engineering of the Environment Water tests, Dar Al-Hakma publishing company, Baghdad, 296p.

Alhadithi, M. (2004). Groundwater evaluation of a typical watershed in piedmont zone of Himalaya, India. Ph D thesis, IIT Roorkee, Roorkee.

Alhadithi, M. (2014). Use of Water Quality Index Technique to Assess Groundwater Quality for Drinking Purposes in Saqlawiyah. Tikit Journal of Pure Science, 19: 89-95.

Alhadithi, M. (2016). Water wells quality assessment for drinking purposes using water quality index and correlation study in Al-qaim City, Al-Anbar, Iraq. Al-Anbar Journal of Agriculture Science, 14: 3e-14e.

Al-Jawad, S.B., Al-Dabagh R.H., Mussa, M.S., and Al-Hady, H.A. (2002). Hydrogeology of the Aquifers in the Western Desert -west and south of the Euphrates River, sections I and II, the national program, unpublished.

Al-Jiburi H.K., (2002). Hydrological and hydrochemical study of Kerbala. Quadrangle Sheet (NI-38-14), State Company of Geological Survey and Mining, Iraq.

Al-Saadi, R.J.M. (2013). Contour Maps and Evaluation of Groundwater Quality in Karbala Region, Journal of Kerbala University, 11(1): 204-222.

Antonopoulos, V.Z., Papamichail, D.M., and Mitsios, K.A. (2001). Historical and trend analysis of water quality and quantity data for the Strymon River in Greece. Hydrology and Earth System Sciences Discussions, European Geosciences Union, 2001, 5(4): 679-692.

Backman, B., Bodis, D., Lahermo, P., Rapant, S., and Tarvaine, T. (1998). Application of groundwater contamination index in Finland and Slovakia. Environmental Geology, 36(1-2): 55-64.

Brown, R.M., McClelland, N.I., Deininger, R.A., and Tozer, R.G. (1970). A water quality index: Do we dare? Water & Sewage Works, 117: 339-343.

Chanda, D.K. (1999). A proposed new diagram for geochemical classification of natural waters and interpretation of chemical data. Hydrology Journal, 5(7): 431-439.

Consortium-Yugoslavia, (1977). Water development projects, western desert-Blook7, hydrogeological explorations and hydrotechnical work, hydrogeology, Vol. (5), Republic of Iraq, and Directorate of western desert development projects.

Deshpande, S.M., and Aher, K.R. (2012). Evaluation of Groundwater Quality and its Suitability for Drinking and Agriculture use in Parts of Vijapur, District Aurangabad, MS, India. Jour. Chem. Sci., 2(1): 25-31.

Dewangan, S., Vaishnav, M.M., and Chandrakar, P.L. (2010). Pre-monsoon statistical analysis of physicochemical parameters and heavy metals in different water bodies of Balco area, Korba (C.G.). Rasayan Journal of Chemistry, 3: 710-720.

Dhirendra M.J., Narendra, S.B., Alok, K., and Namita, A. (2009). Statistical analysis of physicochemical parameters of water of river Ganga in Haridwar district. Rasayan Journal of Chemistry, 2(3): 579-587.

Horton, R. K. (1965). An index number system for rating water quality. Journal-Water Pollution Control Federation, 37: 300-305.

Israil, M., Al-hadithi, M.S., Singhal, D., Bhishm Kumar, C., Rao, M.S., and Verma, S.K. (2006). Groundwater resources evaluation in the Piedmont zone of Himalaya, India, using Isotope and GIS techniques. Journal of Spatial Hydrology, 6(1): 34-48.

Jackson, M.L. (1976). Soil Chemical Analysis. Prentice Hall Inc. Englewood Cliffs, NJ, USA, pp. 227-267.

Joshi, D.M., Bhandari, N.S., Kumar, A., and Agrawal, N. (2009). Statistical analysis of physicochemical parameters of water of River Ganga in Haridwar district. Rasayan Journal of Chemistry, 2: 579-587.

Karant, K.R. (1987). Groundwater Assessment, Development and Management, Tata McGraw Hill publishing company Ltd., New Delhi, 725p.

Khalid H, L. (2011). Evaluation of Groundwater Quality for Drinking Purpose for Tikrit and Samarra Cities using Water Quality Index. European journal of scientific research, 58(4): 472-481.

Mahmood, A.A., Eassa, A.M., Mohammed, M.H., and Shubbar, I.Y. (2013). Assessment of ground water quality at Basrah, Iraq by water quality index (WQI). Journal of Babylon University/Pure and Applied Sciences, 21(7): 2531-2543.

- Navneet, K., and Sinha, D.K. (2010). Drinking water quality management through correlation studies among various physico-chemical parameters: A case study. *International Journal of Environmental Sciences*, 1(2): 235-259.
- Piper, A.M. (1944). A graphic procedure in the geochemical interpretation of water analyses. *Trans. American. Geophysical Union*, 25: 914-923.
- Ramakrishnalal, C.R., Sadashivalah, C., and Rangann, G. (2009). Assessment of water quality index for the groundwater in Tumkur Taluk, Karnataka state, India. *E Journal of chemistry*, 6(2): 523-530.
- Rao, N.S. (1986). Hydrogeology and hydrogeochemistry of Visakhapatnam. Ph.D Thesis unpublished.
- Rasul, M.K., and Waqed, H.H. (2015). Evaluation of irrigation water quality index (IWQI) for al-dammam confined aquifer in the west and southwest of Karbala city, Iraq. *International Journal of Civil Engineering (IJCE)*, 2(3): 21-34.
- Rizwan, R., and Gurdeep, S. (2010). Assessment of Ground Water Quality Status by Using Water Quality Index Method in Orissa, India. *World Applied Sciences Journal*, 9(12): 1392-1397.
- Saeedi, M., Abess, O., Sharifi, F., and Meraji, H. (2009). Development of groundwater quality index. DOI: 10.1007/s: 10661-009-0837-5.
- Schoeller, M. (1972). Etude geochemical de la nappes dans les Ferieuresdubas d' Aquitaine *journal of hydrology*, 15(4): 317-328.
- Sissakian, V.K. (1995). Geologic map of Karbala quadrangle, sheet NI-38-14, Geologic map of Iraq GM 26, Scale 1:250000, 1st Edition, Baghdad, Iraq.
- Soltan, M.E. (1999). Evaluation of groundwater quality in Dakhla Oasis (Egyptian Western Desert). *Environmental Monitoring and Assessment*, 57(2): 157– 168.
- SPSS Inc. (2009). PASW Statistics for Windows, Version 18.0. Chicago: SPSS Inc.
- Stigter T.Y., Ribeiro, L., and Carvalho Dill, A.M.M. (2006a) Application of a groundwater quality index as an assessment and communication tool in agro environmental policies—Two Portuguese case studies. *Journal of Hydrology (Amsterdam)*, 327: 578–591.
- Stigter, T.Y., Ribeiro, L. and Carvalho Dill, A.M.M. (2006b). Evaluation of an intrinsic and a specific vulnerability assessment method in comparison with groundwater salinisation and nitrate contamination levels in two agricultural regions in the south of Portugal, *Journal of Hydrogeology*, 14(1–2): 79–99.
- Suhaimi –Othaman M., Ahmad, A., Mushrifah, I., and Lim, E.C. (2007). Seasonal influence on water quality and heavy metal concentration in Tasik Chini, Peninsular Malaysia, *Proceedings of Taal, The 12th World Lake Conference*, 300-303.
- Udayalaxmi, G., Himabindu, D., and Ramadass G. (2010). Geochemical evaluation of groundwater quality in selected areas of Hyderabad, A.P., India, *Indian Journal of Science and Technology*, 3(5): 546-553.
- USSL., 1954. Diagnosis and improvement of saline and alkali soils. USDA Agr. Handbook No. 60, Washington DC.
- Wilcox LV (1955). Classification and use of irrigation water, US Department of Agri., Circ. No. 969, Washington, DC.

The Effectiveness of Continuous Contour Ridges and Intermittent Trenches Constructed Using the Vallerani in Water Harvesting in Arid Regions

Kefah I. Yousef, Ahmad M. Abu-Awwad*, Michel Rahbeh

Department of Land, Water and Environment, Faculty of Agriculture, The University of Jordan, Amman, Jordan.

Received 31 May, 2018; Accepted 9 August, 2018

Abstract

Rainwater harvesting (RWH) is the most economic and sustainable management method utilized to overcome the problem of water penury in arid regions. Jordan is one of the countries in the Middle East most suffering from water deficit since more than 80% of the country's area receives 50-150 mm of annual rainfall. Different water harvesting techniques (WHT) have been used in many countries in arid and semi-arid regions. An evaluation experiment was conducted at two sites; one is at Al Mwaqar, southeast of Amman, and the other is at Al Grain, west of Al Azraq city. The objective of the current research is to evaluate and determine the effectiveness of two water harvesting techniques constructed by the common Vallerani system using continuous contour ridges and intermittent trenches (bunds) upon effective rainfall (runoff) affected by different land slopes, contour ridges spacing, and water harvesting structures. The results indicated that RWH increases water storage in planted area by two to three, fold depending on land slope and the contour ridges space, but with no significant differences between the applied WHT. Runoff amount increases with the increase of slope gradient (more than 5%), especially in small ridges space, which has shown the highest seasonal runoff range from 300 to 362 m³ha⁻¹ at Al Mwaqar site and from 192 to 243.5 m³ha⁻¹ at Al Grain site. Regression results indicated that there is high coloration between rainfall storms and runoff amount for all treatments. The best regression trend line was obtained from continuous contour ridges CT1 and CT2 with R² being 0.95 and 0.96, respectively, at Al Mwaqar site. At Al Grain site R² for continuous contour ranges between 0.70 and 0.76 compared to R² which ranges from 0.80 to 0.93 for Vallerani intermittent trenches, due to the effect of rock fragments on the catchment surface in the continuous contour area.

© 2018 Jordan Journal of Earth and Environmental Sciences. All rights reserved

Keywords: Water harvesting, Vallerani, Contour ridges, Intermittent trenches, Runoff, Arid regions.

1. Introduction

Jordan is a developing country located to the southeast of the Mediterranean Sea between 35° and 39° East and latitudes 29° and 33° North. Its area is about 90,000 km² and consists of various distinctive topographic units trending in a north-south direction. These units are the Rift Valley, heights and the arid-desert region called locally Badia (Alayyash et al., 2012). Historically, the term 'Badia' refers to the region where Bedouins live, with an annual rainfall of about 50–150 mm. Jordanian Badia is subdivided into three geographical areas (Allison et al., 1998): Northern Badia with an area of 25,900 km² (about 35% of the total Badia area), Middle Badia with an area of 9,600 km² (about 13%), and Southern Badia with an area of 37,100 km² (about 51%). Jordan weather is severe and the variations in the hydrological parameters such as rainfall, runoff and evaporation are wide. They vary from day to day, from summer to winter, and from one year to another.

Water scarcity is one of the main challenges that Jordan has been consistently facing. The current per-capita annual share of water is estimated at 140 m³ which is well below the 1000 m³ threshold (Al-Adamat et al., 2012). The rising air temperatures, coupled with the change in precipitation patterns,

are expected to increase water scarcity (Al-Bakri et al., 2013). By the year 2025, the per-capita water share is expected to fall below 91 m³ per annum due to the limited water resources and the increase in population (Al-Bakri et al., 2013).

This severe water shortage has to be resolved by a comprehensive approach to manage both the water supply and water demand. While meeting domestic water needs has been given priority by the national government, the importance of the agricultural sector to rural employment requires an approach heedful of improving agricultural water security. The sustainable use of water can maintain a balance between the demands and supply (Rahman et al., 2014). Rainwater harvesting (RWH) is the most traditional and sustainable method which can be easily used in the Badia region to improve range lands (FAO, 2016).

Naseef and Thomas (2016) defined rainwater harvesting as a technique used to effectively trap the surface runoff. In technical terms, water harvesting is defined as the process of concentrating precipitation through runoff. Instead of causing erosion, the runoff will be harvested and utilized for beneficial uses (Critchley and Siegert, 1991). Rainwater harvesting has emerged as a vital means for improving water management and soil water conservation in scarce-water environments

* Corresponding author. e-mail: abuawwada@gmail.com

(Ziadat et al., 2006). Wisseret et al., (2010) defined rainwater harvesting as a beneficial tool of used 'green water' which consists of consumptive water used in biomass production as a nutrition chain/cycle which begins with plants and ends with humans.

The objectives of RWH include improving water availability for plants, improving soil structure by increasing organic matter, decreasing soil erosion rates, reducing the impact of drought, reducing surface runoff, and improving the capacity of the soil to store water (Shawaheen et al., 2011). Therefore, RWH is a direct productive form of soil and water conservation. Yield and production reliability can be significantly improved through rainwater harvesting (Critchley and Siegert, 1991; Ziadat et al., 2006). Consequently, human intervention through using water harvesting can enhance the ecosystem functions in scarce-water areas.

Rainwater harvesting systems are typically classified into three categories based on the size of the runoff-producing area: on-farm systems, in situ, micro-catchment systems, and macro-catchment systems (Studer and Liniger, 2013). In situ systems capture rainfall where it falls and ensures that crops make the most effective use of scarce water. These include the use of deep tillage, dry seeding, mixed cropping, ridges and borders, terraces, and trash lines. Micro-catchment systems include pitting, strip catchment tillage, contour bunds, and semi-circular bunds that create a distinct division between a runoff-generating catchment area and a cultivated basin where the runoff is concentrated, stored, and productively used by the plants. Macro-catchment rainwater harvesting is characterized by large catchment areas, where the catchment area for this system is located outside the cropped area.

In Jordan, water-harvesting techniques can help re-establish the productive functioning of rangeland environments. These rangelands are fragile and subject to severe degradation due to drought and misuse, limited feed resources for livestock, and the desertification process. Since sheep are an integral part of the Bedouins' life, representing a source for food and clothing as well as a symbol of wealth and pride, grazing in the Badia used to be sustainable (Allison et al., 1998; Oweis et al., 2006). This lifestyle induced a set of values and laws and formed an environment-friendly system based on the principles of sustainability and self-sufficiency. It has been reported that water harvesting in these areas has resulted in improved fodder shrubs survival, productivity, and water-use efficiency (Abu-Zanat, 2004).

Micro catchment water harvesting is a method used for collecting surface runoff/sheet (and sometimes rill) flow from small catchments of short length, and water is concentrated in an adjacent application area, and is stored in the root zone for direct use by plants. Catchment and application areas alternate within the same field; thus, rainwater is concentrated within a confined area where plants are grown. Hence, the system is replicated many times in an identical pattern. Micro catchment water harvesting techniques are often combined with specific agronomic measures for annual shrubs (Hai, 1998).

The most important factors to be taken into account in the establishment of a water harvesting project include rainfall intensity and distribution, catchment runoff characteristics,

soil depth, physical properties of the cultivated area, type of crops, and the social and economic conditions of the farmers (Shatanawi, 1995).

Generally speaking, a water harvesting project consists of an area divided into two sections: the catchment area (C) or the harvest area where runoff-rainwater is taken from and the cultivated area (CA) where the water is concentrated and stored. The ratio of catchment area to cultivated area (C: CA) can range from 1:1 up to 100:1 (FAO, 1991). Usually, trenches and contour ridges for water harvesting are constructed manually by laborers. The Vallerani System provides the possibility to establish micro catchments along contour lines in a fast and cheap manner (FAO, 2016).

Vallerani trenches are established using a tractor with adequate power (minimum 190 hp) in order to pull the special type of ploughs. The ploughs have been specifically designed by Venanzio Vallerani (1988) to be used under arid and semi-arid conditions for fast rehabilitation of large extensions of land at a low cost (Vallerani system web). It can be adapted to various needs, with different spacing between the contour ridges lines and adjusting the depth and length of work (GIZ, 2012).

The basic parameters needed to determine trenches spacing (Vallerani System) are: soil depth (at least 60 cm), land slope, and rainfall characteristics (FAO, 2016). The recommended number of Vallerani trenches (micro catchments) and the spacing between trenches according to Karrou, et al. (2011) are 250-400 trenches/hectare, five- seven meters apart for a gentle slope (4% to 9%) and 400-600 trenches/hectare, three to four meters apart for a steeper slope (more than 15%).

Youssef (1998) stated that the most efficient and applicable type of water harvesting technique is the contour ridges, with runoff catchment area to cultivated area ratio of 6:1. The highest amount of runoff yield was 6.7 mm for contour ridges compared with 4.1 mm for semi-circle technique at a 67% probability; about 24 mm rainfall.

This study is aimed at evaluating the effectiveness of the water harvesting techniques constructed by the common Vallerani system using continuous contour ridges and intermittent trenches (bunds) on runoff yield (effective rainfall) at two different sites.

2. Methodology

2.1 Investigated Area:

Two study sites were selected. The first site is at Al Mwaqar (N:31.76109 and E:36.27274), located southeast of Amman with an annual rainfall ranging between 120 mm and 150 mm and the land slope ranges between 0% and 15%. The second site is at Al Grain (N:31.9695 and E:36.68367) located to the west of Al Azraq with an annual rainfall between 70 and 100 mm and the land slope ranging between 0% and 10%. The two sites are located within the arid zone area of Jordan under the Badia Restoration Program (Figure 1). Most of the time, rainfall at both sites is characterized by rapid showers with poor distribution.

Contour ridges and intermitted bunds were constructed by the Vallerani plow according to land slope and land use by the National Center for Agriculture Research and Extension (NCARE).

2.2 Rainwater Harvesting Design

Area and the spacing between contour ridges were calculated using the following equations (FAO, 1991):

$$\text{Spacing between Contours} = \frac{WR - RFLT}{RFLT \times RC \times Eff} \dots\dots\dots 1$$

Equation (2) is a simplified form of equation (1):

$$\frac{C}{CA} = \frac{WR - DR}{DR \times RC \times Eff} \dots\dots\dots 2$$

Where:

C: catchment area (m²)

CA: cultivated area (m²)

WR: annual water requirement (mm)

RFLT: rainfall long term (mm)

DR: annual design rainfall (mm)

RC: runoff coefficient

Eff: efficiency factor, normally ranges between 0.5 and 0.7 (FAO, 1991).

The design rainfall represents the amount of rainfall that equals to or exceeds the seasonal rainfall, calculated at a certain probability of occurrence at which the system is designed to provide enough runoff to meet the crop water requirement. If rainfall is below the “design rainfall,” there will be a risk for crop failure due to moisture stress. On the other hand, if rainfall is above the “design rainfall”, runoff will be a surplus and may overtop the bunds (FAO, 1991).

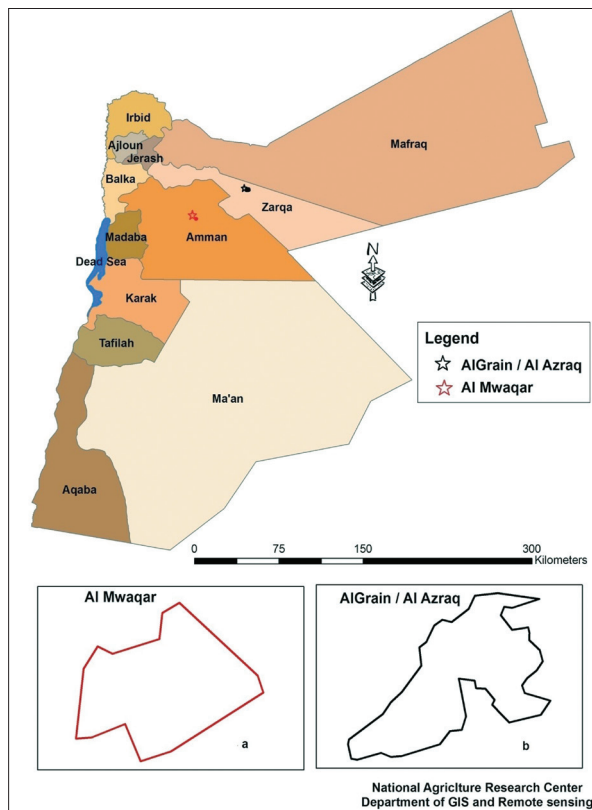


Figure 1. Research sites location; (a) for Al Mwaqar site map and (b) for Al Grain site map.

Increasing the C:CA ratio for high probability will decrease such risks. For example, if the probability of occurrence is set at 67%, this means that design rainfall will be met or exceeded (on average) in two years out of three years and the harvested rain will satisfy the crop water requirements also in two out of three years (FAO, 1991).

The runoff coefficient (RC) is a dimensionless coefficient relating the amount of surface runoff to the amount of rainfall received. It has a larger value for areas with low infiltration

and high runoff (such as pavement and steep gradient), and a lower one for permeable, well-vegetated areas (such as forests or flat lands) and ranges between 0.2 and 0.35 for poorly-graded clay loamy, silty clay loamy soil and soil with a slope ranging between 2% and 10% (FAO, 1991).

The total worked areas at Al Mwaqar and Al Grain sites were 120.6 and 122 hectares, respectively. For both sites, spacing between continuous contour ridges and/or intermittent trenches ranges from 10 m for the land surface slope that exceeds 5% to 17 m for that below 5%. The width of the trench was 1 m.

In this research, eight treatments were investigated in an area that was not planted using two land surface slopes <5% and >5% and four spacing 10-12, 12-14 as small space, and 14-16, 16-18 m as large space (Table 1).

Table 1. Treatments: “V” represents intermittent trenches and “CR” represents continuous contour ridges

Technique	Slope (%)	Spacing (m)	Area (m ²)	Treatment symbol
Intermittent trenches (V)	< 5	17-18	35: (17.5x2)	V T1
	< 5	12-14	26:(13 x2)	V T2
	> 5	10-12	22: (11x2)	V T3
	> 5	15-16	31: (15.5x2)	V T4
Continues Contour (C)	< 5	17-18	35: (17.5x2)	C T1
	< 5	12-14	26: (13x2)	C T2
	> 5	10-12	22: (11x2)	C T3
	> 5	15-16	31: (15.5x2)	C T4

The effective rainfall (Runoff) volume stored was estimated by measuring the soil moisture at three depths (0-10 cm, 10-30 cm and 30-50 cm) in the cultivated area within 24-48 hours after each significant rainfall event. Effective rainfall stored in the crop root zone represents the difference in the soil moisture between the day before and the day after the rainfall event. Evaporation amounts were calculated based on weather data (Equation 3); then they were added to the effective rainfall equation (5).

$$Ev = (1 - kcb \times f(tw)) \times Fw \times Etr \dots\dots\dots 3$$

Where:

Ev: wet soil evaporation adjustment in mm/day

Kcb: basal crop coefficient for the day of wetting

f(tw): a time dependent decay function

$$f(tw) = 1 - \left(\frac{tw}{td} \right)^2 \dots\dots\dots 4$$

where

Fw: proportion of gross land area which was wetted.

Etr: reference crop ET in mm/day

tw: time or days since wetting

td: time in days required for the soil surface to become dry

$$\text{Effective rainfall (runoff)} = SWCa - SWCb + Ev \dots\dots\dots 5$$

where

SWCa: soil water content after significant rainfall event (mm).

SWCb: soil water content before significant rainfall event (mm).

Ev: evaporation (mm)

2.3 Relationship between Effective Rainfall and Calculated Runoff Yield

Runoff was calculated using the direct relationship between rainfall and runoff using runoff coefficient (Boers, 1994):

$$\text{Runoff Volume} = \text{Rainfall} \times \text{catchment Area} \times \text{Runoffcoefficient} \dots\dots\dots 6$$

2.4 Rainwater Harvesting Design

• **Soil water content:** Gravimetric method was used to measure the soil moisture at three depths 0-10 cm, 10-30 cm and 30-50 cm (Black, 1965). Measurements were taken before and within 24 - 48 hours after any significant rainfall event along the trench. For each treatment, a composite of two soil samples were collected from the three depths in three replications, for both sites.

• **Soil Physical and Chemical Properties:** Infiltration rate, soil texture, bulk density, soil water holding capacity, soil acidity (pH), soil salinity (EC), CaCO₃ and total nitrogen were determined, spatially distributed, and depth-integrated (20 cm incremental depth) at four locations for each research site.

2.5 Statistical Analysis

Split plot design with three replicates was used as experimental design. Season runoff for all treatments was analyzed by using SAS program a Duncan's Multiple Range Test.

3. Results and Discussion

3.1. Soil Properties

Some soil physical and chemical properties, for both sites, are presented in Tables 2 and 3. The results showed that

soil texture is the same for both sites being clay loam. Basic infiltration rate varies from 3.2 mm/hr at the catchment area to 4.0 mm/hr at the cultivated area; and from 2.6 mm/hr at the catchment area to 3.7 mm/hr at the cultivated area for Al Mwaqar and Al Grain sites, respectively. Soil texture, or the percentage of sand, silt, and clay in a soil, is the major inherent factor affecting infiltration. Water moves more quickly through the large pores in sandy soil than it does through the small pores in clayey soil, especially if the clay is compacted and has little or no structure or aggregation. Infiltration rate is most affected by the conditions near the soil surface, and can change drastically according to management. Indeed, infiltration capacity which was determined based on the final infiltration rate, is the most important factor controlling runoff generation in the hill slopes land (Roth, 2004).

The low infiltration rate for both sites could be attributed to the high silt percentage (40.6 – 43.0%) at the soil surface layer, causing surface crust and enhancing surface runoff at the catchment area. This result is consistent with Lal and Shukla (2004), who noted that soils that have surface sealing of pores and crusting consequently have less infiltration and high runoff.

Table 2. Soil physical properties at Al Mwaqar and Al Grain sites

Site	Soil depth (cm)	Texture			Bulk Density Kg/m ³	Water Holding Capacity (mm/m)	Hydraulic Conductivity (mm/hr)	Basic Inflation Rate	
		Clay %	Silt %	Sand %				CA (mm/hr)	C (mm/hr)
Al Mwaqar	0-10	35.8	40.6	23.6	1.32	162	2.8	3.2	4
	10-30	33.7	37.3	29	1.23		2.4		
	30-50	36.6	42.2	21.1	1.16		2.6		
Al Grain	0-10	33.5	43	23.5	1.26	210	2.4	2.6	3.7
	10-30	32.9	41.7	25.4	1.17		2.37		
	30-50	33.6	39.1	27.3	1.23		2.28		

Table 3. Soil chemical properties at Al Mwaqar and Al Grain sites

Site	Soil depth (cm)	pH	ECe(dS/m)	Ca	Mg	Na	Total Cation	SAR	CaCO ₃ %	N %
				Meq/L						
Al Mwaqar	0-10	8.3	1.05	1.7	2.4	8	12.1	6.1	18	0.036
	10-30	8.3	1.06	2.05	1.6	6.7	10.35	5	24.1	0.037
	30-50	8.2	0.82	1.5	1.4	4.8	7.7	4.4	23.8	0.031
Al Grain	0-10	8.2	1.18	2.5	2.4	6.5	11.4	4	22.7	0.057
	10-30	8.3	1.15	3	2.5	6.7	12.2	4.5	22.5	0.058
	30-50	8.1	1.69	3.5	3.6	10.4	17.4	5.8	36.5	0.040

3.2 Effective Rainfall (Runoff)

Seasonal rainfall (2016/2017) was 100 and 79 mm at Al Mwaqar and Al Grain sites, respectively. Table 4 shows the seasonal effective rainfall (runoff per unit area in m³/ha) for the different treatments at the two sites (Al Grain and Al Mwaqar), for the most effective rainfall storms.

3.2.1 Water Harvesting Technique

Results showed that there were no significant differences (Table 5: P= 0.2879; and Table 6: P=0.4211) in the seasonal effective rainfall resulted from surface runoff between intermittent trenches (195 and 273 m³/ha) and continuous contour techniques (188 and 277 m³/ha), at Al Grain and Al Mwaqar sites, respectively.

Table 4. Seasonal effective rainfall (m³/ha) for all treatments at Al Grain and Al Mwaqar sites

Site	Al Grain				Al Mwaqar			
	R1	R2	R3	Average	R1	R2	R3	Average
V T1	189.6	180.8	147.2	172.5	207.4	181.2	230.0	206.2
V T2	186.3	168.7	166.4	173.8	237.3	214.4	235.4	229.0
V T3	252.4	236.5	222.9	237.3	361.0	328.2	375.9	355.0
V T4	188.3	190.5	206.1	195.0	311.9	283.8	314.0	303.2
C T1	162.3	136.8	152.8	150.6	204.4	179.9	220.2	201.5
C T2	171.2	156.4	164.3	164.0	262.8	213.8	245.9	240.8
C T3	282.6	241.1	225.3	249.7	386.1	354.9	364.7	368.6
C T4	185.3	186.5	195.7	189.2	317.7	285.9	288.7	297.4

Table 5. ANOVA table seasonal effective rainfall (runoff), Al Grain site.

Source	df	SS	MS	F Value	P > F
Replicates	2	1402.96	701.48	3.61	0.0545
Technique	1	237.26	237.26	1.22	0.2879
Slope	1	16560.31	16560.31	85.17*	<.0001
Space	1	2911.16	2911.16	14.97*	0.0017
Technique x slope	1	550.79	550.79	2.83	0.1145
Technique x space	1	13.98	13.98	0.07	0.7925
Slope x Space	1	5165.83	5165.83	26.57*	0.0001
Technique x slope x space	1	342.98	342.98	1.76	0.2054

* Means significant at $P < 0.05$.

Table 6. ANOVA table seasonal effective rainfall (runoff), Al Mwaqar site.

Source	Df	SS	MS	F Value	P>F
Replicates	2	1702.96	401.48	4.2417	0.0678
Technique	1	82.14	82.14	0.69	0.4211
Slope	1	74812.02	74812.02	625.66*	<.0001
Space	1	1385.25	1385.25	11.58*	0.0043
Technique x slope	1	0.16	0.16	0.0	0.9711
Technique x space	1	2.90	2.90	0.02	0.8784
Slope*Space	1	12855.9	12855.89	107.51*	<.0001
Technique x slope x space	1	480.26	480.26	4.02	0.0648

* Means significant at $P < 0.05$.

3.2.2 Slope Effect

Results showed that slope gradient has significant impact on surface runoff, the greater the slope gradient is, the higher the potential for surface runoff (effective rainfall) will be. Using both water harvesting techniques (WHTs) on slope gradient more than 5% resulted in significantly higher amounts of effective rainfall (217.8 m³/ha) compared with 162.2 m³/ha using the same WHTs on slope gradient less than 5%; at $P < 0.0001$ for Al Grain site. The same trend was obtained at Al Mwaqar site, where WHTs gave 331 and 219 m³/ha with slope more than 5% and less than 5%, respectively; at $P < 0.0001$. Thus, as slope gradient increased soil infiltration will decrease and the surface runoff will increase. These results agree with Nasseef, et al. (2016), Sharma, et al. (1983) and Wenbin, et al.(2015).The big differences in the effective rainfall yield between the two study sites (Al Grain and Al Mwaqar) may be attributed to the condition of the site as explained by Agassi, et al. (1990). They measured the effect of the slope aspect with wind (wind ward vs. leeward) where on the leeward aspect runoff

decreases as slope increases, but with no effect of the slope on the windward aspect. On the other hand, 50-60% of the catchment area in Al Grain site which is covered by rock and a high amount of rock fragments contributes to a delay in ponding resulting in delayed runoff flow and increased infiltration rates (Zavala, et al. 2010).

3.2.3 Space Effect

Results indicate that runoff and consequently effective rainfall significantly increased and inversely proportional with contour ridges spacing. In Al Grain site, effective rainfall was significantly higher ($P = 0.0017$) with contour ridges 10-12 m and 12-14 m apart being 202.5 m³/ha compared to 180.5 m³/ha with contour ridges 15-16 m and 17-18 m apart. The same trend was obtained in Al Mwaqar site at which the effective rainfall was significantly higher ($P = 0.0043$) with small spacing (10-12 m and 12-14 m) being 282.8 m³/ha as compared with 267m³/ha with large spacing (15-16 m and 17-18 m).

Ali, et al. (2007) conducted a study in the Syrian Badia and found out that the resulting runoff per unit area from

100 m² catchment area was significantly different from that obtained from an area of 25m². Also, Ali et al., (2010) found out that the harvested water amount was higher for the smaller catchments with 6 m spacing than for larger catchments with 12 m spacing because of the longer flow path and the higher abstraction losses in larger catchments compared with shorter flow path and lower abstractions in smaller catchments. Zougmore et al. (2000) concluded that the effect of stone lines on soil water content depends on the space between the stone lines, and that the efficiency of stone lines in checking runoff and in improving soil water storage increases with a reduced stone line spacing.

3.2.4 Interaction Effect:

In the two study sites (Al Grain and Al Mwaqar), there was a significant interaction between the effects of the contour ridges spacing and the slope gradient on the runoff yield (P< 0.0001), while, there was no significant interaction between the effects of the water harvesting techniques, slope gradient, and contour ridges spacing on the runoff yield (P=0.2054). Tables 7 and 8 present the interaction effect on the seasonal runoff and consequently the effective rainfall affected by slope gradient and distance between contour ridges, at Al Mwaqar and Al Grain sites, respectively.

The significantly highest seasonal runoff (effective rainfall) values were 362 and 243.5 m³/ha, with land surface slope gradient being more than 5% and contour ridges spacing 10-14m, at Al Mwaqar and Al Grain sites, respectively. While the significantly lowest seasonal runoff (effective rainfall) values were obtained with land surface slope being less than 5% and contour ridges spacing 15-18m being 235 and 161.6 m³/ha at Al Mwaqar and Al Grain sites, respectively. Fang et al., (2008) indicated that a shorter slope length gave the highest runoff coefficient which means a higher runoff or effective rainfall.

Table 7. Seasonal runoff (m³/ha) as affected by land surface slope and contour ridges spacing at Al Mwaqar site (P<0.0001)*.

Slope	Space	
	15-18m	10-14m
> 5%	204 d	362 a
< 5%	235 c	300 b

*Means with the same letter are not significantly different.

Table 8. Seasonal runoff (m³/ha) as affected by land surface slope and contour ridges spacing at Al Grain site (P=0.0001)*.

Slope	Space	
	15-18m	10-14m
> 5%	169 c	243.5 a
< 5%	161.6 c	192 b

*Means with the same letter are not significantly different.

3.3 Predicted Runoff versus Actual Runoff (Effective Rainfall)

The correlation between actual runoff (effective rainfall) estimated by using the gravimetric method by measuring soil water content before and after a significant rainfall event. Predicted runoff is represented in Figure 2. The correlation coefficient of 0.76 indicates a strong positive correlation between actual and predicted runoff. The lowest observed ratio between actual and predicted runoff was 0.45 which almost related to small rainfall storm, which was due to the threshold

of runoff. Runoff began from 2-3 mm after the soil surface was saturated, and these amounts consisted (by 30-50%) of small storm. The highest ratio ranged from 1.2 to 1.7 for both sites and almost related to a large rainfall storm. NSE of 0.776 (Nash–Sutcliffe model efficiency coefficient) corresponds to a good match of predicted runoff to the observed data.

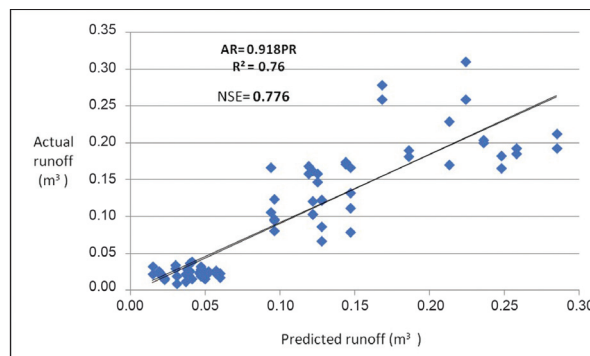


Figure 2. Regression analysis between actual and predicted runoff for both sites.

3.4 Runoff-Rainfall Relation

In general, regardless of the water harvesting technique, contour ridges spacing and slope gradient for both sites regression analysis indicate a good correlation between rainfall (mm) and runoff (effective rainfall) in cubic meter per unit area (m³/ha), with a regression coefficient of R² = 0.84 (Figure 3). Details of regression correlation between runoff (m³/ha) and rainfall (mm), for each treatment is presented in Table 9. The results indicate that there is a strong relation between effective rainfall and rainfall for all treatments. The best relations were obtained from continuous contour ridges which related to CT1 and CT2 with R² equal to 0.95 and 0.96 respectively, and R² range from 0.83 to 0.88 for small space (CT3, CT4). These results were consistent with previous results of Youssef (1998). Intermittent Vallerani trenches had given the same trend but were lower than continuous contour (Table 9). Al Grain site showed linear relation in continues contour (R² range from 0.72 to 0.77) lesser than Vallerani trenches (R² range from 0.79 to 0.93). These differences were due to the nature of land at Al Grain site which related to the slope aspect with wind and a rocky surface as previously mentioned. These results agree with Ali et al., (2010) who found out that runoff per unit area showed increase with rainfall amount following a linear trend. Linear regressions also indicated a rainfall of about 3-4 mm as rainfall-runoff threshold.

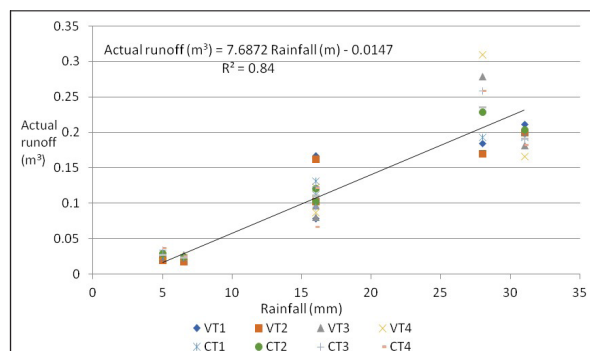


Figure 3. General regression correlation between average actual runoff (effective rainfall) and rainfall amount for all treatment at different rainfall amount.

Table 9. Detailed regression correlation between actual runoff (m^3/ha) and rainfall (mm).

Site	Treatment	Regression Equation	Regression Coefficient (R^2)
Al Mwaqar	VT1	Runoff = 2.1537 Rainfall - 3.1107	0.86
	VT2	Runoff = 2.2832 Rainfall - 1.607	0.86
	VT3	Runoff = 4.1229 Rainfall - 12.425	0.82
	VT4	Runoff = 3.5610 Rainfall - 9.6701	0.73
	CT1	Runoff = 2.0556 Rainfall - 2.0245	0.95
	CT2	Runoff = 2.6062 Rainfall - 4.9386	0.96
	CT3	Runoff = 3.9837 Rainfall - 7.4633	0.88
	CT4	Runoff = 3.2345 Rainfall - 7.0728	0.83
Al Grain	VT1	Runoff = 2.9438 Rainfall - 5.9642	0.93
	VT2	Runoff = 2.4367 Rainfall - 0.6682	0.85
	VT3	Runoff = 3.9098 Rainfall - 5.3416	0.81
	VT4	Runoff = 2.5496 Rainfall - 2.0319	0.79
	CT1	Runoff = 2.2605 Rainfall - 0.0233	0.72
	CT2	Runoff = 2.2605 Rainfall - 0.0233	0.72
	CT3	Runoff = 3.5997 Rainfall - 4.7331	0.77
	CT4	Runoff = 2.9211 Rainfall - 3.5611	0.77

4. Conclusions

Based on previous results, RWH increases water storage in the cropping area by two-three fold depending on land slope gradient and contour ridges spacing. The following conclusion and recommendations were extracted from the results:

Slope gradient plays a significant factor in site selection for RWH. Results indicate an increase in the runoff amount with the increasing of slope, especially in small contour ridges space.

The effective rainfall per unit area or runoff collected in soil profile varied from 5 to $139 m^3 ha^{-1}$. This variation is related to the variation in the rainfall amount, antecedent soil moisture conditions, micro catchment areas, and water harvesting techniques in the two sites area.

Although the relation between effective rainfall and rainfall amount showed a linear trend with strong relation for all treatments, it was the highest for continuous contour ridges ($R^2 = 0.95$).

A high percentage rock fragment cover on the catchment area surface contributes to a delay and decrease in the runoff flow as the results indicated, especially at Al Grain site.

Small and large ridges space was given an effective amount of runoff yield; however, small ridges space is recommended.

References

- Abu-Zanat, M. (2004). Increasing Range Production from Fodder Shrubs in Low Rainfall Areas. *Journal of Arid Environments*, 59: 205-216.
- Agassi, M.; Morin, J.; and Shainberg, I. (1990). Slope, aspect, and phosphogypsum effects on runoff and erosion. *Soil Science. American Journal*, 54: 1102-1106.
- AlAyyash, S., Rida Al-Adamat, R., Al-Amoush, H., Al-Meshan, O., Rawjefih, Z., Shdeifat, A., Al-Harahsheh, A. and Al-Farajat, M. (2012). Runoff Estimation for Suggested Water Harvesting Sites in the Northern Jordanian Badia. *Journal of Water Resource and Protection*, 4: 127-132.
- Allison, R.J., Higgitt, D.L., Kirk A.J., Warburton, J., Al-Homoud, A.S., Sunna, B.F., and White, K. (1998). Geology, geomorphology, hydrology, ground water and physical resources. in *Arid Land Resources and Their Management; Jordan's Desert Margin* (Dutton, W.R., J.I. Clarke and A.M. Battikhi, ed.). Kegan Paul International, London, pp. 22-39.
- Ali, A., Yazarb, A., Abdul Aal, A., Owes, T., and Hayekd, P. (2010). Micro-catchment water harvesting potential of an arid environment. *Agricultural Water Management*. 98: 96-104.
- Ali, A., Oweis, T., Rashid, M., El-Naggar, S. and Abdul Aal, A. (2007). Water harvesting options in the drylands at different spatial scales. *Land use water resources research*, 7: 1-13.
- Al-Adamat, R.; AlAyyash, S.; Al-Amoush, H.; Al-Meshan, O.; Rawjefih, Z.; Shdeifat, A.; Al-Harahsheh, A.; and Al-Farajat, M. (2012). The combination of indigenous knowledge and geoinformatics for water harvesting siting in the Jordanian Badia. *Journal of Geographical: Information System*, 4(4): 366-376.
- Al-Bakri, J.T.; Salahat, M.; Suleiman, A.; Suifan, M.; Hamdan, M.R.; Khresat, S.; and Kandakji, T. (2013). Impact of climate and land use changes on water and food security in Jordan: Implications for transcending "the tragedy of the commons". *Sustainability*, 5: 724-748.
- Black C.A. (1965). *Methods of Soil Analysis: Part I Physical and mineralogical properties*. American Society of Agronomy, Madison, Wisconsin, USA.
- Boers, T.M. (1994). *Rainwater harvesting in arid and semi-arid Zones*. International institute for land reclamation improvement (ILRI). Wageningen, Netherlands.
- Critchley, W., and Siegert, K. (1991) *A Manual for the Design and Construction of Water Harvesting Schemes for Plant Production*. Water harvesting; FAO: Rome, Italy.
- Fang, H. Y., Cai Q. G., Chen, H., and Li, Q.Y. (2008). Effect of Rainfall Regime and Slope on Runoff in a Gullied Loess Region on the Loess Plateau in China *Environmental management*. 42: 402-411.
- FAO, (2016). *Assessment of the water harvesting sector in Jordan*, final report. FAO. Rome, Italy.
- FAO, (1991). *Water Harvesting: A manual for the Design and Construction of Water Harvesting Schemes for Plant Production*. AGL/MISC/17/91. FAO. Rome, Italy.
- GIZ, Deutsche Gesellschaft für internationale Zusammenarbeit GmbH, Sector Network Rural Development Africa (SNRD) / Natural Resource Management. 2012: *Good practices in Soil and Water Conservation; A contribution to adaptation and farmers' resilience towards climate change in the Sahel*, study-handbook.
- Hai, (1998). *From manual Water Harvesting: An Illustrative Manual for Development of Micro-Catchment Techniques for Crop Production in Dry Areas*.
- Karrou, M., Oweis, T., and Ziadat, F. (2011). Rehabilitation and integrated management of dry rangelands environments with water harvesting. *Community-based optimization of the management of scarce water resources in agriculture in Central and West Asia and North Africa*, Report no. 9. ICARDA, Aleppo, Syria, 216 pages, chapters 3, 4 & 6.
- Lal, R., and Shukla, M.K. (2004). *Principle of soil physics*, Marcel, Dekker, Inc., New York.

- Naseef, A., and Thomas, T. (2016). Identification of Suitable Sites for Water Harvesting Structures in Kecheri River Basin. *Science Direct Journal*, 24: 7-14.
- Oweis, T., Benli, B., Bruggeman, A., and Farahani, H. (2006). Characteristics of Benchmark. *Research Agroecosystems in WANA: Rainfed, Irrigated, and Marginal Drylands*. ICARDA, Aleppo, Syria. Strategy for Badia Development. A paper presented at the workshop on selection of Benchmark Sites Badia, NCARE, Jordan, pp. 6-12.
- Rahman, S., Khan, M., Akib, S., Che Din, N., Biswas, S., and Shirazi, S. (2014). Sustainability of Rainwater Harvesting System in terms of Water Quality. *The Scientific World Journal*, 2014: 1-10.
- Roth, C.H. (2004). A framework relating soil surface condition to infiltration and sediment and nutrient mobilization in grazed rangelands of northeastern Queensland, Australia, *Earth Surface Processes and Landforms*, 29: 1093–1104.
- Sharma, K.; Singh, H., and Pareek, O. (1983). Rainwater infiltration into a bare loamy sand. *Hydrol. Sci. J.*, 28: 417–424.
- Shatanawi, M.R. (1995). Report of water harvesting Guideline in selected Arab countries. Water and Environment Research and study Center, University of Jordan.
- Shawaheen, N.; Saoub, H.; Oweis, T.; Haddad, N., and Karrou, M. (2011). Impact of Micro Catchment Water Harvesting on the Diversity of the Badia Rangelands of Jordan. In *Rehabilitation and Integrated Management of Dry Rangelands Environments with Water Harvesting*; Report no. 9; International Center for Agricultural Research in the Dry Areas (ICARDA): Aleppo, Syria, p. 85.
- Studer, R., and Liniger, H. (2013). *Water Harvesting: Guidelines to Good Practice*. Centre for Development and Environment (CDE), Bern; Rainwater Harvesting Implementation Network (RAIN), Amsterdam; Meta, Wageningen; The International Fund for Agricultural Development (IFAD), Rome.
- Vallerani Systems webpage. Overview on the Vallerani system and its implementation: http://www.Vallerani.com/wp/wp-content/uploads/2015/09/Eng%20VS_D3-D3s%20...
- Wenbin, M., Fuliang, Y., Chuanzhe, L., Yuebo, X., Jiyang, T., Jia, L., and Zhao, N. (2015). Effects of Rainfall Intensity and Slope Gradient on Runoff and Soil Moisture Content on Different Growing Stages of Spring Maize. *Water Journal*, 7: 2990-3008
- Wisser, D., Frolking S., Douglas, E., Fekete, B., Schumann, A., and Vörösmarty, C. (2010). The significance of local water resources captured in small reservoirs for crop production – A global-scale. *Analysis. Journal*, 384: 264-275.
- Youssef K. (1998). Evaluation of different water harvesting techniques at two different sites of Jordan. M.Sc thesis, University of Jordan, Amman.
- Zavala, L., Jordan, A., Bellinfante, N., and Gil, J. (2010). Relationships between rock fragment cover and soil hydrological response in Mediterranean environment. *J. Soil Science and plant Nutrition*, 56: 95-104.
- Ziadat, F.K.; Mazahreh, S.S.; Oweis, T.Y., and Bruggeman, A. (2006). A GIS Based Approach for Assessing Water Harvesting Suitability in a Badia Benchmark Watershed in Jordan. In *Proceedings on the Fourteenth International Soil Conservation Organization Conference: Water Management and Soil Conservation in Semi-Arid Environments*, Marrakech, Morocco, May 14–19.
- Zougmore, R., Guillobez, S., Kambou, N., and Son, G. (2000). Runoff and sorghum performance as affected by the spacing of stone lines in the semiarid Sahelian zone. *Soil and Tillage Research*, 56: 175-183.

Evaluation of the DSSAT Vertical Drainage Model for Vertisols

Fatima Ali Bani Khaled* and Ayman A. Suleiman

Department of Land, Water and Environment, Faculty of Agriculture, University of Jordan, Amman, Jordan.

Received 13 September, 2018; Accepted 29 October, 2018

Abstract

The increasing competition for water has led to the need for a better water resources management, especially for crops irrigation. A water balance tool in crop models is useful for the determination of the best agricultural water management practices that maximize the crop yield and the water productivity while avoiding the need for costly field experiments. This requires that crop models simulate water balance accurately. Suleiman and Richie (2004) (SR2004) developed a vertical drainage equation which has been incorporated into the Decision Support System for Agrotechnology Transfer (DSSAT) which is the most widely used crop model in the world. The objective of this study is to test the performance of SR2004 in Vertisols of Jordan. A laboratory trial was conducted on three Vertisols columns. The soil water content was measured daily at different soil depths during drainage cycles to test the vertical drainage model. The root mean square difference between the simulated and measured volumetric soil water contents across the three replicates ranged between 0.0039 and 0.0471 cm³/cm³. Excellent estimation was obtained for soil water content during the drainage cycles for columns (1 and 2) at all depths with the nRMSE ranging from 2.6212 to 6.4606 cm³/cm³. While for column (3), the soil water content was at an excellent estimated level except at the depths of 12 cm and 16 cm where it was estimated as good. The simulation results obtained revealed that the SR2004 overestimated the soil water content during the drainage cycle, thus, the SR2004 model needs modification to perform better regarding Vertisols.

© 2018 Jordan Journal of Earth and Environmental Sciences. All rights reserved

Keywords: Vertical Drainage, DSSAT, Vertisols.

1. Introduction

The increasing competition for water has led to a pressing need for a better use and management of water resources so that the needs of the people can be met properly. One of the major users of water are the agricultural irrigated crops (Ines et al., 2001). A water balance equation can be used to describe the flow of water in and out of a system. A system can be one of several hydrological domains, such as a column of soil or a drainage basin. It can be used in the design of subsurface drainage systems which may be horizontal (i.e. using pipes, tile drains or ditches) or vertical (drainage by wells). To estimate the drainage requirement, the use of hydrogeological water balance and groundwater models may be instrumental (Singh, 1998).

A number of water balance models exist which have different input requirements and achieve slightly different outcomes. All water balance models are aimed at estimating the different components of the water balance such as soil evaporation, deep drainage and runoff. Modeling helps identifying the factors (such as soil properties and weather variables) that may be confounding in experimental studies (Connolly et al., 2002). A model is similar to but simpler than the system it represents. Model validity is an important issue in modeling, where it includes simulating the model under known input conditions and comparing the model output with the system output. Mathematical model classifications include deterministic (input and output variables are fixed values), or stochastic (at least one of the input or output variables is probabilistic); static (time is not taken into

account) or dynamic (time-varying interactions among variables are taken into account). Typically, simulation models are either stochastic or dynamic (Law and Kelton, 1991; Nelson, 1995). The accuracy of the models depends on the correct estimation of the input data and on their simplifying assumptions (Panigrahi and Panda, 2003).

The Decision Support System for Agrotechnology Transfer (DSSAT) helps decision-makers analyze complex alternative decisions by reducing the time and human resources required (Tsuji et al., 1998). The DSSAT is a suite of crop models sharing a common simulation of soil processes. Soil water drainage is estimated based on a tipping bucket approach. Drainage takes place if the soil water present in the layer exceeds its field capacity. For the estimation of the soil water dynamics during vertical drainage, a functional model is used. Functional models such as DSSAT need less input than the mechanistic models such as hydraulic conductivity function for each soil layer (Suleiman and Ritchie, 2003). The change in the soil water content caused by vertical drainage is calculated by multiplying the drainable soil water by a coefficient (C, the fraction of drainable soil water that can be drained on a day) (Suleiman and Ritchie, 2003). Ritchie et al. (1986) assumed that C is the function of the soil porosity. Ritchie (1998) assumed that C can be assumed to be constant of 0.55 days⁻¹ or different soils, while other studies such as (Gabrielle et al., 1995; Gerakis and Ritchie, 1998) found that the DSSAT drainage model must be calibrated in order to give good estimates of the soil water drainage.

The Suleiman and Richie (2004) SR2004 model

* Corresponding author. e-mail: eng_fatima2003@yahoo.com

presented some modifications from the DSSAT vertical drainage model to improve the soil water dynamics estimation and the vertical drainage rate. The performance of the original DSSAT and of the modified DSSAT models as a whole was evaluated for two soils during the summer of 1997. The modified DSSAT with SR2004 equation estimated the daily soil water content reasonably well at the different depths throughout the drainage cycle (maximum root mean square difference (RMSD) < 0.013 m³ /m³), outperforming the original DSSAT by reducing the RMSD 2–4 fold at most of the soil depths (Suleiman and Ritchie, 2004).

Vertisols or cracked soils are clay-rich soils that shrink and swell with changes in the moisture content. Among the ten orders of the soils recognized in Soil Taxonomy (Soil Survey Staff, 1992), Vertisols are recognized by their propensity to shrink when dried and to swell when wetted. During dry periods, the soil volume shrinks, and deep wide cracks form (Rycroft and Amer, 1995). Vertisols and the associated soils cover approximately 2,570,000 million m² of the earth's surface in seventy-six countries (Dudal and Bramao, 1965). Vertisols form an important part of the agricultural land in Jordan. This soil occupies more than half of the cultivable land in northern Jordan (Battikhi et al, 2010). Due to the properties of these soils, they face various agricultural and engineering problems. When properly managed, they are productive. Although during the first rain or irrigation of the soil, the water infiltrates quickly to large depths via large cracks, subsequent infiltration and permeability are very low. Poor drainage may be a problem and crops may become waterlogged. Since changes in the soil water content is the main governing factor for the shrinking and swelling of soils and the formation of cracking, measuring the soil water content is equally important to measuring the cracks. Numerous studies have been conducted on Vertisols in Jordan with different purposes.

In a study on Vertisols at Mushaqar Agricultural Research Station, Suleiman (1994) found that the bulk density increased from 1.01 to 1.19 g/cm³ when volumetric water decreased from 40.4% to 24.51%, and the tillage tended to the Vertisols moisture storage from rainfall. This effect was reduced when residues were present on the soil surface. The surface soil water content was higher with the moldboard plow treatment than with the chisel plow treatments. Significant differences disappeared when the soil was too wet (i.e. water content by volume is more than 35 %), or too dry (i.e. water content by volume is less than 10 %), while residue incorporation had no significant effect on the water content. In Jordan, several other studies have been carried out on Vertisols characterization and management such as Abu-Hammad, 1993; Suleiman, 1994; Battikhi et al., 1998; however, there has been no attempt to evaluate the water balance of any crop simulation models for Vertisols. Therefore, this study is aimed at evaluating the SR2004 vertical drainage model of DSSAT for Vertisols in Jordan.

2. Materials and Methods

2.1 Suleiman and Ritchie (2004) Model Description

Understanding the movement of water in a saturated soil is important in drainage. Darcy's equation works well in describing the soil water flow during vertical drainage for

homogeneous soils with a uniform initial soil water content (Youngs, 1957a and b; Philip, 1957). It can be written as:

$$Q = \frac{-KA(h_2 - h_1)}{z_2 - z_1} \dots\dots\dots 1$$

where Q is the quantity of water per second such as in cubic centimeters per second, often called the "flux"; K, centimeters per second, is the "hydraulic conductivity" (the law defines K); hydraulic heads h1 and h2 and distances z1 and z2 are as shown in Figure1. The reference level here is x=0. The head h1 is the hydraulic head for all points at the bottom of the soil column, that is, at z= z1, and similarly, the head h2 applies to all points at the top of the soil column, z = z2. The length of the column is z2 -z1 = L (Kirkham and Powers, 1972).

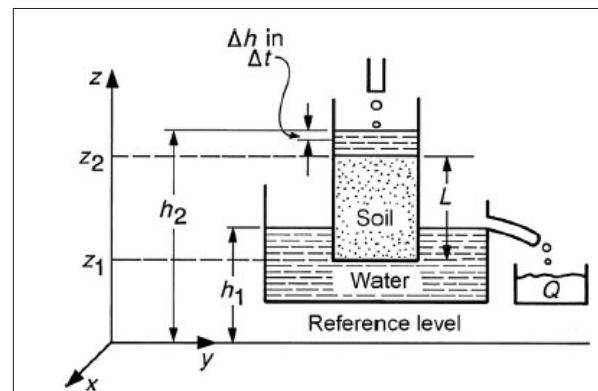


Figure 1. Illustration of Darcy's law. From Kirkham and Powers (1972).

The hydraulic gradient may be assumed to be 1 for the vertical saturated flow or for the soil water flow during vertical drainage without serious errors (Black et al., 1969). Based on such assumption, the soil water flow can be described as (Gabrielle et al., 1995):

$$q = K(\theta) \dots\dots\dots 2$$

When a layer of soil, initially at a uniform water content θ_s , has its surface covered, the initial. Assuming that the soil water content is uniform with depth (for each layer) throughout the drainage cycle, the soil water content of a soil layer subject to (the initial and boundary conditions), may be assumed to have an exponential relationship with time (Ritchie, 1985) as:

$$\theta = \theta_{dul} + (\theta_s - \theta_{dul})exp(-Ct) \dots\dots\dots 3$$

where C (d⁻¹) is a constant that can vary greatly among soils, and is related to the slope of the drainage curve (Ritchie and Amato, 1990). In DSSAT 4.0,

$$\frac{d\theta}{dt} = -C(\theta - \theta_{dul}) \dots\dots\dots 4$$

Equation (4) is used to simulate the daily soil water dynamics caused by vertical drainage using a dt of one day. The minimum value of C in a soil profile is assigned to the whole profile. The soil water drainage of each layer in the profile is assumed to move out of the profile without cascading through the different layers if no restricted layers exist. To study C and its values for different soils, an analysis of soil water redistribution for a couple of days during vertical drainage subject to the initial and boundary conditions mentioned above is presented in Suleiman and Ritchie (2004). Considering that C1 is the fraction of drainable soil water that can be drained from a soil layer

on the first day (d^{-1}) subject to (the initial and boundary conditions mentioned above), Eq (4) can be written as:

$$\Delta\theta = -C(\theta_s - \theta_{dul}) \dots\dots\dots 5$$

Although using C1 in Eq. (3) and Eq. (5) would produce different results because of the large time step (1 day), theoretically, a value of C1 that gives the correct soil water content after one day of drainage using Eq. (5) can be found for every soil. A quadratic polynomial relationship was developed to estimate C from θ_{dul} . This equation may be written as:

$$C = 3\theta_{dul}^2 - 2.6\theta_{dul} + 0.85 \dots\dots\dots 6$$

During free drainage, the amount of drainage from a soil layer subject to the initial and boundary conditions depends not only on its hydraulic properties and initial water content, but also on its position in the profile.

The incoming water flow (Q_i) defined as the amount of water that drains from and through one layer to the other is the contributor to this vertical soil water dynamics pattern. To account for the impact of the incoming water flow from the above layer on the change of the soil water content of a certain layer during drainage, a new coefficient (F) was added to Eq (4) as follows (Suleiman and Ritchie, 2004):

$$\frac{d\theta}{dt} = FC(\theta - \theta_{dul}) \dots\dots\dots 7$$

Having in mind that (1) when $Q_i = 0$, F has to be 1 and (2) when $Q_i = K_s$, F has to be 0, a generic relationship between F and Q_i was introduced as follows when $Q_i \leq K_s$:

$$F = 1 - \frac{\ln(Q_i + 1)}{\ln(K_s + 1)} \dots\dots\dots 8$$

if $Q_i > K_s$, F is 0.

During a drainage cycle, the incoming flow to a particular layer is equal to the cumulative drainage (from the layers above), and can be calculated by summing the change in the soil water content for all the layers (above that particular layer) multiplied by their thickness.

2.2 Laboratory Experiment

A soil sample from Maru Agricultural Research Station Vertisols was collected from the surface layer to evaluate the performance of the drainage model in simulating the soil water dynamics during vertical drainage. The Maru Station is located in the Northern region of Jordan (32°33' N; 35°51' E) with an elevation of 530 m above the sea level. Its soil is classified as: fine, smectitic, thermic, typic chromoxerert. The land slope is less than 6 % (Taimeh and Khreisat, 1988).

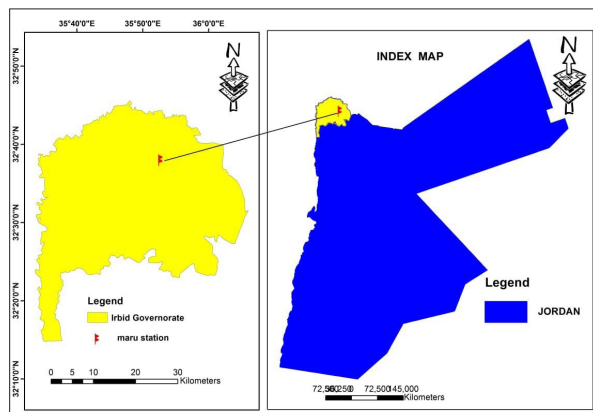


Figure 2. Maru location

Soils of Maru is clayey (59.2 % clay, 12.7 sand, and 1.09 g cm^{-1} bulk density), and dark reddish brown. The organic matter content (1.16 %) was determined by the potassium dichromate method (Schollenberger, 1931).

The soil sample was air-dried, sieved through a 2-mm screen, and was then assembled uniformly into three insulated poly vinyl chloride (PVC) columns of 150 cm in height and 30 cm in diameter by adding soil in small increments while shaking the columns continuously until the soils stopped settling (Suleiman and Ritchie, 2004).

Thirteen 20-cm time domain reflectometry (TDR) probes were installed horizontally at the depths of 4, 8, 12, 16, 20, 30, 40, 50, 60, 70, 100, and 120 cm from the surface. The soil in the columns was saturated from the bottom using a constant head of 150 cm (Suleiman and Ritchie, 2004). These soils were allowed to drain for sixteen days with the surface covered, during this time the soil water content was monitored on a daily basis at these thirteen soil depths. The column was closed by using valve and gravel sand underneath to prevent any soil loss. A digital balance was placed under each column to monitor the total weight of the soil columns on a daily basis at the same time of the soil moisture readings as shown in Figure 3.



Figure 3. Column of soil and the digital balance.

2.3 Soil Physical and Chemical Characteristics

The Maru soil is alkaline because it is mostly derived from calcareous or base-rich parent material pH values ranging from 7.3 to 7.4 (Table 1). The electrical conductivity values of the saturation extracts E_{ce} ranged from 0.28 to 0.46 dS m^{-1} , indicating that the soil is not saline (Table 1). Generally, shrink-swell soils have a relatively high Cation Exchange Capacity (CEC) which ranged from 22.5 to 24.4 cmol kg^{-1} (soil). The basic property of Vertisols that endows them with a high moisture-holding capacity is their clay content, which commonly lies between 40 to 60 %, but it can be as high as 80 % (Dudal 1965, De Vos and Virgo 1969).

Table 1. Soil properties of Maru Site.

Depth (cm)	CEC (cmol kg^{-1})	Ph	EC (dS m^{-1})	Sand (%)	Silt (%)	Clay (%)	Bulk Density (g cm^{-3})
0-20	24.4	7.3	0.5	12.7	28.1	59.2	1.1
20-60	23.5	7.3	0.3	12.8	29.0	58.2	1.1
60-120	24.2	7.3	0.3	13.4	29.9	56.7	1.3
120-150	22.5	7.4	0.4	13.2	27.5	59.3	1.3

The pipette method was used to determine the soil texture (Franzmeier et al., 1977). A core sampler is used with several cylindrical rings of known dimensions driven manually into the soil. The extruded soil from the core sampler or the soils and rings are weighed and oven-dried to a constant weight

at 105 °C. The oven-dry weight divided by the volume of the core sampler or cylindrical ring is the bulk density usually expressed in g/cm³ (Rawls and Brakensiek, 1982).

2.4 Volumetric Water Content

The measurements of the volumetric water content were taken using Time Domain Reflectometer (TDR), and were performed manually by taking samples from the site, taking into consideration the calibration between the observed readings and the device. The relationship between the volumetric soil water content, θ_v , and the soil water potential, ψ obtained by the ceramic plate method can be seen in the Figure 4.

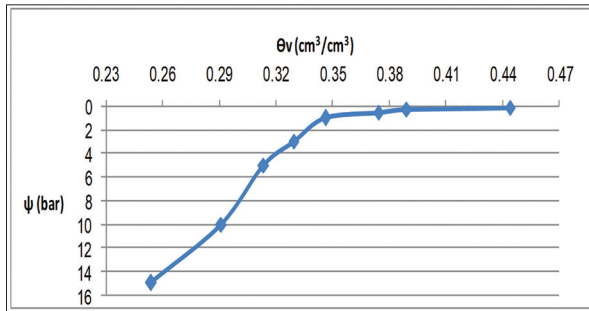


Figure 4. Soil characteristic curve of soil sample.

The calibration of the TDR was performed using samples of the gravimetric water content and the TDR device as shown in Figure (5), where the samples were taken every day for twelve days coupled with TDR readings followed by finding R² which was 0.98, 0.91, 0.80 for columns 1, 2 and 3, respectively.

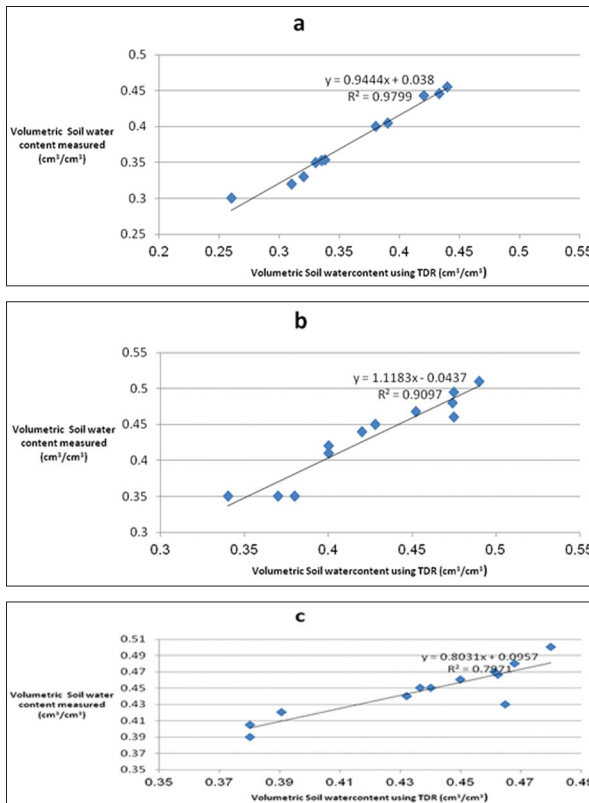


Figure 5. The calibration of TDR device for a. column 1, b. column 2 and c. column 3.

2.5 Statistical Analysis

Different statistical criteria for determining the goodness of fit for the simulation model were used to evaluate the output data and to compare the measured and the predicted results. Root mean square error (RMSE), normalized root mean square error (nRMSE) (Loague and Green 1991), and the degree of agreement index (d-index) (Willmott et al., 1985) were implemented. The predicted values are considered excellent when the nRMSE is less than 10 %. They were considered good when nRMSE ranged from 10 % to 20 %, fair if greater than 20 % to less than 30 %, and poor if nRMSE exceeded 30 % (Jamieson et al., 1991).

For d-index, the better the agreement for a certain variable between the observed and simulated values, the closer the index value is to one. The RMSE, nRMSE and d can be computed as follows:

$$RMSE = \sqrt{\sum_{i=1}^n (P_i - O_i)^2 / n}$$

$$nRMSE = RMSE * 100 / M$$

$$d = 1 - \left(\frac{\sum_{i=1}^n (P_i - O_i)^2}{\sum_{i=1}^n (|P'_i| + |O'_i|)^2} \right)$$

where P_i and O_i indicate predicted and observed values for the studied variable, respectively, n is the number of used observations, M is the mean of the observed variable, P'_i=P_i-M and O'_i=O_i-M.

3. Results and Discussions

3.1 Suleiman and Ritchie (2004)

The volumetric soil water content (θ_v) at the end of the drainage cycle (day 16) at each soil depth was assumed to be the drained upper limit (dul) at that depth. The dul in column (1) ranged from 0.39 to 0.42 cm³/cm³ and at column (2) the dul ranged between 0.38 and 0.42 cm³/cm³ while for column (3) it fluctuated from 0.31 to 0.46 cm³/cm³ (Table 2).

Boote et al. (2008) concluded that the tipping bucket soil water balance model in DSSAT generally works better when the soil water-holding properties (a drained upper limit (dul), and a lower limit of plant-extractable soil water, (ll)) are estimated properly, and when the rooting depth and root length distribution are predicted adequately. Nevertheless, the approach is inherently more than the soil water flow calculations used in many hydrological models such as HYDRUS-1D, which can estimate soil moisture distribution in the soil profile with more accuracy (Scanlon et al., 2002).

Table 2. Drained upper limit (dul) (cm³/cm³) in three soil columns.

Depth (cm)	Column 1	Column 2	Column 3
	θ_v at F.C(dul) (cm ³ /cm ³)	θ_v at (dul) (cm ³ /cm ³)	θ_v at (dul) (cm ³ /cm ³)
4	0.380	0.380	0.380
8	0.380	0.380	0.381
12	0.380	0.432	0.430
16	0.380	0.437	0.437
20	0.380	0.391	0.391
30	0.380	0.315	0.315
40	0.445	0.380	0.380
50	0.429	0.462	0.463
60	0.421	0.465	0.463
70	0.419	0.461	0.460
80	0.392	0.424	0.436
100	0.392	0.426	0.436
120	0.391	0.420	0.446

The C values estimated from θ_{dul} for the SR2004 model ranged from 0.287 to 0.293 days⁻¹ for column 1, and from 0.287 to 0.295 days⁻¹ for the column 2. They ranged from 0.287 to 0.329 days⁻¹ for column 3 (Figure 6). The C values did not change much for the three columns at the different soil depths because C is dependent on θ_{dul} which did not vary a lot in the different columns. The highest C value was at the soil depth of 40 cm of column 3 because it had the lowest θ_{dul} as C and is inversely related.

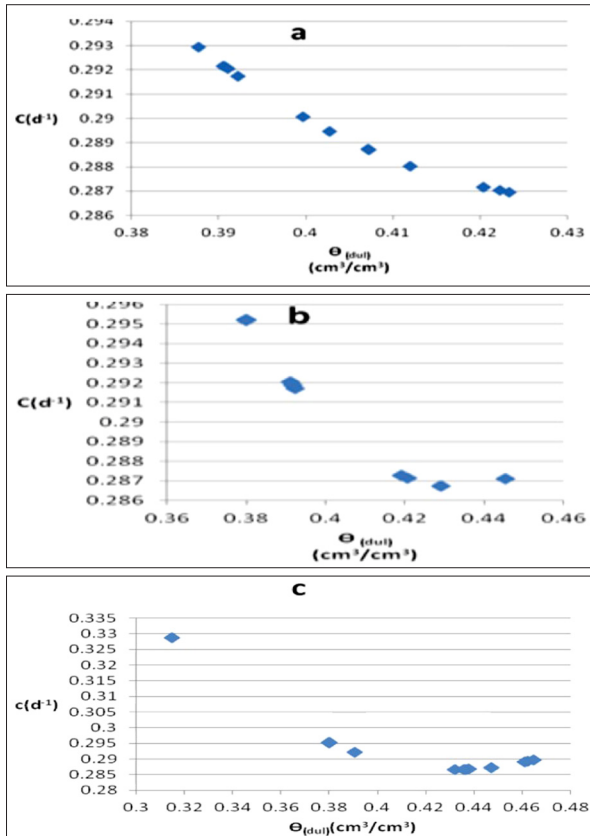


Figure 6. Relationship between C (SR2004) and θ_{dul} for the three columns of Vertisols for a. column 1, b. column 2, and c. column 3.

3.2 Measured Volumetric Soil Water Content:

Column (1) and column (2) had a higher initial soil water content because of the Vertisols having a high water-holding capacity. The initial soil water content in column 1 and column 2 was similar ranging from 0.52 cm³/cm³ at the depth of 4 cm and 0.44 cm³/cm³ at depth of 120 cm, while in column 3 the volumetric soil water content ranged between 0.38 and 0.58 cm³/cm³ at different depths (Figure 7 and 8). The initial θ_v for column (1) was higher at the soil depths of 4, 8 and 12 cm than at the lower depths.

At the end of the drainage cycle, θ_v was the least at the depth of 4 cm, while at the depth of 40 cm θ_v was the highest. The initial value of θ_v for column (2) was the highest at the depth of 8 cm and the lowest at the depth of 120 cm. At the end of the drainage cycle, the lowest θ_v was at an 8 cm soil depth, while the highest θ_v was at a soil depth of 30 cm. The initial value of θ_v for column (3) was the highest at the depth of 20 cm and lowest at the depth 40 cm. At the end of the drainage cycle, the lowest θ_v was at a 4 cm soil depth, while the highest θ_v was at a soil depth of 50 cm. Soil moisture content decreases faster on the first three days.

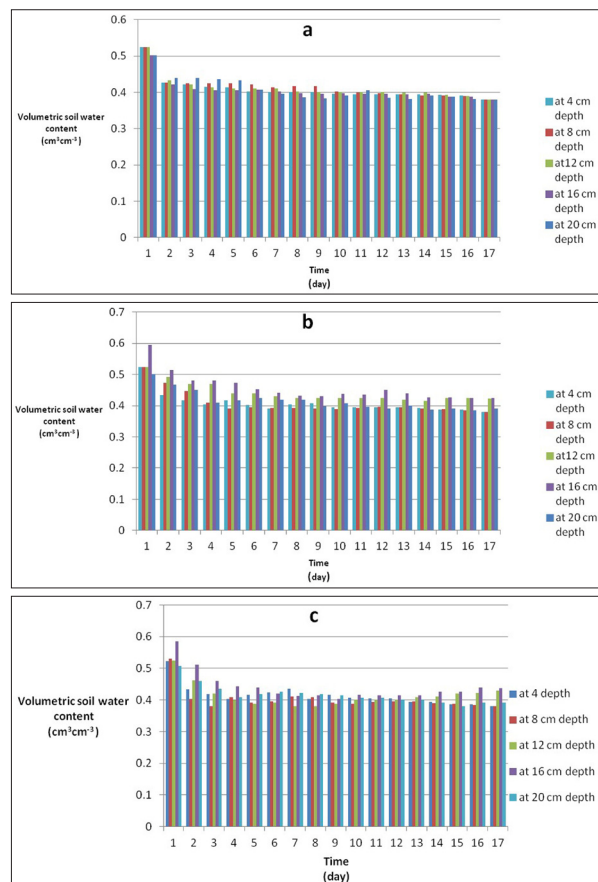


Figure 7. Volumetric Soil Water Content at the depths of (4, 8, 12, 16, 20 cm) for a. columns 1, b. columns 2, and c. columns 3.

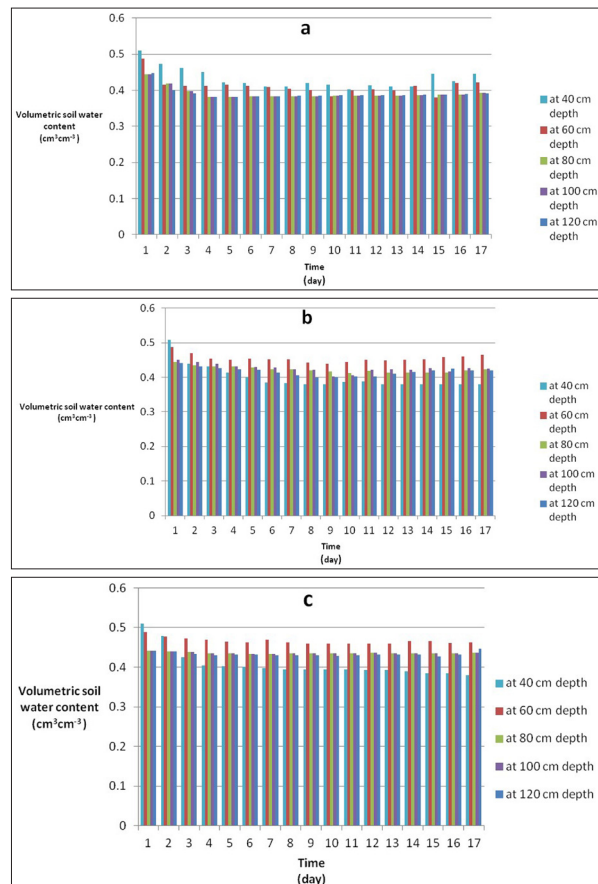


Figure 8. Volumetric Soil Water Content at the depths of (40, 60, 80, 100, 120 cm) for a. columns 1, b. columns 2, and c. columns 3.

3.3 Comparison between the Simulated and Measured Soil Water Content

Soil moisture simulations from SR2004 models were evaluated to determine the accuracy of the simulated soil water content. The differences between the simulated and measured Θ_v are shown in Figures 9, 10, and 11. The simulated value of the soil water content Θ_v column (1), column (2) and column (3) overestimated the soil water content for Vertisols at the different soil depths.

The soil water content at all depths was overestimated except at the depths of 4, 8, 12, and 16 cm, where it was close to the measured values. For the first four days and at all the soil depths except at 4, 16, and 20 cm, Ritchie (1998) estimated the soil water content relatively well in Case 3, then tended to underestimate it for the rest of the days. Concerning, the soil depths of 9 and 12 cm in Case 3, Ritchie (1998) overestimated the soil water content. For column (1) at the soil depth of 4 cm, the measured Θ_v was more than the

simulated Θ_v within the first four days, and from day ten to sixteen.

The simulated Θ_v after the depth of 40 cm was more than the measured ones throughout the drainage cycle. The simulated Θ_v after depth 50 cm was more than the measured Θ_v . The simulated change in Θ_v showed a similar pattern of the three columns with the highest change being on day 1, and the least change being at the last day of the drainage cycle. In a study done in Spain, the original DSSAT drainage simulation was unable to reproduce the small drainage amounts occurring over extended periods of time (Martinez et al., 2013). It exhibited a steep curve with strong variations of drainage in a short period of time. The drainage simulation improved after the optimization. In their study, the original DSSAT underestimated the soil water content at all depths from surface to 170 cm.

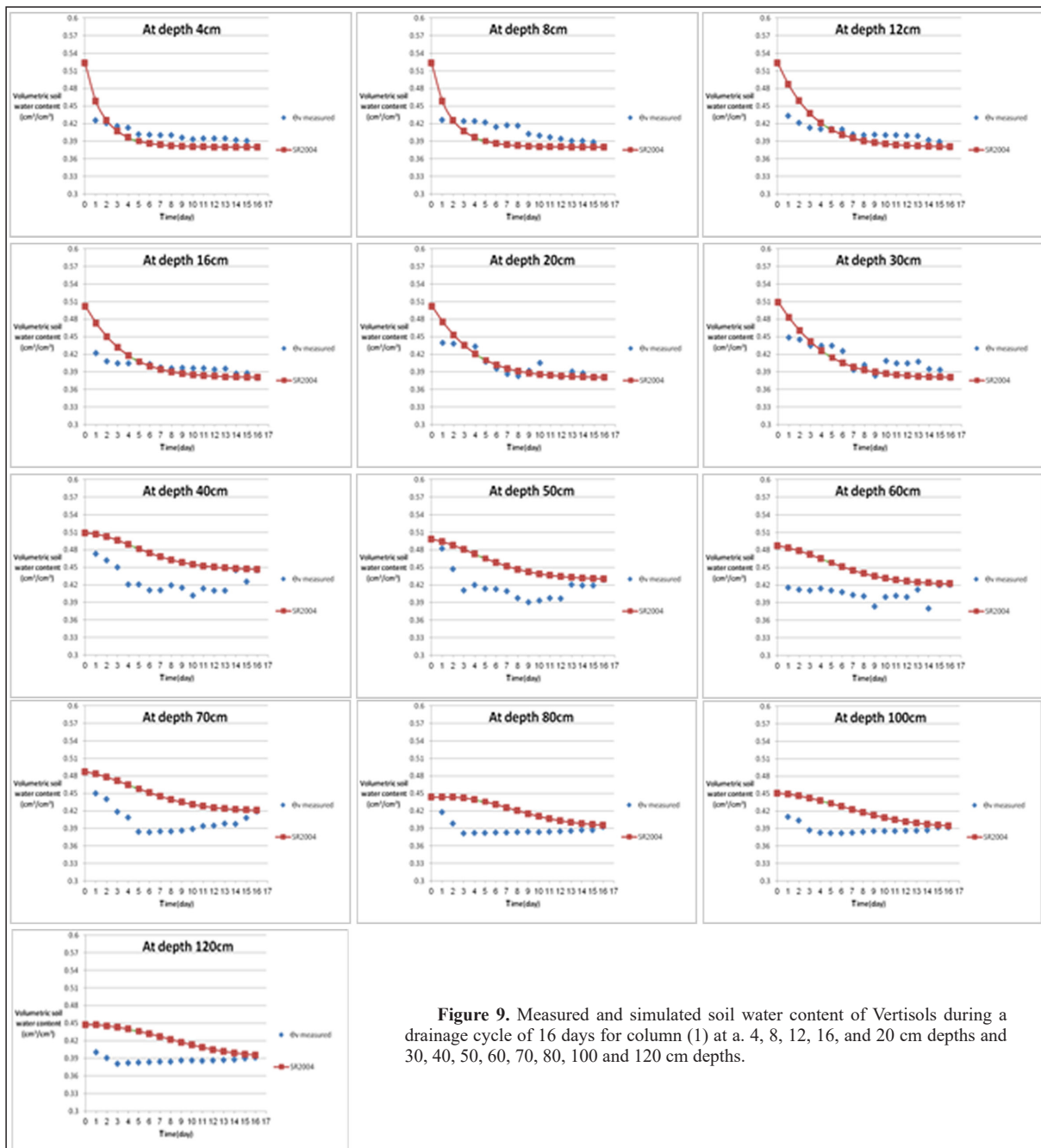


Figure 9. Measured and simulated soil water content of Vertisols during a drainage cycle of 16 days for column (1) at a. 4, 8, 12, 16, and 20 cm depths and 30, 40, 50, 60, 70, 80, 100 and 120 cm depths.

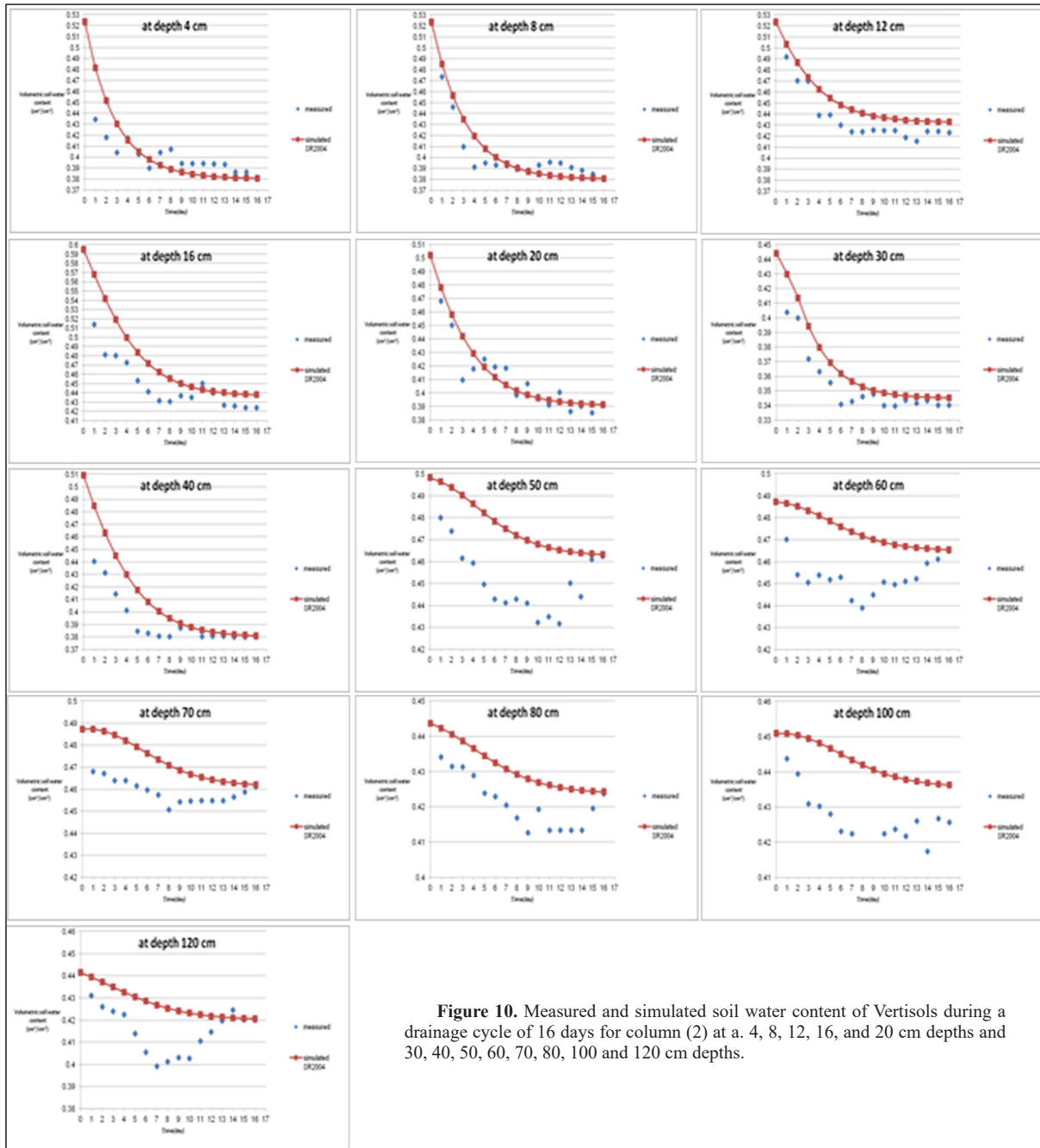


Figure 10. Measured and simulated soil water content of Vertisols during a drainage cycle of 16 days for column (2) at a 4, 8, 12, 16, and 20 cm depths and 30, 40, 50, 60, 70, 80, 100 and 120 cm depths.

The root mean square difference (RMSD) between the simulated and measured soil water content, ranged from 0.0103 to 0.0279 $\text{cm}^3 \text{m}^{-3}$ for column (1). For column (2), it was between 0.0098 and 0.028, and for column (3) it ranged between 0.0039 and .0471 (Table 3). This demonstrates that the drainage model overestimated the soil water contents at different depths and days for the Vertisols. In the lab experiment, the RMSD for column (1) was 0.0177, 0.0118, 0.0279, 0.0108, 0.0103 and 0.012 $\text{cm}^3 \text{cm}^{-3}$ at 4, 20, 40, 80, 100 and 120 cm soil depths, respectively. One would conclude that the SR2004 at column (1) performed best at the depth of 100 cm, then at 80 cm, 20 and 120 cm, respectively. The least was at 40 and 4 cm depths. While, for column (2) the RMSD was 0.0175, 0.0103, 0.0206, 0.0098, 0.0192 and 0.0146 $\text{cm}^3 \text{cm}^{-3}$ at 4, 20, 40, 80, 100 and 120 cm soil depths, respectively.

One would conclude that the SR2004 at column (2) performed best at 80 cm, then at 20 cm, 120 and 4 cm, 100

cm, respectively. The least was at a 40 cm depth. Also, the RMSD for column (3) was 0.0223, 0.0131, 0.0165, 0.0039, 0.0041 and 0.0073 $\text{cm}^3 \text{cm}^{-3}$ at 4, 20, 40, 80, 100 and 120 cm soil depths, respectively. One would conclude that the value for SR2004 in column (3) performed best at 80 cm, 100 cm, 120, 20 and 40 cm, respectively, and the least performance was at a 4 cm depth.

The results of a study conducted by (Suleiman and Richie, 2004) showed that the RMSD between the simulated (by the DSSAT) and the measured soil water contents, ranged from 0.002 to 0.37 $\text{m}^3 \text{m}^{-3}$ at the end of the drainage cycle for the sandy loam soil, and from 0.003 to 0.27 $\text{m}^3 \text{m}^{-3}$ for the loamy soils. The RMSD between the simulated water contents using the modified DSSAT and the measured soil water contents, ranged from 0.002 to 0.013 $\text{m}^3 \text{m}^{-3}$ at the end of the drainage cycle for the sandy loam soil and from 0.002 to 0.01 $\text{m}^3 \text{m}^{-3}$ for the loamy soils.

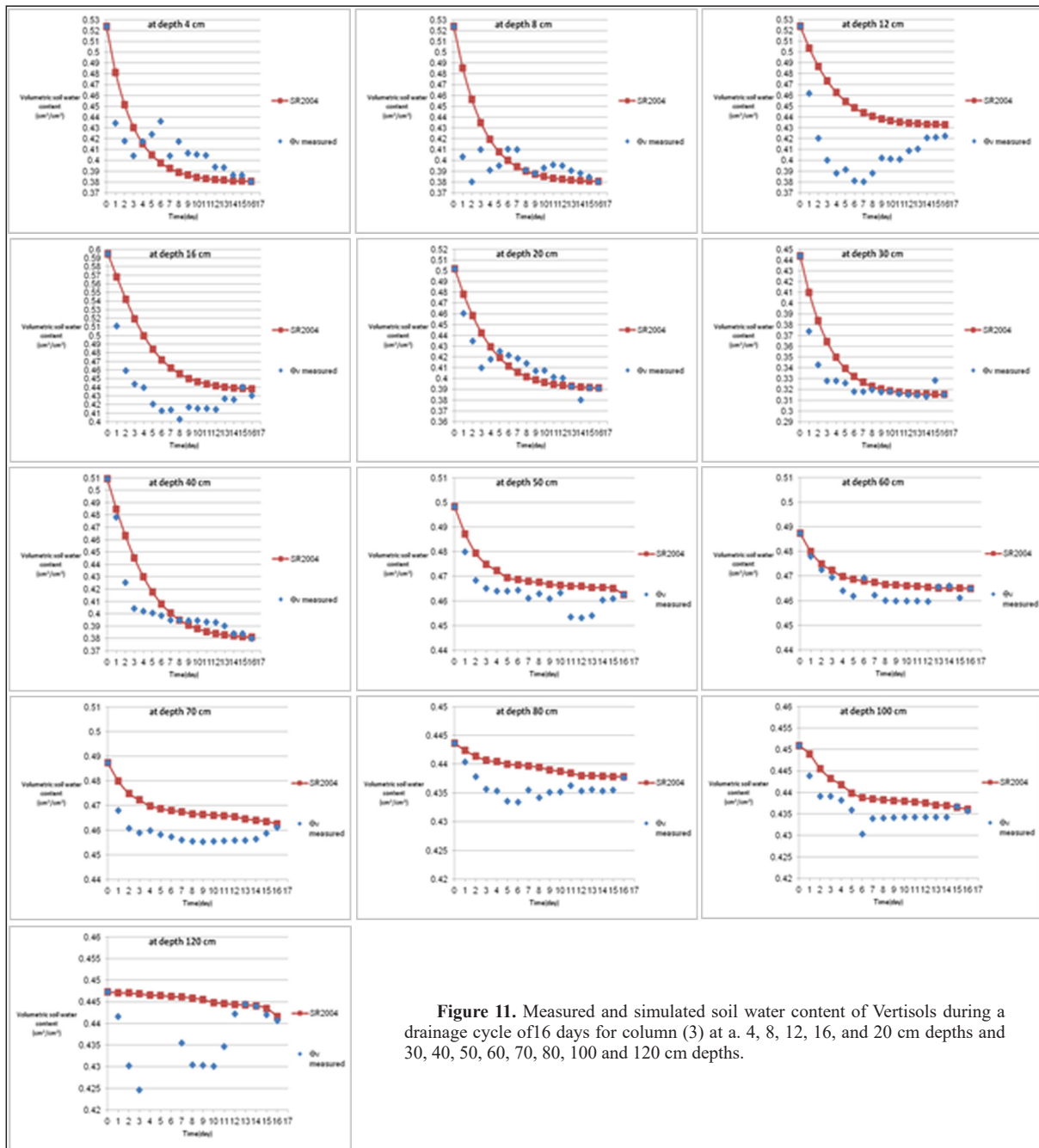


Figure 11. Measured and simulated soil water content of Vertisols during a drainage cycle of 16 days for column (3) at a 4, 8, 12, 16, and 20 cm depths and 30, 40, 50, 60, 70, 80, 100 and 120 cm depths.

Based on nRMSE, the simulation of soil water content which resulted from the SR2004 model, exhibited excellent simulation for volumetric soil water content in Vertisols in column (1) and column (2) during the drainage cycle at all depths with nRMSE ranging from 2.6212 to 6.4606 cm³/cm³. The simulation for volumetric soil water content was excellent for column (3) except at the depths of 12 and 16cm where they were estimated as good.

A value of 1 for d means a perfect agreement, while a value of 0 for d means a poor agreement (Krause et al., 2005). The d-test was conducted between the simulated values and the values ranging between 0.7437 and 0.9687 for column (1), for column (2) between values from 0.8159 to 0.9857, and for column (3) between values ranging from 0.3802 to 0.9546. The perfect agreement between the measured and the simulated values was for column (2) as in (Tables 3, 4 and 5).

Table 3. Root mean square difference (RMSD) and some statistical indices between the simulated and measured soil water contents for the Vertisols for column 1.

Depth	RMSE (Column 1)	n RMSE (Column 1)	d-test (Column 1)	Simulation Level
	SR2004	SR2004	SR2004	SR2004
4	0.0177	4.3354	0.9349	Excellent
8	0.0205	4.9634	0.9153	Excellent
12	0.0198	4.8176	0.9198	Excellent
16	0.0189	4.6776	0.8988	Excellent
20	0.0118	2.888	0.9687	Excellent
30	0.0166	3.9828	0.942	Excellent
40	0.0279	6.4606	0.8898	Excellent
50	0.024	5.703	0.8717	Excellent
60	0.0246	5.9839	0.7437	Excellent
70	0.0258	6.3347	0.7805	Excellent
80	0.0108	2.7721	0.9208	Excellent
100	0.0103	2.6212	0.9321	Excellent
120	0.012	3.0807	0.9083	Excellent

Table 4. Root mean square difference (RMSD) and some statistical indices between the simulated and measured soil water contents for the Vertisols for column 2.

	RMSE (Column 2)	n RMSE (Column 2)	d-test (Column 2)	Simulation Level
Depth	SR2004	SR2004	SR2004	SR2004
4	0.0175	4.2898	0.9384	Excellent
8	0.0119	2.912	0.9764	Excellent
12	0.0143	3.2474	0.9778	Excellent
16	0.0281	6.1638	0.964	Excellent
20	0.0103	2.4919	0.9745	Excellent
30	0.0127	3.543	0.9857	Excellent
40	0.0206	5.155	0.9168	Excellent
50	0.0259	5.7112	0.9508	Excellent
60	0.0219	4.8166	0.963	Excellent
70	0.0142	3.0883	0.9856	Excellent
80	0.0098	2.3113	0.9416	Excellent
100	0.0192	4.5076	0.8798	Excellent
120	0.0146	3.5152	0.8159	Excellent

Table 5. Root mean square difference (RMSD) and some statistical indices between the simulated and measured soil water contents for the Vertisols for column 3.

	RMSE (Column 3)	n RMSE (Column 3)	d-test (Column 3)	Simulation Level
Depth	SR2004	SR2004	SR2004	SR2004
4	0.0223	5.3910	0.8979	Excellent
8	0.0297	7.3782	0.8342	Excellent
12	0.0471	11.3947	0.6512	Good
16	0.0460	10.4566	0.7832	Good
20	0.0131	3.1414	0.9546	Excellent
30	0.0179	5.3857	0.9353	Excellent
40	0.0165	4.0553	0.9469	Excellent
50	0.0077	1.6472	0.8665	Excellent
60	0.0045	0.9667	0.9014	Excellent
70	0.0105	2.2873	0.6620	Excellent
80	0.0039	0.8907	0.5164	Excellent
100	0.0041	0.9497	0.8099	Excellent
120	0.0073	1.6869	0.3802	Excellent

4. Conclusions

Water balance is a useful tool in crop models that can be used to find the best agricultural water management practices that maximize the crop yield and water productivity while avoiding the need for costly field experiments. An evaluation of the SR2004 model for the simulation of vertical drainage in Vertisols was conducted in this study. From the current results, the root mean square difference (RMSD) between the simulated and measured Θ_v , ranged from 0.0103 to 0.0279 $\text{cm}^3 \text{cm}^{-3}$ for column (1), and between 0.0098 and 0.0281 for column (2). For column (3), it ranged between 0.0039 and 0.0471.

Excellent estimation was obtained for the soil water content during the drainage cycles for columns (1 and 2) at all depths with nRMSE ranging between 2.6212 and 6.4606 cm^3/cm^3 . While for column (3) estimation was excellent except at the depths of 12 cm and 16 cm where it was estimated as good.

The index of agreement (d) between the simulated and the measured values for the volumetric soil water content indicated that the measured and SR2004 simulated values were very similar for column (2) at all depths, then column (1). While in column (3) and at the depths of 60, 80 and 120 cm, the values of d index were very low. Generally, the SR2004 model overestimated the soil water content during the drainage cycle, thus it needs modification to perform better concerning Vertisols.

References

- Abu-Hammad, A.Y. (1993). Effect of Different Crop Rotations, Tillage-Residue Management on soil moisture storage, soil physical properties, and yields in rainfed areas. M.Sc. Thesis, University of Jordan, Amman, Jordan, 1993.
- Battikhi, A.M., Suifan, M.S., and Al-Bakri, J.T. (1998). Effect of Tillage and Plant Residue Management Practices on Some Physical Properties of vertisols. *Dirasat, Agricultural Sciences*. 25(3): 362-374.
- Battikhi, A.M., B. Snobar, S. Khattari, and Suifan, M. (2010). Effect of tillage systems and wheat residue management methods under different crop rotations on soil moisture storage and crop yields in 3 rainfed areas of Jordan. *Jordan Jour. of Agr. Sciences*
- Black, T.A., Gardner, W. R., and Thurtell, G.W. (1969). The prediction of evaporation, drainage, and soil water storage for a bare soil. *Soil Sci. Soc. Am. J.*, 33: 655–660.
- Boote, K.J., Sau, F., Hoogenboom, G., and Jones, J.W. (2008). Experience with Water Balance, Evapotranspiration, and Predictions of Water Stress Effects in the CROPGRO Model. Response of crops to limited water: Understanding and modeling water stress effects on plant growth processes. *Advances in Agricultural Systems Modeling Series 1*. ASA, CSSA, SSSA, 677 S. Segoe Rd., Madison, WI 53711, USA. pp. 59–103.
- Connolly, R.D., Bell, M., Huth, N., Freebairn, D.M., and Thomas, G. (2002). Simulating infiltration and the water balance in cropping systems with APSIM-SWIM. *Australian Journal of Soil Research* 40: 221-242.
- De Vos, J. H., Virgo, K.J. (1969). Soil Structure in Vertisols of The Blue Nile Clay Plains, Sudan. *European J. Soil Sci.*, 20(1): 189-206.
- Dudal, R. (1965). Dark Clay Soils of Tropical and Subtropical Regions. *Agric. Dev.* Paper 83, FAO, Rome, Italy. 161 p.
- Franzmeier, D.P., Steinhardt, J.F., Crum, and Norton, L.D. (1977). Soil Characterization in Indiana: I. Field and Laboratory Procedures: *Research Bulletin No. 943*, p. 13-14.
- Gabrielle, B., Menasseri, S., and Houot, S. (1995). Analysis and field evaluation of the CERES models water balance component. *Soil Sci. Soc. Am. J.*, 59: 1403–1412.
- Gerakis, A., and Ritchie, J.T. (1998). Simulation of atrazine leaching in relation to water table management using a CERES model. *J. Environ. Manag.*, 52: 241–258.
- Gijsman, A.J., Jagtap, S.S., and Jones, J.W. (2003). Wading through a swamp of complete confusion: how to choose a method for estimating soil water retention parameters for crop models. *Eur. J. Agron.*, 88: 77–106.
- Ines, AVM, Droogers, P, Makin, LW, and Das Gupta, A. (2001). Crop growth and soil water balance modelling to explore water management options. IWMI Working Paper 22. Colombo, Sri Lanka: International Water Management Institute.
- Jamieson, P., Porter, J., and Wilson, D. (1991). A test of the computer simulation model ARC-WHEAT on wheat crops grown in New Zealand. *Field Crops Res.* 27: 337–350.
- Kirkham, D., and Powers, W.L. (1972). *Advanced Soil Physics*. Wiley, New York.
- Krause, P., Boyle, D.P., and Base, F. (2005). Comparison of different efficiency criteria for hydrological model assessment. *Adv. Geosci.*, 5: 89–97.

- Law, A.M., and Kelton, W.D. (1991). *Simulation Modeling and Analysis*, Second Edition, McGraw-Hill.
- Law, A. M., and McComas, M G. (1991). *Secrets of Successful Simulation Studies*, Proceedings of the 1991 Winter Simulation Conference, ed. J. M. Charnes, D. M. Morrice, D. T. Brunner, and J. J. Swain, 21-27. Institute of Electrical and Electronics Engineers, Piscataway, New Jersey.
- Loague, K., and Green, R. (1991). Statistical and graphical methods for evaluating solute transport models: Overview and Application, *Journal of Contaminant Hydrology*, 7(12): 51-73.
- Martinez, S., López-Urrea, R., Martínez-Molina, L. and Quemada, M. (2013). Improving Simulation of Soil Water Balance Using Lysimeter Observations on a Semiarid Climate M. ETSIA, Technical University of Madrid, Avenida Complutense s/n, 28040 Madrid, Spain. *Estudios en la Zona no Saturada del Suelo*. Vol XI 77
- Nelson, B.L. (1995). *Stochastic Modeling: Analysis and Simulation*, McGraw-Hill.
- Panigrahi, B., and Panda, N.S. (2003). Field test of a soil water balance simulation model. *Agric. Water Manag.* 58: 223–240.
- Philip, J.R. (1957). Numerical solution of equations of the diffusion type with diffusivity concentration dependent. II. *Aust. J. Phys.* 10: 29–42.
- Rawls, W.J., Brakensiek, D.L., and Saxton, K.E. (1982). Estimation of Soil Water Properties. *Transactions of the ASAE*, 25: 1316- 1328.
- Ritchie, J.T. (1985). A user-oriented model of the soil water balance in wheat. In *Wheat Growth and Modeling. Series A: Life Sciences*, Vol. 86. Day, W. and Atkin, R.K. (eds.). Plenum Press, New York, pp. 293–305.
- Ritchie, J.T., Kiniry, J. R., Jones, C.A., and Dyke P.T. (1986). Model inputs. In *CERES-Maize, A Simulation Model of Maize Growth and Development*. Jones, C.A. and Kiniry, J.R. (eds.). Texas A&M Press, College Station, TX, pp. 37–48.
- Ritchie, J.T., and Amato, M. (1990). Field evaluation of plant extractable soil water for irrigation scheduling. *Acta Hort.* (Wageningen), 278: 595–615.
- Ritchie, J.T., Gerakis, A., and Suleiman, A.A. (1999). Simple model to estimate field-measured soil waterlimits. *Trans. ASAE*, 42: 1609–1614.
- Rycroft, D.W., and Amer, M.H. (1995). Prospects for the drainage of clay soils. (FAO irrigation and drainage paper, 51, 2nd edition, 147pp). Food and Agriculture Organization. Rome, Italy. ISBN 978-9251036242.
- Scanlon, B.R., Christman, M., Reedy, R.C., Porro, I., Šimůnek, J., and Flerchinger, G.F. (2002). Intercode comparisons for simulating water balance of surficial sediments in semiarid regions. *Water Resources Research*, 38, 12, 1323, 59.1–59.16
- Shelia, V., Šimůnek, J., Boote, K., and Hoogenboom, G. (2017). Coupling DSSAT and HYDRUS-1D for simulations of soil water dynamics in the soil-plant-atmosphere system. Department of Agricultural and Biological Engineering & Institute for Sustainable Food Systems, University of Florida, Gainesville, FL 32611, USA. *J. Hydrol. Hydromech.*, 66(2): 232–245.
- Soil Survey Staff. (1992). *Keys to Soil Taxonomy: Vertisols*. Fifth edition, pp. 14- 57.
- Singh, V.P. (1998). A Review on Monthly Water Balance Models for Water Resources Investigations. *Water Resources Management*. 12 (1): 31–50.
- Suleiman, A.A. (1996). *Moisture Content and Some Physical Properties of Vertisols Under Different Tillage and Crop Residue Management Practice*. M.Sc. Thesis, University of Jordan, Amman, Jordan.
- Suleiman, A.A., and Ritchie J.T. (2001). Estimating saturated hydraulic conductivity from soil porosity. *Trans. ASAE* 44: 235–239.
- Suleiman, A.A., and Ritchie J.T. (2003). Modeling soil water redistribution during second stage evaporation. *Soil. Sci. Soc. Am. J.*, 67: 377–386.
- Suleiman, A.A., and Ritchie, J.T. (2004). Modifications to the DSSAT vertical drainage model for more accurate soil water dynamics estimation. *Soil Sci.*, 169(11): 745–757.
- Suleiman, A.A. (2008). Modeling daily soil water dynamics during vertical drainage using the incoming flow concept. *Soil Sci. Soc. Catena*, 73: 312-320.
- Taimah, A.Y., and Khreisat, S.A. (1988). *Vertisols in Jordan. Properties and Distribution*. 1st Edition, Publications of the University of Jordan, Amman, 1988, pp. 43-46.
- Tsuji, G.Y. , Hoogenboom, G., and Thornton, P.K. (1998). Understanding options for agricultural production. *Systems Approaches for Sustainable Agricultural Development*. Kluwer Academic Publishers, Dordrecht, The Netherlands 1998, p. 400.
- Willmott, C., Ackleson, S., Davis, R., Feddema, J., Klink, K., Legates, D., O'Donnell, J., and Rowe, C. (1985). Statistics for the evaluation and comparison of models, *Journal of Geophysical Research*, 90(5): 8995-9005.
- Youngs, E.G. (1957a). Redistribution of moisture in porous materials after infiltration. 1. *Agric. Res. Council Soil Phys.*, 117–125.
- Youngs, E.G. (1957b). Redistribution of moisture in porous materials after infiltration. 2. *Agric. Res. Council Soil Phys.*, 202–207.

Characterization and Origin of Selected Basaltic Outcrops in Harrat Irbid (HI), Northern Jordan

Ali Al Smadi¹, Ahmad Al-Malabeh², Sana'a Odat^{3*}

¹Ministry of Education, Jerash, Jordan

²Department of Earth and Environmental Sciences, The Hashemite University, Zarqa, Jordan

³Department of Earth and Environmental Sciences, Yarmouk University, Irbid, Jordan

Received 19 October, 2018; Accepted 20 December, 2018

Abstract

This research is conducted to investigate the mineralogy, geochemistry and the petrology of Harrat Irbid (HI), in northern Jordan. Petrographic, mineralogical, and geochemical data were obtained from twenty representative samples selected from the studied HI outcrops. Mineralogical data show that HI consists of plagioclase, olivine, pyroxene, Feldspathoids, alkali feldspar, opaques, carbonates, iddingsite and chlorite minerals. The petrographical data show that the basalt is mesocratic and has hypocrySTALLINE minerals. Modally, three petro-types are recognized, olivine-plagioclase-pyroxene phyric (23%), olivine-pyroxene phyric (53%) and olivine phyric basalt (24%). The HI minerals are arranged mainly according to the porphyritic, glomeroporphyritic, paliotaxitic, vesicular, radiate and intergranular textures. Geochemically, all of the inspected samples of HI are located within plate alkaline basalt. They belong to the sodic series and are produced from undersaturated magma which resulted from a primitive mantle source. The rare-earth elements showed a depletion in the heavy rare earth elements and a strong negative Europium anomaly and enrichments in some lithophile elements, suggesting that the basalt resulted from a partial melting of a slightly differentiated pattern later. Magmas, which are analyzed for petrogenesis modeling, may have been derived from low degrees (about 10%) of partial melting of an enriched deeper garnet peridotite mantle source (>100km) with a limited crustal contamination.

© 2018 Jordan Journal of Earth and Environmental Sciences. All rights reserved

Keywords: Harrat Irbid, Porphyritic, Alkaline, Under-saturated, Mantle Source.

1. Introduction

Basaltic rocks cover approximately 18% of Jordan's area (Fig. 1a). According to Bender, 1974; Al-Malabeh, 1993; and El-Hasan and Al-Malabeh, 2008, the basaltic rocks in Jordan occur as Harrat Al-Sham that emerge in the eastern and northern parts, and some eastern marginal basaltic occurrences (Fig. 1b) also appear in the Jordan Rift and central Jordan (Ibrahim et al., 2014).

Harrat Al-Sham is believed to be generated by a paleo-volcanic activity, accompanied by opening continental rifts since the beginning of the Oligocene and frequently in the

Miocene, Pliocene and Pleistocene (e.g. Ibrahim, 1993; Ibrahim et al., 2001; Illani et al., 2001; Tarawneh et al., 2000). The results of this study can shed light on the span and duration of the upper-mantle upwelling beneath the western Arabian plate based on previous studies (Al-Amoush, 2010; Illani et al., 2001).

Basaltic rocks in the Jordanian Harrat cover about 11,400 km² (Al-Malabeh, 2009; Al-Oufi et al., 2012). The geology of Irbid area is an extension of south Syria's geology, and the samples taken from the area proved that the basaltic rocks exposed along the Irbid area are part of Harrat Al-Sham (Abu-Mahfouz et al., 2016; Al-Malabeh, 2009).

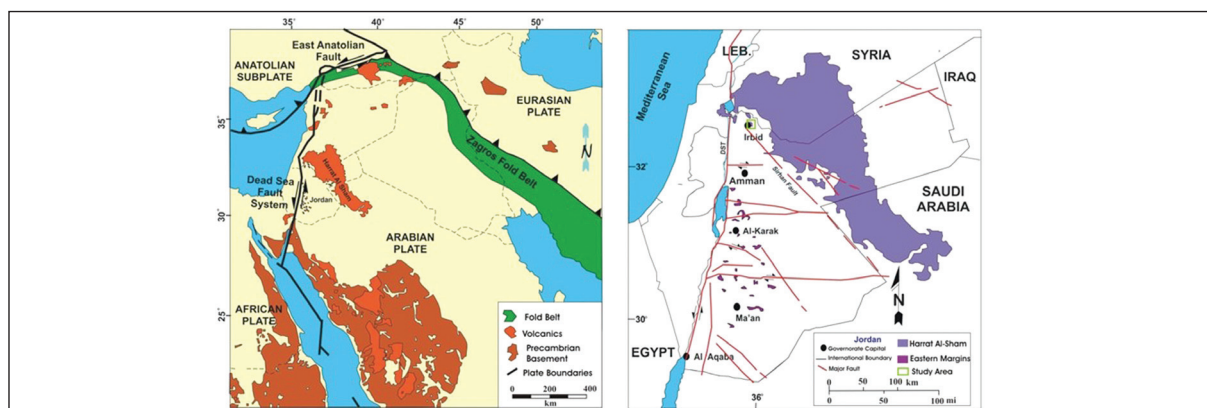


Figure 1. a. Location map of volcanic fields along the western Arabian plate (after Garfunkel, 1989; Camp and Roobol, 1989). **b.** Tectonic setting of Jordan and location of study area (Modified after Abed, 2000; and Ibrahim et al., 2014).

* Corresponding author. e-mail: sanaa.owdat@yu.edu.jo

2. Geology of Study Area

The study area geology characterized by sheet to gentle dipping and formation of wadis. The wadis resulted from head-way erosions formed by faulting and subsidence of the Dead Sea rift. The formation of this rift was followed by faulting, tectonic movements, and volcanic activity. The volcanic activity of HI is of the Pliocene to recent age and occurs as thick patches of basalt in the study area (Mo'hd, 1997).

Basaltic outcrops of the central parts of Irbid are located about 69km north of the Jordanian capital Amman; Irbid city is considered as one part of the study area. The study area lies between 35°48'40" to 35°55'41" longitude and between 32°31'30" to 32°36'36" latitude (Fig. 2). The basalt covers an area of about 10 Km² in NW-SE trend (Moh'd, 1997). Depending on the field survey, Geographic position system (GPS) and Google Earth images, seven HI's outcrops (Hw, Bu, Hk, DM, HZ, ST and DS) are shown on the location map (Fig. 2) to find out the spatial, mineralogical and geochemical relationships of basalt in the study area.

The slope of land, abundance of vesicular basalt and thicknesses of the basalt (Bryant, 1991) are evidences that the source of basalt comes from Irbid city and flows on to the surrounding low-lying areas (Fig. 2).

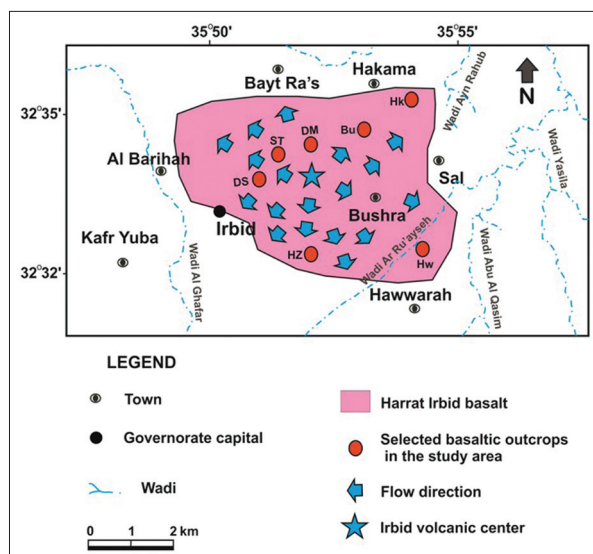


Figure 2. Location map of the study area showing that the selected basaltic outcrops and representative columnar sections will be correlated subsequently for these outcrops (Modified after Moh'd, 1997).

3. Sampling and Analytical Methods

Twenty fresh hand rock samples were collected randomly from different depths of HI outcrops for petrological, mineralogical and geochemical analyses. Three samples have been taken from DM, HZ, ST, DS, Hk & Hw, and two samples were taken from Bu basaltic outcrop. Fifty thin sections were prepared at the Department of Earth and Environmental Sciences at Yarmouk University and the Ministry of Energy and Mineral Resources (MEMR) for petrographic investigations. Seven microscopic slides were selected from each sample except DM, from which eight slides were taken. After preparation, they were evaluated using Leica Optical Microscope (LOM) and obtained using LEICA-DMEP Canon camera. After grinding approximately 100 g of each

HI sample to a very fine powder using a crusher and a ring mill at the Institute of Earth and Environmental Sciences at Al al-Bayt University, they were dried at 90°C, and then powdered to be ready for analysis by X-ray fluorescence. X-ray fluorescence (XRF) analyses were carried out in the Jordan Atomic Energy Commission (JAEC) and at the Ministry of Energy and Mineral Resources (MEMR). XRF was used for the analysis of major and some trace elements (V, Ni, Zr and Zn) in the HI samples. Other trace elements can be defined by using Inductive coupled plasma (ICP) in MEMR. PetroGraph and Iqpet softwares have been used to visualize, elaborate, and model the geochemical data for igneous petrology purposes.

4. Results

After studying thin sections under a microscope, the petrographic results of the HI samples from seven locations mostly indicate having the same texture (Aphanitic fine-grained rock, such as a basalt containing minerals that can't be distinguished with the naked eye). The basalt samples are characterized by a hypocrySTALLINE texture which consists of a mixture of groundmass and crystals where the ratio of crystals to groundmass is greater than 3:5.

Olivine and augite form the main phenocrysts phases with small amounts of plagioclase phenocrysts (Table 1) in these rocks. Typically, three petro-types are recognized, Olivine- Plagioclase- Pyroxene Phyric Basalt (23 %), Olivine- Pyroxene Phyric Basalt (53 %) and Olivine Phyric Basalt (24 %).

Table 1: Texture and mineralogy of the Harrat Irbid basalt

Outcrop	Textures	Relative abundance of minerals	Relative abundance of phenocrysts
Hw	Porphyritic, Glomeroporphyritic, Vesicular, Amygdaloidal, Seriate, Paliotaxitic	Pl > Px > Ol	Ol
Bu	Porphyritic, Glomeroporphyritic, Ophitic & Sub-Ophitic, Seriate, Radiate, Paliotaxitic	Pl > Px > Ol	Ol > Px > Pl
Hk	Porphyritic, Glomeroporphyritic, Amygdaloidal, Vesicular, Embayment, Paliotaxitic	Pl > Px > Ol	Ol
DM	Porphyritic, Glomeroporphyritic, Sub-Ophitic, Seriate, Radiate, Paliotaxitic	Pl > Px > Ol	Ol > Px > Pl
HZ	Porphyritic, Glomeroporphyritic, Sub-ophitic, Vesicular, Seriate, Intergranular	Pl > Px > Ol	Ol > Px
ST	Porphyritic, Glomeroporphyritic, Ophitic & Sub-Ophitic, Seriate, Intergranular	Pl > Px > Ol	Ol > Px
DS	Porphyritic, Glomeroporphyritic, Amygdaloidal, Vesicular, Sub-ophitic, Intergranular	Pl > Px > Ol	Ol > Px

4.1.1 Plagioclase

Plagioclase minerals, which are generally small-microliths within the matrix phase, form 32-43 % of the basaltic rocks. They are often euhedral or subhedral in shape and rarely show zonation (Fig. 3a). Labradorite plagioclase is the most abundant phenocryst in the HI samples. The average extinction angle of all the samples ranges between (29° - 32°).

4.1.2 Clinopyroxene

The Clinopyroxenes are the second dominant (18-27 %) mineral phase in the basalt. They have euhedral or subhedral crystal shape with olivine and plagioclase, and are observed in the microcrystalline matrix. The bluish red to violet-brownish clinopyroxene is characterized primarily by 35° - 50° extinction angle and other optical properties such as;

inclined extinction, higher birefringence and sector zoning (Fig. 3b).

4.1.3 Olivine

There are two generations of olivine in the HI samples. The first one is usually colorless to pale yellow in thin sections, displays a parallel extinction, fractures and a higher birefringence, and ranges from 0.5 to 1.5 mm in diameter. Olivine phenocrysts in the three petrotypes are euhedral to subhedral, tabular, fine-grained and fractured with embayment textures (Fig. 3c) produced from complete or partial alteration to iddingsite by hydration or oxidation processes. The second generation of olivine (Fig. 3d) is characterized by serpentinized macrocrysts, and may be derived from small-volume ultramafic magmas.

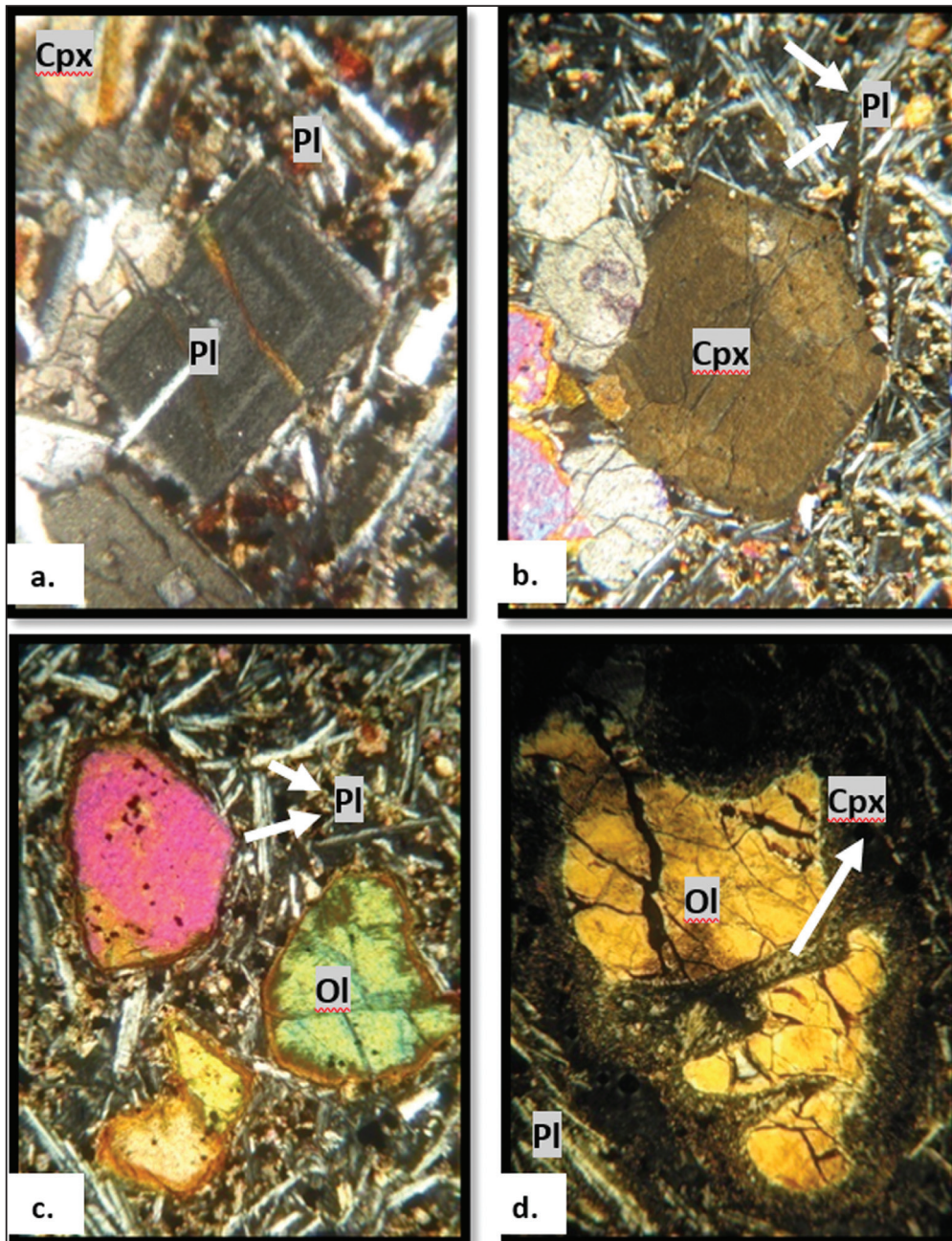


Figure 3. Photomicroscope images showing Oscillatory zoning of **a.** Plagioclase under XPL, $4\times 10\times$ magnification (Sample No. Hk1, $4\times = 2.25$ mm) and **b.** Clinopyroxene phenocryst, $10\times 10\times$ magnitude (Sample No. ST1, $10\times = 1$ mm). **c.** Photomicrograph showing porphyritic texture of three grains of olivine altered iddingsite on the rims within plagioclase and clinopyroxene groundmass under XPL, $10\times 10\times$ magnification (Sample No. DM1; $10\times = 1$ mm). **d.** Photomicrograph image showing altered and serpentinized olivine macrocryst surrounded closely by fine grained clinopyroxene groundmass under XPL, $4\times 10\times$ magnification (Sample No. DM2, $4\times = 2.25$ mm).

4.1.4 Accessory and Secondary minerals

Other accessory minerals include feldspathoids which consist of leucite (Fig. 4a) and nepheline (Fig. 4b), alkali feldspar (e.g. orthoclase) and magnetite, and secondary minerals such as carbonates, iddingsite and chlorite. The vesicles are filled with gas bubbles and carbonates.

The carbonate group is found to be calcite with a fourth-order interference color (Fig. 4c), perfect cleavage and shows a pale red colour under PPL. It appears as a filling material, and the rock full of them can be called amygdaloidal texture.

4.1.5 Groundmass

The microcrystalline matrix is dominated by plagioclase,

augite, olivine and magnetite. Two generations of microlites are apparent in the HI samples. One of these ranges in diameter between 0.15-0.34 mm and the other ranges between 0.4-0.6 mm due to disparity in the cooling rate.

4.1.6 Vesicles

Vesicles form when magmas generally continue to release gas, which can form bubbles inside; these bubbles get trapped in the solidified rock forming vesicles (Gill, 2010).

4.1.7 Textures

The HI minerals are arranged mainly by the porphyritic, glomeroporphyritic, paliotaxitic, vesicular, Amygdaloidal, sub-ophitic (Fig. 4d), radiate and intergranular textures.

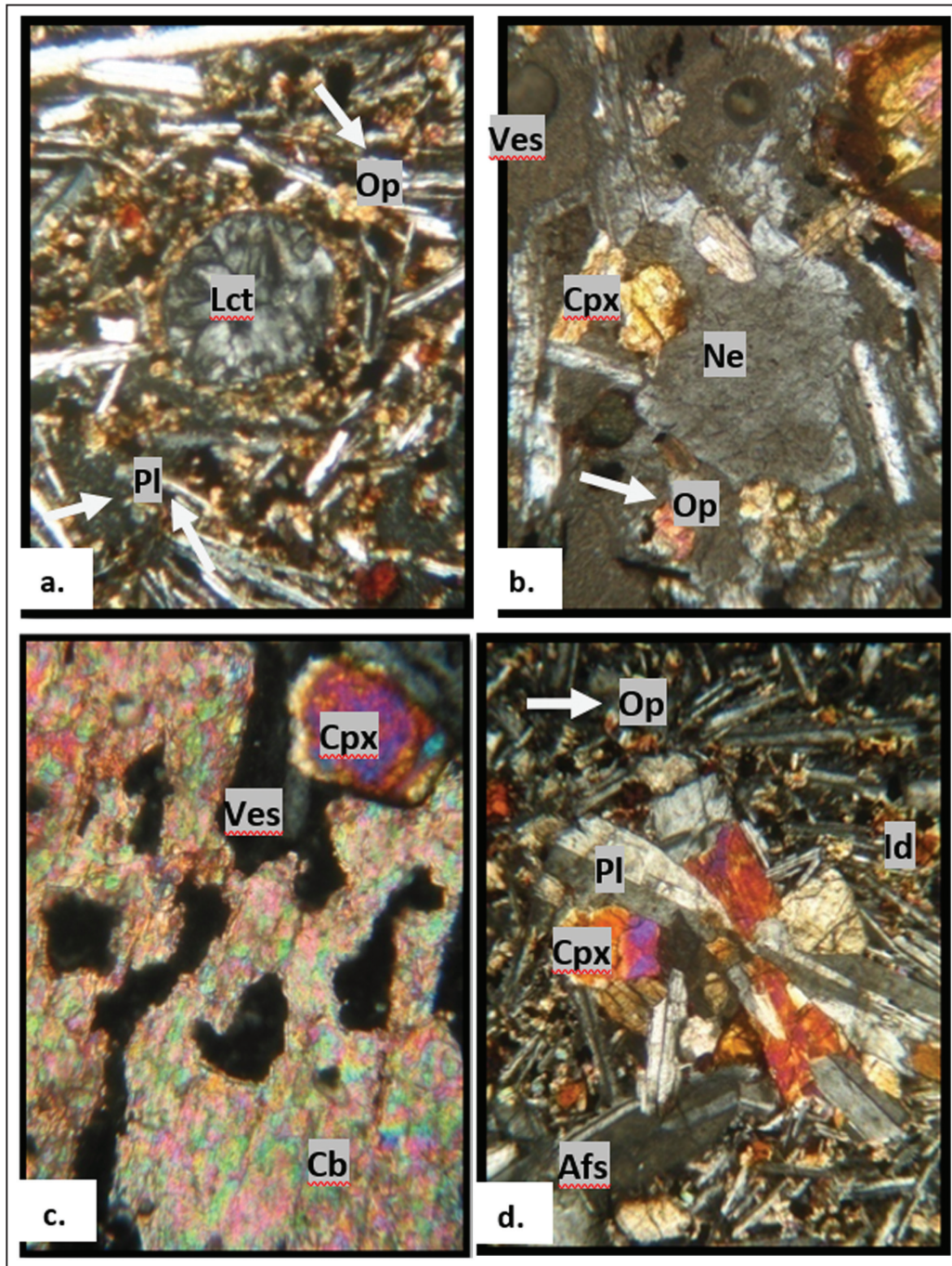


Figure 4. Photomicroscope images showing **a.** Euhedral leucite mineral enclosed within fine grain clinopyroxene groundmass under XPL, 4x*10x magnification (Sample No. ST1; 4x= 2.25 mm), **b.** Anhydrous nepheline mineral under XPL, 4x*10x magnification. (Sample No. DM1, 4x= 2.25 mm), **c.** Carbonates with a fourth-order interference color filled the vesicles under XPL, 4x*10x magnification (Sample No. Hk2, 4x= 2.25), **d.** Clinopyroxene grains are incompletely within plagioclase phenocrysts (Sub-ophitic texture) under XPL, 10x*10x magnification (Sample No. Bu1, 10x= 1 mm).

Table 2. Major, trace elements and CIPW norm data for the HI basalt.

(wt%)	Hw1	Hw2	Hw3	Bu1	Bu2	Hk1	Hk2	Hk3	DM1	
SiO ₂	45.93	44.97	46.19	44.79	46.88	45.04	45.43	44.66	45.50	
TiO ₂	2.18	2.12	2.45	2.37	1.89	2.52	2.19	2.35	2.42	
Al ₂ O ₃	14.37	14.09	15.64	15.29	14.75	15.86	14.29	15.20	15.80	
FeO(t)	11.06	11.14	11.36	11.46	11.36	11.40	11.36	11.38	11.53	
MnO	0.17	0.17	0.17	0.19	0.18	0.24	0.19	0.17	0.19	
MgO	7.19	7.02	6.07	6.43	7.32	4.54	6.85	5.80	6.77	
CaO	11.41	12.27	10.88	11.35	11.17	11.26	11.35	11.53	10.70	
Na ₂ O	3.63	3.40	3.08	2.97	3.27	3.60	3.52	4.25	2.11	
K ₂ O	1.15	1.09	1.23	1.10	0.69	1.21	1.21	1.05	1.02	
P ₂ O ₅	0.32	0.33	0.32	0.46	0.42	0.40	0.30	0.37	0.38	
LOI	1.6	1.73	1.26	2.15	1	1.45	1.74	1.7	1.65	
Total	100.2	99.6	99.9	99.8	100.2	98.77	99.7	99.7	99.3	
Mg#	0.58	0.57	0.53	0.54	0.58	0.46	0.56	0.52	0.55	
Trace elements (ppm)										
V	264	259	278	293	245	315	244	269	248	
Cr	435	420	395	467	455	482	492	376	334	
Co	65	78	71	85	71	76	61	69	62	
Ni	200	185	177	189	180	169	182	190	222	
Cu	44	55	62	60	62	54	49	62	n.d.	
Zn	161	170	192	177	173	183	155	142	175	
Rb	18	21	20	18	17	17	17	19	19	
Sr	510	489	716	509	585	653	530	653	688	
Y	16	17	18	15	19	20	16	15	17	
Zr	161	96	124	188	131	103	174	110	199	
Nb	20	24	20	23	32	17	28	26	42	
Ba	127	418	49	908	473	619	816	138	229	
La	36	38	34	30	37	30	40	36	35	
Sm	9.2	7.1	6.6	8.6	7.8	6	6.4	5.7	6.4	
U	0.6	<12	<12	<12	0.6	<12	0.45	-	0.3	
Ti/Zr	80.7	131.6	117.7	75.1	86.0	145.8	75.0	127.3	72.5	
Zr/Nb	8.05	4.00	6.20	8.17	4.09	6.06	6.21	4.23	4.74	
K/Zr	59.3	94.25	82.34	48.57	43.72	97.52	57.73	79.24	42.55	
Y/Nb	0.80	0.71	0.90	0.63	0.59	0.65	0.71	0.62	0.41	
CIPW Norm (wt% normative)										
Or	6.8	6.44	7.27	6.5	4.08	7.15	7.15	6.2	6.03	
Ab	16.39	13.06	21	17.86	23.6	18.38	15.78	13.92	17.85	
An	19.55	19.99	25.26	25.19	23.56	23.57	19.65	19.33	30.63	
Ne	7.76	8.51	2.74	3.94	2.2	6.55	7.59	11.94	0	
Di	28.36	31.4	21.79	23.01	23.69	24.43	28.21	28.96	16.16	
Hy	-	-	-	-	-	-	-	-	9.99	
Ol	8.73	7.25	8.87	9.12	11.15	5.19	8.35	6.03	5.08	
Mt	5.34	5.38	5.48	5.54	5.48	5.51	5.48	5.5	5.57	
Il	4.14	4.03	4.65	4.5	3.59	4.79	4.16	4.46	4.6	
Ap	0.74	0.76	0.74	0.86	1.06	0.93	0.7	0.86	0.88	
An%	52.9	59.2	53.1	57.1	50	54.7	54	56.7	63.2	
C.I.	46.57	48.06	40.79	44.95	42.17	43.91	39.92	46.20	41.40	
D.I.	30.95	28.01	31.01	32.06	28.30	29.88	32.08	30.52	23.88	
S.I.	63.07	63.80	67.51	68.53	66.42	63.27	73.59	64.80	65.41	
R.S.	3.62	4.56	2.70	6.39	4.55	2.04	4.72	3.89	2.50	

	DM2	DM3	HZ1	HZ2	HZ3	ST1	ST2	ST3	DS1	DS2	DS3
	46.36	45.27	45.64	46.02	45.90	45.37	45.40	45.40	45.27	45.50	46.40
	2.18	2.43	2.22	2.17	2.22	2.20	2.18	2.19	2.22	2.40	2.19
	14.43	15.39	14.54	14.38	14.70	14.38	14.80	14.60	13.92	14.80	14.70
	11.04	11.72	11.09	11.11	10.81	11.05	10.99	10.81	11.34	11.08	10.72
	0.18	0.18	0.17	0.16	0.16	0.16	0.16	0.17	0.17	0.17	0.17
	7.45	6.45	7.19	7.40	7.74	6.15	7.01	7.01	7.00	6.58	8.19
	11.05	10.94	11.55	11.24	11.30	12.08	11.70	11.70	12.09	11.20	10.80
	3.49	3.24	3.52	3.56	2.96	3.75	3.07	2.99	3.66	3.56	3.05
	1.13	1.20	1.10	1.14	1.11	1.14	1.11	1.11	1.10	1.41	1.11
	0.31	0.34	0.34	0.29	0.35	0.33	0.31	0.32	0.34	0.42	0.31
	1.24	1.6	1.14	0.84	1.36	1.26	1.14	1.21	1.72	1.34	1.21
	100.1	100.1	99.7	99.5	99.8	99.1	99.1	98.7	100.1	99.7	100
	0.59	0.54	0.58	0.58	0.60	0.54	0.57	0.58	0.56	0.56	0.62
	270	256	262	248	200	275	215	214	314	223	223
	380	377	377	350	485	470	466	423	392	477	557
	78	55	69	56	52	72	60	53	78	136	94
	202	175	170	180	220	165	189	174	170	199	227
	46	65	52	47	50	55	42	42	47	70	50
	163	159	196	137	119	131	107	155	189	197	160
	20	20	18	21	20	17	18	18	19	20	18
	524	n.d.	537	528	628	520	566	589	499	634	616
	19	17	15	15	19	15	19	18	15	14	19
	216	200	227	212	164	171	166	145	180	191	191
	30	28	27	22	24	19	21	20	24	32	30
	463	348	222	258	285	366	401	184	280	264	275
	40	37	34	38	32	28	34	32	30	32	30
	8.3	8	5.6	6	6.2	8	7	7.4	7.1	6.6	7
	-	-	0.45	<12	<12	0.6	-	<12	0.4	<12	-
	60.1	72.4	58.3	61.0	80.7	76.7	78.3	90.0	73.5	74.9	68.3
	7.20	7.14	8.41	9.64	6.83	9.00	7.90	7.25	7.50	5.97	6.37
	43.43	49.81	40.22	44.64	56.19	55.34	55.51	63.55	50.73	61.28	48.24
	0.63	0.61	0.56	0.68	0.79	0.79	0.91	0.90	0.63	0.44	0.63
	6.68	7.09	6.5	6.74	6.56	6.74	6.56	6.56	6.5	8.33	6.56
	18.67	17.93	15.99	16.96	18.47	14.27	16.45	16.96	13.47	15.9	20.12
	20.4	23.94	20.65	19.92	23.55	19.07	23.32	23.14	18.33	20.24	23.14
	5.88	5.14	7.47	7.13	3.56	9.46	5.16	4.52	9.48	7.71	3.08
	26.27	22.97	27.93	27.55	24.32	31.51	26.39	26.47	32	26.32	22.82
	-	-	-	-	-	-	-	-	-	-	-
	9.93	9.45	8.85	9.44	10.9	5.69	9.03	8.89	7.25	8.11	12.21
	5.34	5.65	5.35	5.36	5.22	5.34	5.31	5.22	5.48	5.35	5.18
	4.14	4.62	4.22	4.12	4.22	4.18	4.14	4.16	4.22	4.56	4.16
	0.72	0.79	0.79	0.66	0.81	0.76	0.72	0.74	0.79	0.97	0.72
	52.2	57.18	56.36	54.02	56.04	57.19	58.64	57.7	57.64	56.01	53.49
	45.68	42.69	46.35	46.47	44.66	46.72	44.87	44.74	48.95	44.34	44.37
	31.23	30.16	29.96	30.83	28.59	30.47	28.17	28.04	29.45	31.94	29.76
	62.18	66.86	63.13	62.49	60.79	66.61	63.51	63.12	64.27	65.15	59.23
	2.75	3.91	3.50	3.11	2.80	4.12	3.48	3.42	4.19	3.98	2.45

4.2 Geochemistry

Major and trace elements and CIPW norm analyses (Table 2) are useful for the interpretation of geochemical and petrologic data trends. They can be used also to classify and name individual igneous rocks, a method that is useful for volcanic rocks which may have few identifiable minerals (Kelsey, 1965).

4.2.1 Biveriant Diagrams

Major element analysis (Table 2) is useful for the interpretation of geochemical and petrologic data trends and the classification of volcanic rocks. Basalt samples are classified to mesocratic basalt (with an average 45) defined by Colour Index [C.I. = Ol+ Hy+ Di+ Mt+ Il]. The Differentiation Index [D.I.= Q+ Ab+ Or+ Ne+ Kp+ Lc] of HI samples ranges from 24 to 32, and the Solidification Index [SI= 100 MgO / (MgO +FeO +Fe₂O₃ +Na₂O +K₂O)

extends from 63 to 68 indicating a high fractionation of crystals of mafic minerals. The Rittmann Serial Index [R.S. = (Na₂O+ K₂O)*2/ (SiO₂ - 43)] (Rittmann, 1957 & 1962)) is used as a convenient petrochemical parameter to analyze the igneous rock series based on alkalinity: calcic- ($\sigma < 1.2$), calcalkaline- (1.2-3.5), alkaline- (3.5-8.8), and peralkaline-series (>8.8). Therefore, the Rittmann Serial Index of the HI equals at average ~3.62, and Indicates that they are located at the beginning of the alkaline phase.

The decrease in Fe₂O₃ and CaO as SiO₂ increases (Fig. 5) is consistent with the removal of early-forming plagioclase and/or pyroxene from the cooling magma. The samples have a relatively high FeO content, which may indicate small degrees of melting at high pressure (Wilson, 1989). Positive correlation between MgO and SiO₂ can be attributed to the low degree of the fractional crystallization temperature of olivine.

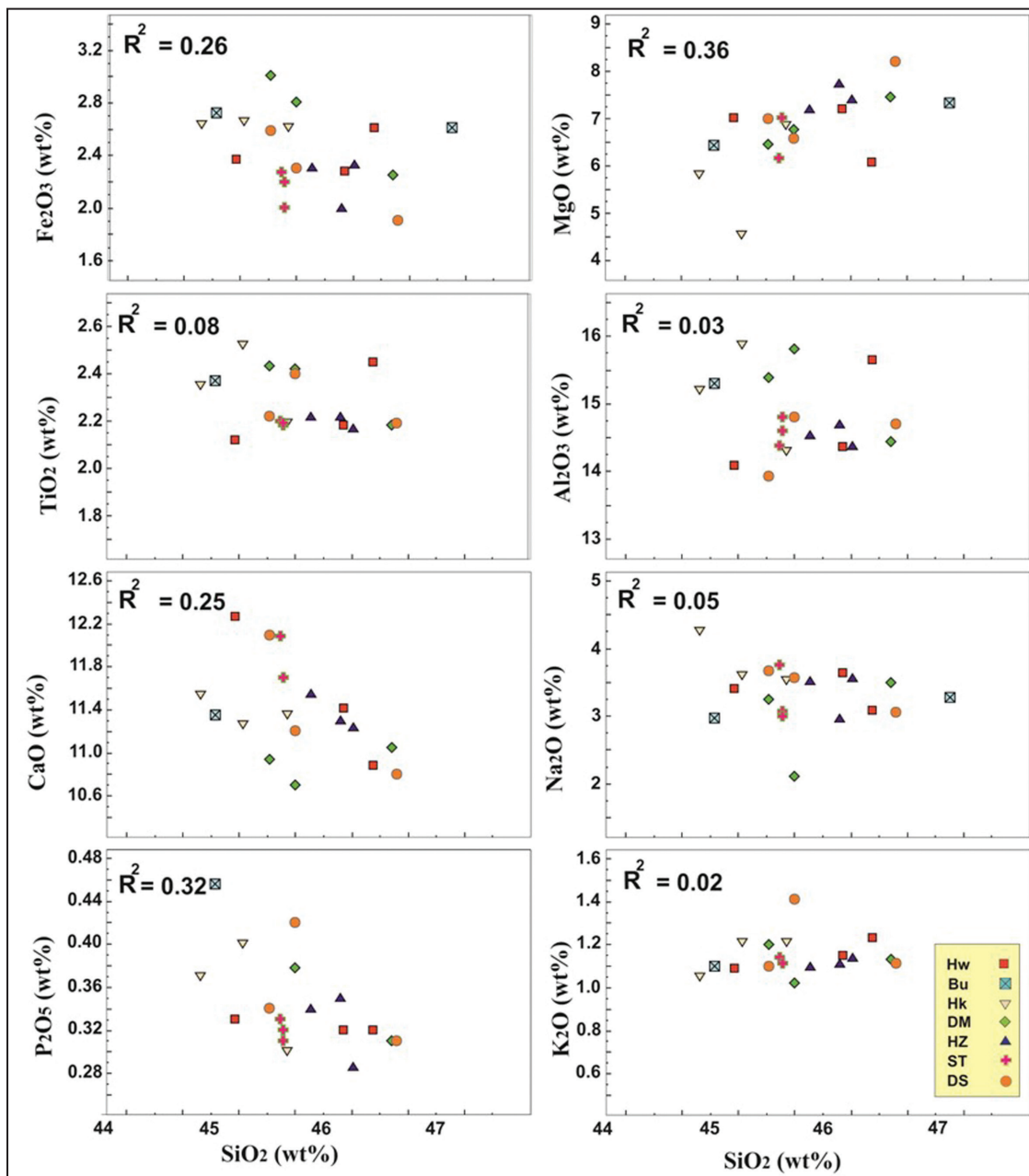


Figure 5. Harker variation diagrams for volcanic HI rocks. All major oxides are characterized by their unique trend as SiO₂ progresses from 44 – 48 wt %.

The Al_2O_3 curve shows a little negative to constant relation with SiO_2 . Because CaO decreases continuously, these trends can be reconciled by speculating that clinopyroxene was removed early on removing Ca, but Al, and plagioclase began to crystallize later, removing both Ca and Al. The apparent constant to weakly- negative correlation of Na_2O and K_2O with SiO_2 indicates that the alkalis undergo two stages. First, the alkalis are not incorporated into crystallizing phase and are conserved in the magma. After that, the alkalis began to crystallize under low melting degrees, removing both K and Na.

At low SiO_2 concentrations, both TiO_2 and P_2O_5 raise systematically as neither oxide is incorporated in the early fractionating phases (e.g. olivine, Opx, or Ca-plagioclase), causing these two oxides to remain in the liquid phase. At lower temperatures, magnetite begins to crystallize and separate from the magma, causing the TiO_2 content of the remaining magma to drop suddenly. At lower temperatures,

apatite begins to crystallize; resulting in another sharp kink in the P_2O_5 vs. SiO_2 plot.

Compatible elements of the HI samples include Ni, Cr, Co and Cu (Fig. 6). The Ni content ranges between 165 and 227 ppm with an average of 188 ppm, and indicates that the rocks suffered through very limited olivine fractionation. The copper lies between 42 and 70 ppm, with an average of 53 ppm.

The Cr, Ni and Co contents may also show the ancestry of the parental magma by the partial melting of a peridotite mantle source (Wilson, 1989). The Co/Mg ratio of the studied samples is relatively negative due to the incorporation of cobalt in the early precipitated Mg minerals. The Cu/Mg ratio in the studied samples is relatively negative compared with positive correlation of Cu/Fe and Cu/Na ratios. Thus, Cu/Fe and Cu/Na ratios should increase during fractionation and Cu substituting for Fe and Na in plagioclase and pyroxene (Alexander and Thomas, 2011).

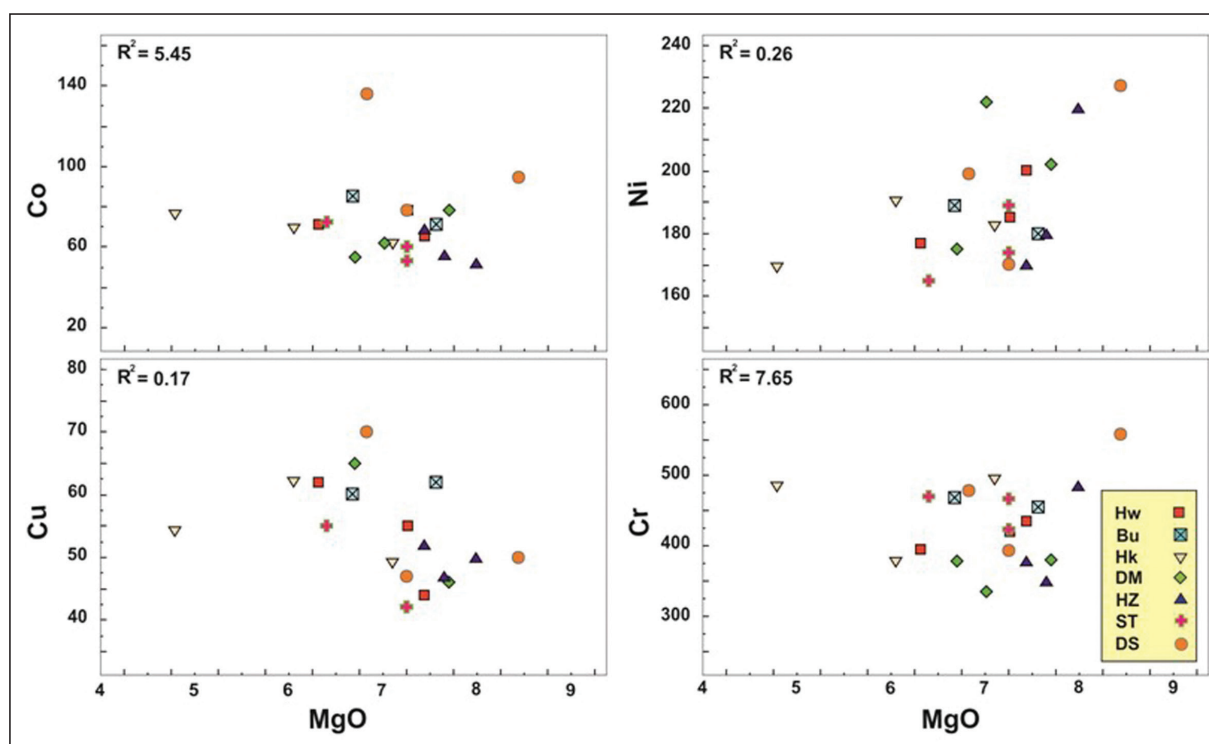


Figure 6. Variation diagrams showing compositional HI rocks ranges of selected major oxide (MgO) and compatible elements.

High-Field Strength (HFS) elements include Zr, Nb and Y (Fig. 7). The HI has a Zr content ranging from 110 to 191 ppm. The studied samples have high Ti/Zr and K/Zr averages of 59 and 85 ppm, respectively. Zr is a little positively correlated with K_2O in all samples, and it is independent with TiO_2 and P_2O_5 . Zr/Nb ratio of HI is 6.7. The low Zr/Nb ratios of the HI samples are attributed to the source heterogeneities and the “enriched” nature of the source region (Pearce and Norry, 1979).

An average Zr/Nb value of 7 is given by Sunkel (1990) as a boundary between an alkaline and tholeiitic basalt, with the earlier investigated values of less than 7. Y contents show approximate constancy from 15 to 20 ppm in the HI with an average value of 17 ppm. The Y/Nb ratio averages 0.68. These ratios are appropriate with the ratio of <1 for intercontinental alkali basalts reported by Pearce and Cann

(1973). The samples have high Zr/Y and Ti/Y ratios which average 10 and 825 in the samples respectively. The high Ti/Y ratio and the constancy of the Y content may indicate that the source magmas originated in garnet-bearing rocks (Frey et al., 1978).

4.2.2 Geochemical Classification of HI Volcanic rocks

Based on TAS diagram that is modified and recommended by Le Base et al. (1986), the typical evolutionary sequence (Fig. 8a) in the alkaline series of the HI rocks starts with an alkali olivine basalt, and proceeds to become alkali trachybasalt and tephrite basanite (Winter, 2001). Most of the HI samples fall in the alkali rocks region depending on the discrimination line of alkali and subalkalic rock fields after Irvine and Baragar (1971).

The alkaline and subalkaline rocks, when plotted on Ne-Ol-Qtz diagram (Fig. 8b) using the normative minerals

include nepheline, olivine and quartz, are marked by the dividing line that is close to the critical plane of silica

undersaturation (Proposed by Irvine and Baragar, 1971). The HI samples fall in the undersaturated area.

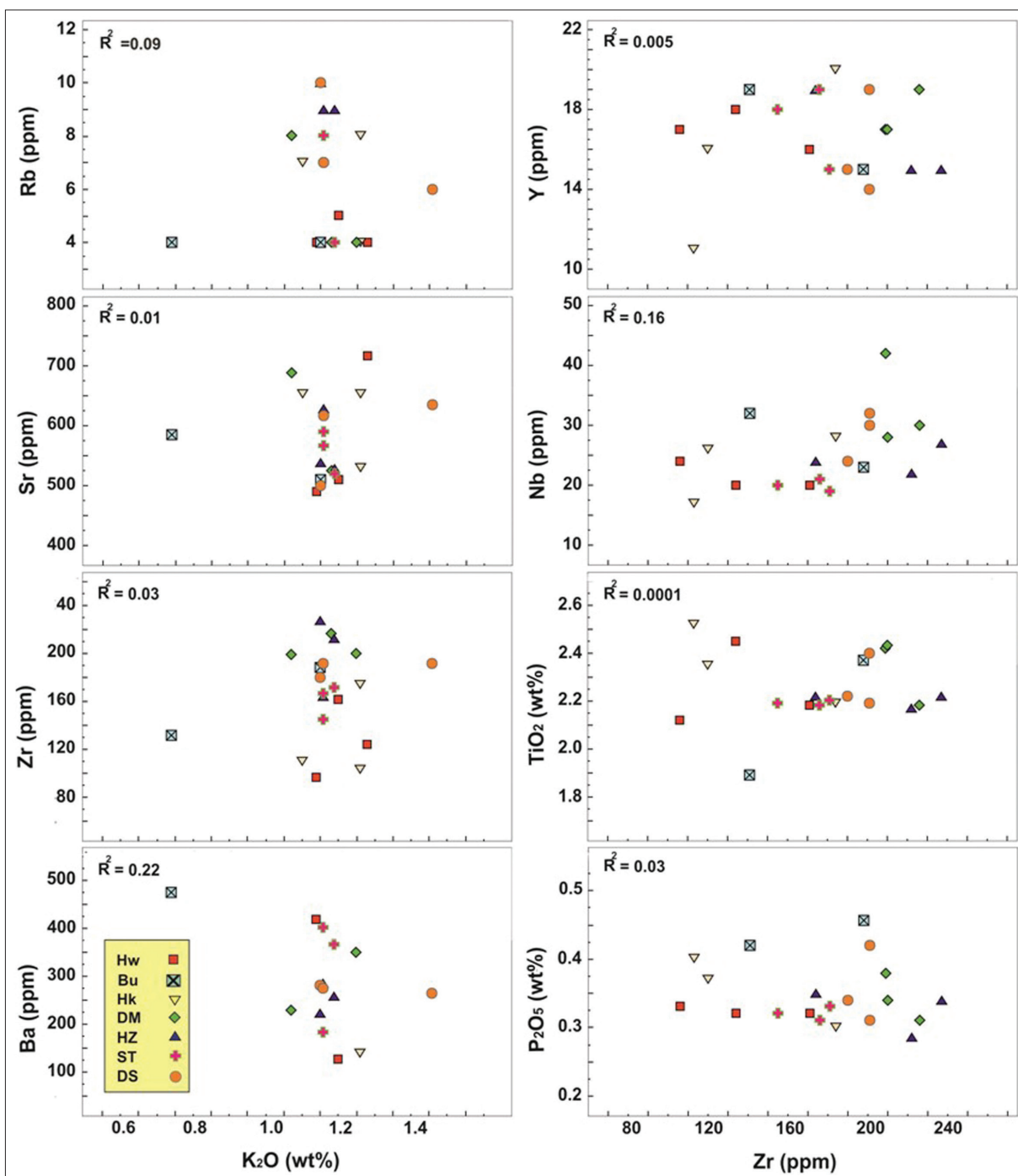


Figure 7. Variation diagrams showing interelemental relationships of the incompatible elements in the studied rocks.

The Nb/Y ratio (Fig. 8c) was first noted as an indicator of alkalinity in basalts by Pearce and Cann (1973), and further studies confirmed this (Floyd and Winchester, 1975); a higher Nb/Y (averages 1.5 in the HI samples) ratio generally reflects the higher Nb content characteristic of alkaline suites (Winchester and Floyd, 1976).

Using the K_2O versus Na_2O subdivision (After Middlemost, 1975) for alkaline magmatic rocks (Fig. 8d), the HI samples have high Na_2O/K_2O ratios; therefore, they belong to the Na-series of alkaline magmatism. This reflects a high albite and feldspathoidal content of these samples.

4.2.3 REE Diagram

The REE diagram normalized to Chondrite-Nakamura (1974) for the HI rocks (Table 3) shows depletion in the heavy rare-earth elements relative to the light ones and a strong negative Eu anomaly (Fig. 9). The HI samples with high abundances of lithophile elements and negative Eu anomalies represent fractionated melts which indicates that the basalt resulted from partial melting with slight differentiation (Anand and others, 2006). The positive relation between total abundance of REE and of other incompatible elements, which may reflect a lower degree of partial melting (Al-Malabeh, 1994).

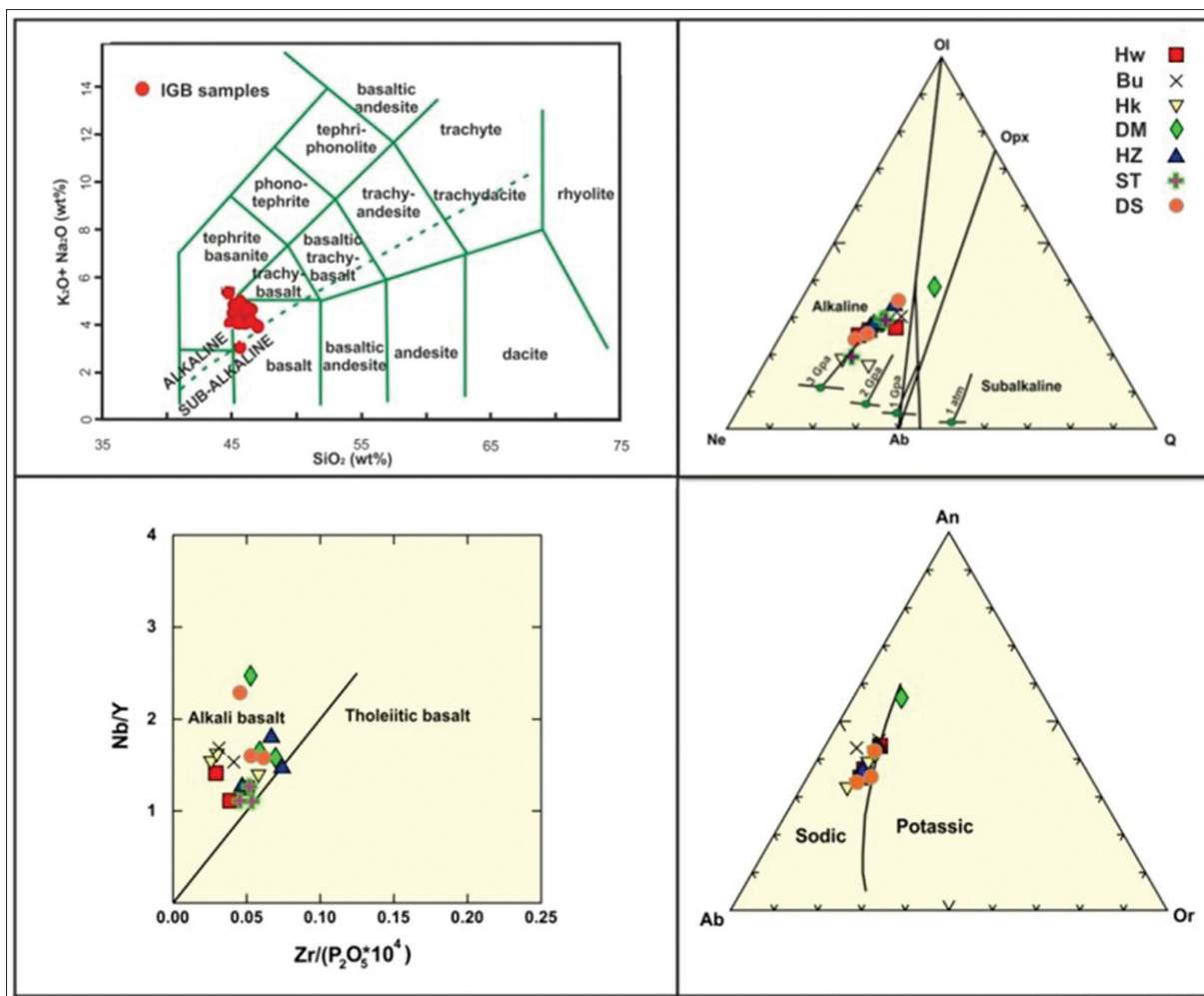


Figure 8. a. Chemical classification and nomenclature of the HI rocks using the total alkali versus silica (TAS) diagram (Le Base et al., 1986). The discrimination line of alkali and subalkali rock fields after Irvine and Baragar (1971). b. A Ne-Ol-Q base of the basalt tetrahedron illustrating the compositions of the HI samples in highly undersaturated alkaline field (Modified after Irvine and Baragar, 1971). Change in the first melt composition with increasing pressure projected onto the base of the basalt tetrahedron (Modified after Kushiro, 1968). c. Zr/ (P₂O₅ * 10⁴) vs. Nb/Y diagram (After Winchester and Floyd, 1976). d. Normative An–Ab–Or diagram showing the sodic and potassic series of alkaline HI samples (After Irvine and Baragar, 1971).

Table 3. The average of REE-element concentrations in the studied HI outcrops (in ppm).

REE	Hw	Bu	Hk	DM	HZ	ST	DS
La	36	36	34	37	35	32	31
Ce	90	75	82	100	96	81	98
Pr	8.9	9.4	7	9	10	10.1	8.8
Sm	9.2	8.6	6.4	8	5.6	7	7.1
Eu	1.1	0.6	1	0.8	0.9	0.7	0.8
Gd	6.6	7.1	8	5.8	6.2	7	6.4
Dy	5.9	5.1	5.2	6.6	7.1	5.7	6.8
Er	3.2	3.9	3.4	2.9	4.2	3.8	3
Yb	1.75	1.9	1.5	1.7	1.3	1.42	1.2
Lu	0.25	0.18	0.15	0.2	0.17	0.15	0.18

4.2.4 Spider Diagram

The normalized trace elements Rb, Ba, U, K, Nb, La, Ce, Sr, P, Zr, Ti and Y spider diagram (Fig. 10) are normalized to the primordial mantle values of Wood et al. (1979) and plotted

on a logarithmic scale. The normalized trace elements of the rock/primitive mantle shows a positive Nb peak, which is a good indicator that HI is a product of the asthenospheric part of the mantle rather than the lithospheric part (Al-Malabeh, 1994; Wilson, 1989).

The Zr and Sr anomalies can be illustrated in selective enrichment of the mantle source regions from which the primitive basalts were borrowed (Al-Malabeh, 1994).

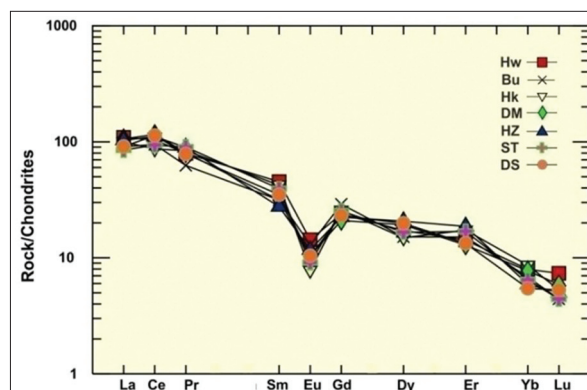


Figure 9. Chondrite normalized (Nakamura, 1974) REE patterns for the HI samples.

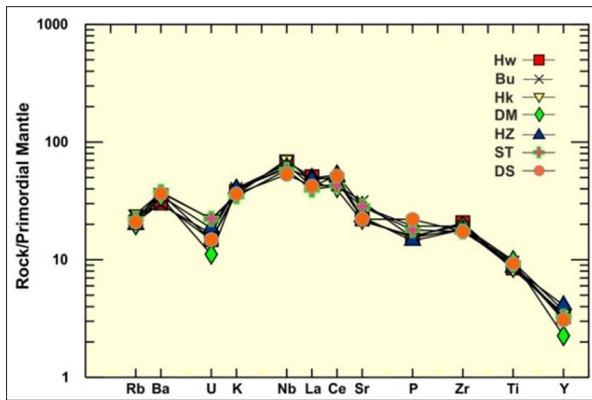


Figure 10. Spider diagram of incompatible elements from HI normalized to primitive mantle source. Elements are arranged in the order of their increasing incompatibility with the mantle rocks. The data are normalized to primordial mantle of Wood et al. (1979).

4.2.5 Tectonic Classification

The HI samples plot in the “within-plate” basalts and alkali field (Fig. 11a) on Ti/Y vs. Nb/Y discrimination plots (after Pearce, 1982). Pearce and Cann (1973) evaluated trace elements data on basalts from four major tectonic settings (Fig. 11b). The most of HI samples in this diagram plotting in “within-plate” basalts. The triangular diagram (Fig. 11c) with apices Zr/4, 2Nb and Y is suggested by Meschede (1986). All the HI samples situated in Al and All regions indicate the within-plate alkali basalt.

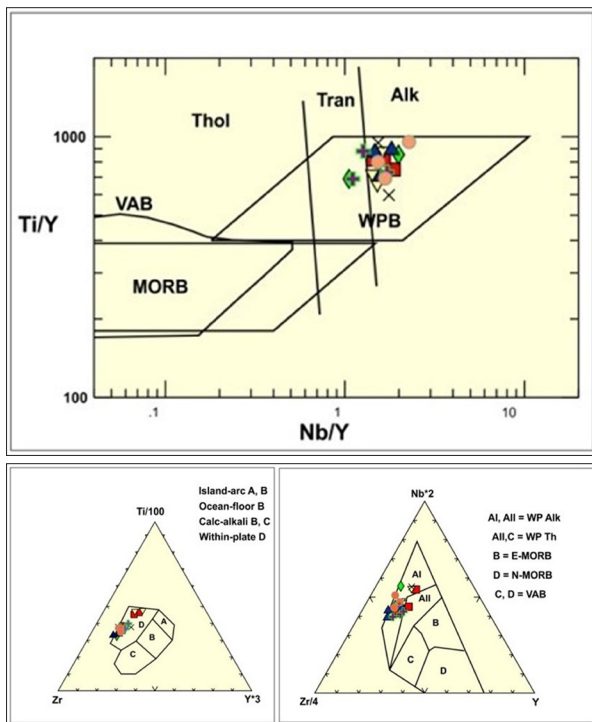


Figure 11. a. Ti/Y vs. Nb/Y discrimination diagram (after Pearce, 1982) displaying most HI samples plot between the alkalic and within-plate basalts. b. Zr, Ti/1000, and Y*3 tectonic discrimination diagram of the HI rocks (Pearce and Cann 1973). The HI samples fall in “within-plate” region. c. 2Nb – Zr/4 – Y discrimination diagram of Meschede (1986). AI: within-plate alkali basalts; AII: within-plate basalts and within- plate tholeiites; B: E-MORB; C: within-plate tholeiites and volcanic arc basalts; D: N-MORB volcanic arc basalts.

4.3 Petrogenesis of HI Samples

4.3.1 Crustal Contamination

The HI samples define a trend of constant La/ Nb compared with SiO₂ which can be imputed to the assimilation

of low-La/Nb crustal contaminants during magma evolution (Walker et al., 2009). Mg# (MgO/ (MgO+FeO)) indicates the level of evolution of a volcanic rock (e.g. Basalt) since leaving its birth place (mantle). Mg# for the HI products ranges from 0.52 to 0.62 values, with an average of 0.57. These values are close to the values of 0.65, 0.77 and >0.70 for primary magmas reported by Wilson (1989) and Al-Malabeh (1994).

The primary nature of the magma, and the Mg#, provide an evidence for a closed-system magma chamber, and suggest that the contamination of the upper crust was minimal. Furthermore, the high K/Rb ratios, and the low Rb/Sr & K/Sr ratios in the HI rocks show a primary uncontaminated magmas (Al-Malabeh, 1994). Trace element modeling (Zr/Y vs. Ti/Y, Zr/Nb vs. La/Sm) indicates that the alkali HI samples were produced by a partial melting of an enriched mantle source that experienced little or no crustal contamination (Floyd et al., 2000).

4.3.2 Fractional Crystallization vs. Partial Melting

MgO contents (4-9 wt. %) were observed in all of the samples, demonstrating that they are close to primary magmas, and may have experienced minimal fractionation of mafic minerals such as olivine and pyroxene, which is consistent with the observed phenocrysts assemblages and argues for a rapid ascent from the mantle. The low Y content, high Zr/Y ratio, high TiO₂/Y ratio (Frey et al., 1978), and the high La/Yb ratio (Saunders et al., 1987) with averages of 20, support the idea that the studied rocks are derived from a mantle of garnet peridotite composition.

The REE pattern may help us illustrate a partial melting trend and a crystal fractionation trend for the HI rocks. The content of the incompatible elements, such as REE (See Fig. 9 and 10), in the melt decreases with increasing the degree of melting and decreasing the degree of fractional crystallization (Winter, 2001).

The negative K anomalies appearing in the more enriched profiles propose that for smaller degrees of partial melting, such K-bearing phases may have been held in the source, but they are depleted with a greater degree of partial melting (Ibrahim and others, 2014; Fitton and Dunlop, 1985; Smedley, 1988).

Because the slope on a REE diagram (See Fig. 9) is a function of F, the melt fraction (10 % partial melts) generated, the differences between HREE depletion and LREE enrichment are due to the low degrees of partial melting (Winter, 2001).

This result is propped by the Sr-Zr plot after Camp and Roobol (1989), where all samples (Fig. 12a) take place into a partial melting trend rather than proposing plagioclase fractionation (El-Hasan and Al-Malabeh, 2008).

4.3.3 Petrogenetic Modeling

The trace elements pattern of alkaline lavas is repeatedly explained as being due to low degrees of melt from a garnet peridotite source (Foulger et al., 2005). As mentioned earlier, a positive Nb peak is a good indicator that HI is a product of the asthenospheric part of the mantle rather than the lithospheric part. The high Ti/Y ratio and the stability of the Y content may indicate that the source magmas originated in garnet-bearing rocks.

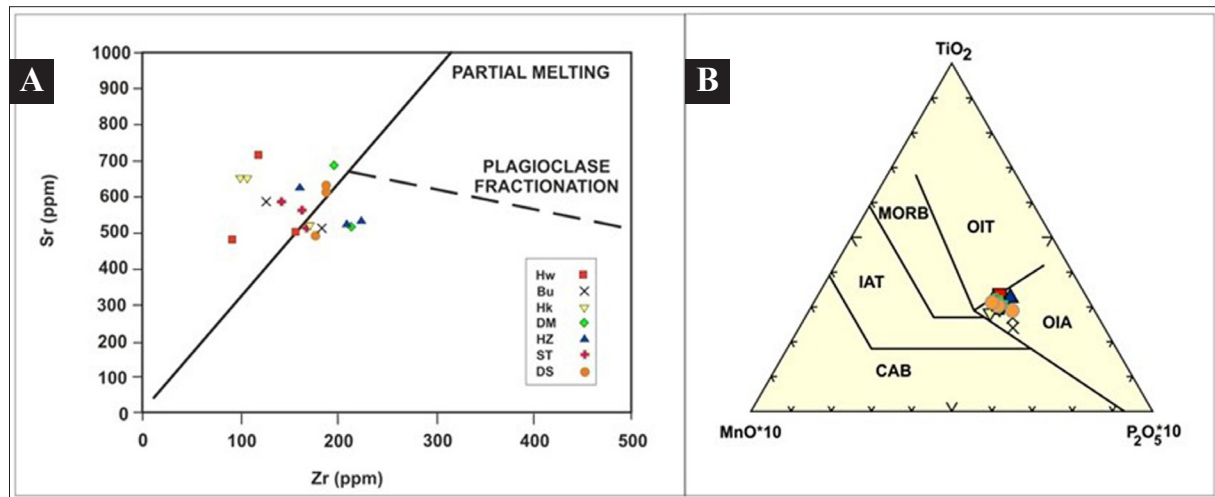


Figure 12. a. Plot of the HI samples on Sr-Zr diagram (Modified after Camp & Roobol, 1989) showing the limited plagioclase fractionation. **b.** MnO-TiO₂-P₂O₅ diagram (Mullen 1983) for the HI samples. (CAB: Calc-Alkaline Basalt, IAT: Island-Arc Tholeiites, MORB: Mid-Ocean Ridge Basalt, OIT: Ocean Island Tholeiites, OIA: Ocean Island Alkaline basalt).

Depending on Mullen (1983) discrimination diagram for basalts, MnO-TiO₂-P₂O₅ for the HI are compared with the oceanic island alkali basalts (OIA). The HI shows restricted major elements' ratios of the studied samples that fall within the range of OIBs (Fig. 12b). These results indicate that the HI samples cannot be created in a subcontinental lithosphere, but are generated from asthenospheric mantle (Al-Malabeh, 1994; Ibrahim et al., 2014).

Petrogenetic modeling of the HI samples depends primarily on the mantle plume activity. Morgan (1971) proposed that hotspot volcanism is produced by mantle plumes, involving the rapid ascent of uncommonly hot and floatable mantle materials from deep thermal boundary layers in the lower mantle (Fig. 13).

We conclude that there is a deeper possible partial source for the HI basalts at > 100 km (Al-Malabeh, 1994; Morgan, 1971). A basalt flow like those in HI has low silica contents and low viscosities so they can flow for long distances similar to Hawai'i (Bryant, 1991).

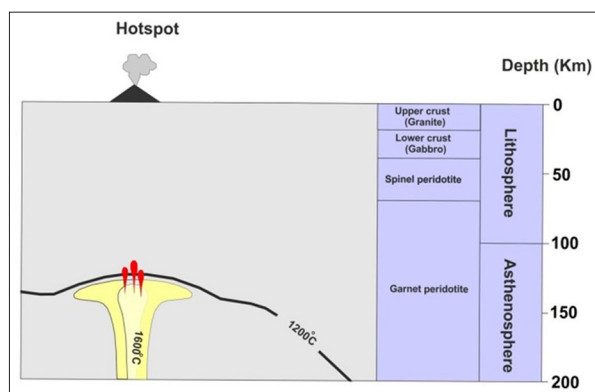


Figure 13. Structure of the crust and mantle below the HI source (After Al-Malabeh, 1994).

4. Conclusions

The basalt samples are characterized by a hypocrySTALLINE texture and mesocratic colour index, Olivine- Plagioclase-Pyroxene Phyric Basalt (23 %), Olivine- Pyroxene Phyric Basalt (43 %) and Olivine Phyric Basalt (24 %). The microcrystalline matrix is dominated by plagioclase, augite,

olivine and magnetite.

HI consists also of other accessory minerals such as nepheline and magnetite and secondary minerals such as carbonates, iddingsite and chlorite in addition to vesicles filled with gas bubbles and carbonates.

Porphyritic, Vesicular, Amygdaloidal, embayment, pilotaxitic, glomeroporphyritic and sub-ophitic are the major textures that emerged in basaltic samples in addition to some less visible textures such as seriate, ophitic, radiate and intergranular textures.

The typical evolutionary sequence in the alkaline series of the HI rocks starts with an alkali olivine basalt, and proceeds to become alkali trachy basalt and tephrite basanite.

The compositions of the HI samples plotted in highly undersaturated alkaline field, resulted from a primitive mantle source, situated in the within-plate alkali basaltic field and were produced by a lesser percentage of partial melting (about 10 %) of an enriched mantle source that experienced little or no crustal contamination.

Similarities between some OIB and continental basalts are another evidence of the asthenospheric source that resulted from mantle plumes producing melts called alkali HI that are very high in potassium and sodium.

References

- Abed, A.M. (2000). Geology of Jordan. Jordanian Geologists Association, Amman.
- Abu-Mahfouz, I., Al-Malabeh, A., and Rababeh, S. (2016). Geo-Engineering of Harrat Irbid Basaltic Rocks, Irbid District-North Jordan. *Arabian Journal of Geosciences*, 8(4): 231-248.
- Al-Amoush, H. (2010). Integration of Vertical Electrical Sounding and Aeromagnetic Data Using GIS Techniques to Assess the Potential of Unsaturated Zone and Natural Basalt Caves for Groundwater Artificial Recharge in NE-Jordan. *Jordan Journal of Civil Engineering*, 4(4): 387-389.
- Al-Malabeh, A. (2009). Cryptic Mantle Metasomatism: Evidences from Spinel 1 Herzolite Xenoliths/Al-Harida Volcano in Harrat Al-Shaam, Jordan. *American Journal of Applied Sciences*, 6(12): 2085-2092.

- Al-Malabeh, A. (1994). Geochemistry of Two Volcanic Cones from the Intra- continental plateau Basalt of Harra El-Jabban, NE-Jordan. In *Basaltic rocks of Various Tectonic Setting, Special Issue of the Geochemical Journal, Japan*, 28: 542-558.
- Al-Malabeh, A. (1993). The volcanology, mineralogy and geochemistry of selected pyroclastic cones from NE – Jordan and their evolution for possible industrial applications, p. 330.
- Al-Oufi, A., Al-Malabeh, A., and Al-Tarazi, E. (2012). Characterization of Lava Caves, Using 2D Induced Polarization Imaging, Umm Al Quttein area, NE Jordan. 15th International Symposium on Vulcanospeology, March 15-22, pp. 71-83.
- Alexander, P., and Thomas, H. (2011). Copper In Deccan Basalts (India): Review Of the Abundance And Patterns Of Distribution. *Boletín del Instituto de Fisiografía y Geología* 79-81, pp. 107-112.
- Anand, M., Taylor, L., Floss, C., Neal, C., Terada, K., and Tanikawa, S. (2006). Petrology and geochemistry of LaPaz Icefield 02205: A new unique low-Ti mare-basalt meteorite. *Geochimica et Cosmochimica Acta*, 70: 246–264.
- Bryant, W.A. (1991). Likely Fault Zone, Lassen and Modoc counties. California Division of Mines and Geology Fault Evaluation Report 218.
- Camp, V., and Roobol, M., (1989). The Arabian continental alkali province: Part I Evolution of Harrat Rahat, Kingdom of Saudi Arabia. *Geological Society of America Bulletin*, 101: 71-95.
- El-Hasan, T., and Al-Malabeh, A. (2008). Geochemistry, Mineralogy and Petrogenesis of El-Lajjoun Pleistocene Alkali Basalt of Central Jordan. *Jordan Journal of Earth and Environmental Sciences*, 1(2): 53-62.
- Fitton, J., and Dunlop, H. (1985). The Cameroon line, West Africa and its bearing on the origine of oceanic and continental alkali basalts. *Earth and Planetary Science Letters*, 72: 23–38.
- Floyd, P., and Winchester, J. (1975). Magma Type and Tectonic Setting Discrimination using immobile trace elements. *Earth Planetary Science Letters*, 27: 211-218.
- Floyd, P., Goncuoglu, M., Winchester, J., and Yaliniz, M. (2000). Geochemical Character and tectonic environment of Neotethyan ophiolitic fragments and metabasites in the Central Antolian Crystalline Complex, Turkey, in *Bozkurt*. *Geological Special Publication*, 173: 183-202.
- Foulger, G., Natland, J., Presnall, D. and Anderson, D. (2005). *Plates, Plumes, and Paradigms*. Geological Society of America Special Papers, Vol. 388, p. 881.
- Frey, F., Green, D., and Roy, S.D. (1978). Integrated Models of Basalt Petrogenesis - Study of Quartz Tholeiites to Olivine Melilitites from South Eastern Australia Utilizing Geochemical and Experimental Petrological Data. *Journal of Petrology*, 19(3): 463-513.
- Garfunkel, Z. (1989). Tectonic setting of Phanerozoic magmatism in Israel: *Israel Journal of Earth Sciences*, 38(2–4): 51–74.
- Gill, R. (2010). *Igneous Rocks and Processes: A Practical Guide*. A John Wiley & Sons, Ltd., Publication, 2: 20-65.
- Ibrahim, K. (1993): The geological framework for Harrat Ash – Shaam basaltic super group and its volcano tectonic evolution”. *Bulletin 25. NRA., Amman, Jordan*.
- Ibrahim, K., Rabba', I., and Tarawneh, K. (2001). Geological and mineral occurrences map of the northern Badia region, Jordan, scale 1:250,000. A Joint Report of the Higher Council for Science and Technology and the NRA, p. 136.
- Ibrahim, K. Moh'd, B. Masri, A. Al-Taj, M. Musleh, S., and Alzughoul, K. (2014). Volcanotectonic evolution of central Jordan: Evidence from the Shihan Volcano. *Journal of African Earth Sciences*, 100: 541–553.
- Illani, S., Harlvan, Y., Tarawneh, K., Rabba', I., Weinberger, R., Ibrahim, K., Peltz, S., and Steinitz, G. (2001). Dating of the Harrat Ash – Shaam basalts ,Northeastern Jordan. *Geological Society of America, Geology*, 29(2): 171-174.
- Irvine, T., and Barager, W. (1971). A guide to the chemical classification of the common rocks. *Canadian Journal of Earth Sciences*, 8: 523-548.
- Kushiro, I. (1968). Compositions of magmas formed by partial zone melting of the earth's upper mantle. *J. geophys. Res.*, 73: 619-634.
- Le Bas, M., Le Maitre, R., Streckeisen, A., and Zanettin, B. (1986). A chemical classification of volcanic rocks based on the total alkalis-silica diagram. *Journal of Petrology*, 27: 745-750.
- Meschede, M. (1986). A method of discriminating between different types of mid-ocean ridge basalts and continental tholeiites with the Nb-Zr-Y diagram. *Chemical Geology*, 56: 207-218.
- Middlemost, E. (1975). The basalt clan. *Earth Science Reviews*, 11: 337-364.
- Mo'hd, B. (1997). Geological Map of Irbid (3155II). 1:50,000, Natural Resources Authority, Amman, Jordan.
- Morgan, J. (1971), Convection plumes in the lower mantle, *Nature*, 230: 42-43.
- Mullen, E. (1983). MnO/TiO₂/P₂O₅—a minor element discriminant for basaltic rocks of oceanic environments and implication for petrogenesis. *Earth Planet. Sci. Lett.*, 62: 53–62.
- Nakamura, N. (1974). Determination of REE, Ba, Fe, Mg, Na, and K in carbonaceous and ordinary chondrites. *Geochim. Cosmochim. Acta*, 38: 757–775.
- Pearce, J. (1982). Trace element characteristics of lavas from destructive plate boundaries. In *Andesites: Orogenic Andesites and Related Rocks* (R.S. Thorpe, ed.). John Wiley & Sons, Chichester, U.K., pp. 525-548.

Pearce, J., and Norry, M. (1979). Petrogenetic implications of Ti, Zr, Y, and Nb variations in volcanic rocks. *Contributions to Mineralogy and Petrology*, 69(1): 33-47.

Pearce, J., and Cann, J. (1973). Tectonic setting of basic volcanic rocks determined using trace element analyses. *Earth Planet. Sci. Lett.*, 19: 290–300.

Rittmann, A. (1957). On the serial character of igneous rocks. *Egyptian Journal of Geology*, 1: 23-48.

Rittmann, A. (1962). *Volcanoes and their activity* (translation P.A. Vincent). Interscience, New York, p. 305.

Saunders, A., Rogers, G., Marriner, G., Terrell, D., and Verma, S. (1987). Geochemistry of Cenozoic volcanic rocks, Baja California, Mexico: Implications for the genesis of post-subduction magmas. *Journal of Volcanology and Geothermal Research*, 32: 223–245.

Smedley, P. (1988). Trace element and isotopic variations in Scottish and Irish Dinantian volcanism: evidence for an OIB-like mantle source. *Journal of Petrology*, 29: 413–443.

Sunkel, G. (1990). Origin of petrological and geochemical variations of Lau Basin Lavas (SW Pacific). *Mar. Min.*, 9: 205–234.

Tarawneh, K. ShimonI, Rabba, I. Harlavan, Y. Peltz, S. Ibrahim, K. Weinberger, R., and Steinitz, G. (2000). "Dating Of the Harrat Ash Shaam Basalts/ NE Jordan (Phase 1)". NRA-GSI Report, p. 65.

Walker, R., Gans, P., Allen, M., Jackson, J., Khatib, M., Marsh, N., and Zarrinkoub, M. (2009). Late Cenozoic volcanism and rates of active faulting in eastern Iran. *Geophys. J. Int.*, 177: 783–805.

Wilson, M. (1989). *Igneous Petrogenesis, a Global Tectonic Approach*. Unwin Hyman, London.

Winchester, J., and Floyd, P. (1976). Geochemical magma type discrimination: application to altered and metamorphosed basic igneous rocks. *Earth Planet. Sei. Lett.*, 28: 459-469.

Winter, Ohn D. (2001). *An Introduction to Igneous and Metamorphic Petrology*. Library of Congress Cataloging-in-Publication Data, USA.

Wood, D., Tarney, J., Varet, J., Saunder, A., Bougault, H., Joron, J., Treuil, M., and Cann, J. (1979). Geochemistry of basalt drilled in the North Atlantic by IPOD leg 49. Implications for mantle heterogeneity. *Earth and Planetary Science Letters*, 42: 77-97.



الجامعة الهاشمية



صندوق دعم البحث العلمي



المملكة الأردنية الهاشمية

المجلة الأردنية
لعلوم الأرض والبيئة

JJEES

مجلة عالمية عالمية محكمة

المجلد (٩) العدد (٣)

<http://jjees.hu.edu.jo/>

ISSN 1995-6681

المجلة الأردنية لعلوم الأرض والبيئة

مجلة علمية عالمية محكمة

المجلة الأردنية لعلوم الأرض والبيئة: مجلة علمية عالمية محكمة ومفهرسة ومصنفة، تصدر عن عمادة البحث العلمي في الجامعة الهاشمية وبدعم من صندوق البحث العلمي - وزارة التعليم العالي والبحث العلمي، الأردن.

هيئة التحرير:

رئيس التحرير:

- الأستاذ الدكتور فايز أحمد
الجامعة الهاشمية، الزرقاء، الأردن.

مساعد رئيس التحرير

- الأستاذ الدكتور نزار الحموري
الجامعة الهاشمية، الزرقاء، الأردن.

أعضاء هيئة التحرير:

- الأستاذ الدكتور نجيب أبو كركي
الجامعة الأردنية
- الأستاذ الدكتور نزار أبو جابر
الجامعة الأردنية الألمانية
- الأستاذ الدكتور محمد عطالله
جامعة اليرموك
- الأستاذ الدكتور أنور جريس
جامعة مؤتة

- الأستاذ الدكتور خالد الطراونة
جامعة الحسين بن طلال
- الأستاذ الدكتور عاطف خرايشة
جامعة البلقاء التطبيقية
- الأستاذ الدكتور عبدالله ذيابات
جامعة آل البيت

فريق الدعم:

المحرر اللغوي
- الدكتورة هاله شريتح

تنفيذ وإخراج
- عبادة الصمادي

ترسل البحوث إلكترونياً إلى البريد الإلكتروني التالي:

رئيس تحرير المجلة الأردنية لعلوم الأرض والبيئة

jjees@hu.edu.jo

لمزيد من المعلومات والأعداد السابقة يرجى زيارة موقع المجلة على شبكة الانترنت على الرابط التالي:

www.jjees.hu.edu.jo



المملكة الأردنية الهاشمية صندوق دعم البحث العلمي الجامعة الهاشمية

JREES

المجلة الأردنية
لعلوم الأرض والبيئة

المجلد (٩) العدد (٣)



مجلة علمية عالمية مدعمة تصدر بدعم من صندوق دعم البحث العلمي